Biomechanical Characterization of Complex Thin Bone structures in The Human Craniofacial Skeleton

by

Asmaa Maloul

A thesis submitted in conformity with the requirements
for the degree of Doctor of Philosophy

Institute of Biomaterials and Biomedical Engineering
University of Toronto

Biomechanical Characterization of Complex Thin Bone structures in The Human Craniofacial Skeleton

Asmaa Maloul

Doctor of Philosophy

Institute of Biomaterials and Biomedical Engineering
University of Toronto

2012

Abstract

In spite of burgeoning of new technologies in the field of maxillofacial surgery, such as novel methods for osteosynthesis, bone substitution and bone regeneration, the reconstruction of the craniofacial skeleton (CFS) remains a challenge. Complications and failure in existing technologies and treatments for the CFS may be attributed in part to an incomplete understanding of the biomechanical environment in which these technologies are expected to perform. Characterizing the morphology and biomechanical behaviour of this complex and unique structure is important to understanding its global response to mechanical demands. This thesis aims to characterize the biomechanical behaviour of thin bone regions and sutures in the CFS. We investigated the impact of image degradation in CT scans on the ability to develop accurate specimen-specific FE models. Image degradation resulted in large increases in cortical thickness and decreases in scan intensity, which corresponded to significant changes in maximum principal strains in the FE models. A new semi-automated connectivity technique was developed to quantify the degree of fusion in sutures and revealed varying degrees of connectivity and interdigitation depending on the suture location. Morphological features characterized using this technique were incorporated into idealized suture FE models and analysed under multiple loading directions. The idealized FE models revealed that the impact of the number of

interdigitations on the strain energy absorption in the suture/bone complex is dependent on the loading direction (inversely related under pressure and directly related under perpendicular and pressure loading); similar behaviour was seen in a μCT based specimen-specific FE model. Three-point bending tests on bone samples containing sutures revealed a positive correlation between the number of interdigitations and bending strength. Finally, experimental testing of full cadaveric heads demonstrated inter-specimen consistency in strain magnitude and direction under muscle loading in spite of morphological differences. Overall, these findings provide new insight into the complex morphology of the CFS, limitations of current clinical imaging and the biomechanical behaviour of thin bone structures and their articulations. This work forms a solid foundation for future development of image analysis, modeling and experimental investigations focused on characterizing the global behaviour of the CFS

ACKNOWLEDGMENTS

I have been fortunate to have received mentorship from numerous outstanding individuals during the last four years of my Ph.D. at the University of Toronto and the Orthopaedic Biomechanics Laboratory. It is to those people that my gratitude and thanks go out to, for without their help and support, this thesis would not have been completed.

First, I would like to thank my research supervisors, Dr. Cari Whyne and Dr. Jeffrey Fialkov. Cari, thank you for your support and guidance everytime I came into your office asking for advice. I would have never had a rewarding experience without your help and encouragement. You always inspired me to work harder towards my goals and dreams. Thank you for everything, from having faith in me from the very beginning and giving me the opportunity to be part of your research team before even meeting me, to keeping up with all my complaints and questions. I thank you for teaching me so much more for my future than just doing research and science. Jeffrey, thank you for always helping me to think of the big picture and the exposure you gave me to your work. It has been a great experience and opportunity to have been able to work with you. Special thanks to my committee, Dr. Craig Simmons, Dr. Kristy Brock, and Dr. Ernest Lam for their support, guidance and helpful suggestions.

To my friends in many parts of the world, you were sources of laughter, joy, and support through your visits to me in Toronto or our long video chats. Special thanks go to Maral Charyeva, Safia Al-Kharsa and June Yeung. I am very happy that even though we are no longer at Smith College, your continued love and support have extended well beyond our time at Smith. Thank you so much for being there for me when I needed your advice.

To the members of the OBL lab, you were like my family in Canada. Each one of you touched my life in a great way. Our lunch times and many breaks brought so much laugh and joy to my Ph.D. experience. You made graduate school such a fun, exciting, and beautiful part of my life. Special thanks to Devin and Zoryana for their support and encouragement through the hard times in my last year. To our great engineer Maarten Beek, thank you for your help especially during mechanical testing.

I am grateful to my family, who through my life believed in me and had always encouraged me to follow my dreams. Thank you Yabba and Yamma for providing me with all the support and

love and be patient with me. To my siblings, Suha, Heba , Salam, Hamodi, and Hala, your smiles and love kept me going always even when I am thousands of miles away from home. To my brother Anas, you always told me you were so proud of me and I should never let anything stop me from following my heart. You will always be with me and your love will always lighten my way. I dedicate this thesis to you, my wonderful brother; you left us too soon. To Mohammed, thank you for your love and support through good and bad times. Thank you for keeping up with my moods, which a lot of the time correlated with the results of my research. Your love provided my inspiration and was my driving force. To all of my family members, I owe you everything and wish I could show you just how much I love and appreciate you.

.

TABLE OF CONTENTS

LIST OF FIGURES

LIST OF TABLES

CHAPTER 1
Background

1.1 Functional Anatomy

The human craniofacial skeleton (CFS) is made up of a series of irregular flattened bones, which can be primarily divided into two parts, the *neurocranium (cranial* vault) and the *viscerocranium* (facial bones). The *neurocranium* consists of eight bones, which include two parietal bones, two temporal bones, frontal bone, occipital bone, sphenoidal and ethmoidal bones (Figure 1-1 and Figure 1-2). The *viscerocranium* consists of fifteen bones: the inferior portion, or mandible, and the superior region, composed of 14 bones (two nasal (2), maxilla (2), lacrimal (2), zygomatic (2), palatine (2), inferior nasal conchae (2), ethmoid (1) and vomer (1)) [1, 2]. Unlike the remainder of the axial skeleton and the appendicular skeleton, the CFS (with exception of the mandible) has no intrinsic moving parts and is joined by static articulations called sutures.

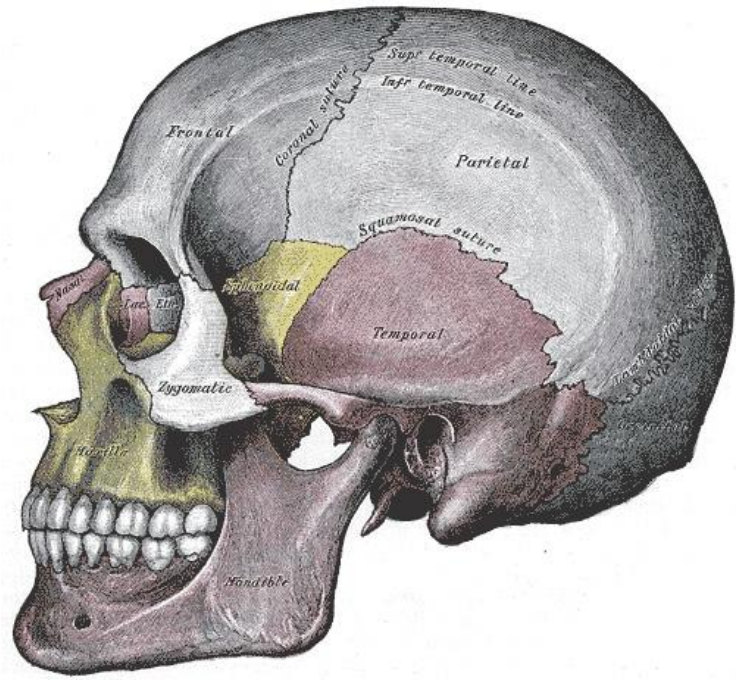

Figure 1-1: Lateral view of the craniofacial skeleton bones
(from Gray's Anatomy, 20th edn., 1918, copyright expired)

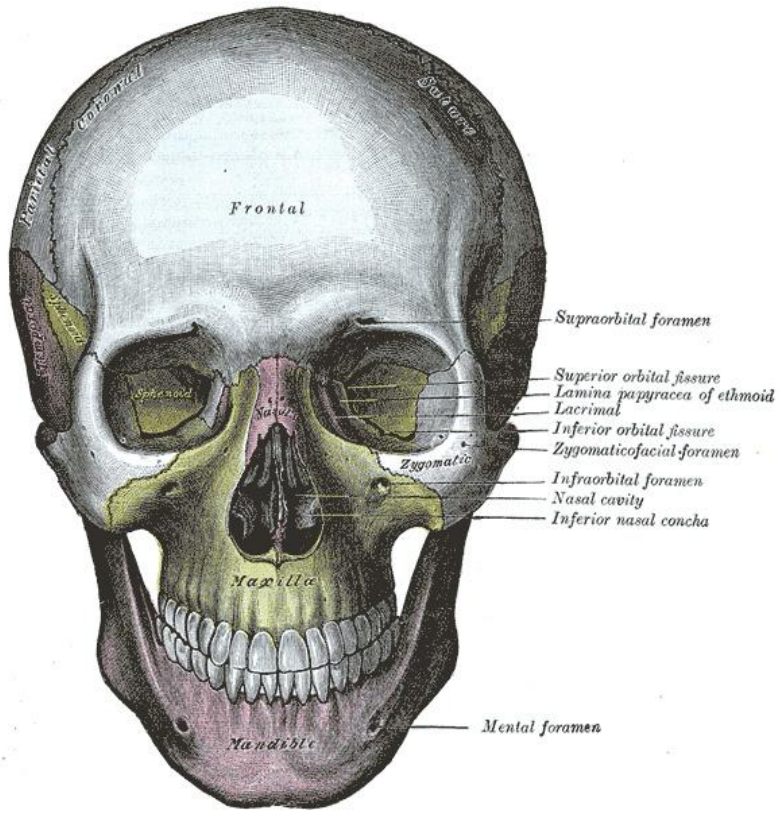

Figure 1-2: Anterior view of the craniofacial skeleton bones
(from Gray's Anatomy, 20th edn., 1918, copyright expired)

1.2 Development and Growth of the Craniofacial Skeleton

Bones of the CFS develop through one of two pathways: desmal ossification or chondral ossification. Desmal ossification is the formation of bone directly from the mesenchyme while chondral ossification is bone formation indirectly through a cartilage stage. All bones of the human CFS develop directly from the mesenchyme with exception of the ethmoid bone, the inferior nasal conchae and the base of the skull. During the prenatal stage the mesenchyme becomes concentrated into an envelope around the brain from which the craniofacial bones ossify directly out of the connective tissues. The proliferation of the bony nuclei in the connective tissues in a lamellar fashion forms the bone of the CFS, thereby reducing the amount of connective tissue remaining to small gaps, called sutures[3]. Longitudinal postnatal bone growth in the CFS occurs at the location of these sutures. Latitudinal bone growth in the CFS occurs appositionally from the periosteum resulting in the thickening of the skull.

The craniofacial sutures form as the margins of the developing bones approximate each other without fusing forming a gap filled with collagen fibres[4, 5]. The sutures function to hold the bones of the skull together while allowing for mechanical stress transmission and deformation (i.e. distortion during childbirth, cyclic loading from muscle activity, forces from therapeutic mechanical devices and traumatic impacts) [6]. The primary function of sutures in the CFS changes with age. In postnatal stages and early development, sutures provide high flexibility to allow for enlargement of the head around the developing organs. Calvarial sutures undergo most of their growth during these early stages of development, where as facial sutures are most active during adolescence. In adulthood, sutures are believed to function primarily as shock absorbers to dissipate stresses transmitted through the skull[7-15].

Morphogenesis and postnatal growth in the adult CFS is mainly influenced by the development of the jaw apparatus due to mastication. For example, the eruption of the 12 year molars results in further growth of the skull in association with the greater functional demands of the masticatory muscles [3]. The postnatal growth of the skull is presumed to peak in mid adolescence and slow dramatically in late adolescence, with no growth occurring in adulthood. Common dates of cessation revolve around 14 years in females and 16 years in males [16]. Thus, the adult CFS is viewed as a stable and static entity in terms of size and shape changes. More recent studies have suggested that during adulthood the depth, width and height of the face increase by several millimetres. One study showed 9 to 14 percent increases in frontal sinuses, 6 percent increases in the upper face, and 5 to 7 percent increases in the mandible during late adulthood [17-19]. This contradicts the initial concept that formation of ossified bridges over the sutures presumably ends its growth and results in full closure of the suture gaps between the ages of 40 and 50 years[3].

1.3 Function

The bones and cavities of CFS provide a housing and protective cover for the brain and the sense organs, and represent the beginning of the respiratory and digestive tract. Similar to most of the bones in human skeleton the CFS serves as the attachment location for all the facial muscles responsible for mastication, breathing and facial expressions (Figure 1-3). The contraction of these muscles results in multiple types and directions of loading applied to the CFS. The force generated through the contraction of the facial muscles, mainly the masseter and temporalis,

results in the movement of the mandible upwards toward the maxilla to cut and grind food[2]. The forces produced by these muscles have an effect on the bones from which they originate, however, little has been written about the effect of these muscles on stress and strain patterns in the CFS. The resultant forces due to the occlusion of the jaws is the highest physiological force acting on the CFS and due to its cyclic nature it is of greatest concern when considering fracture fixation in the head[2, 20, 21]. Other facial muscles, such as the mentalis, medial and lateral pterygoid, generate less forces on the CFS due to their relatively smaller sizes. The lines of action of the different facial muscles are diverse resulting in different types of loading, including shear and torsion.

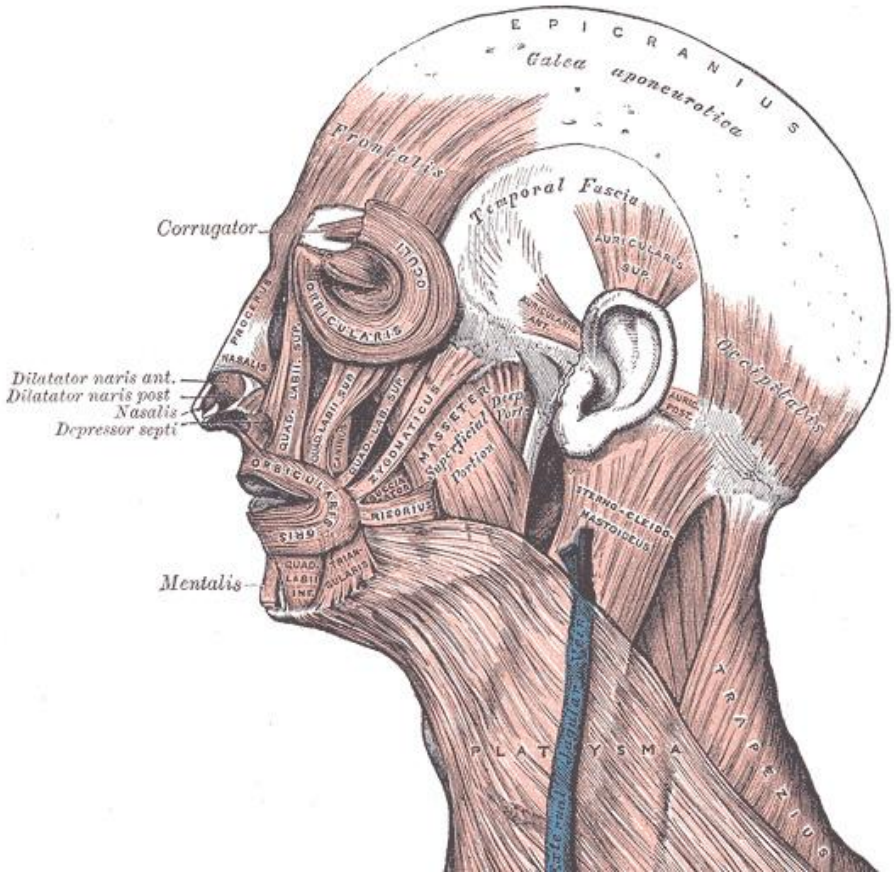

Figure 1-3: Muscles of Mastication in the craniofacial skeleton
(from Gray's Anatomy, 20th edn., 1918, copyright expired)

The facial bones form the foundation for the soft tissues of the face and, as such, the appearance of the facial features. Thus, the shape and quality of the craniofacial bones determine much of the static appearance and distinctness of individuals. Deformities or abnormal alterations in the

shape or structure of the CFS bones can significantly change an individual's appearance and negatively affect facial sensory, respiratory, digestive and masticatory functions. Maintaining the integrity and stability of the CFS is essential both functionally and cosmetically.

1.4 Structural Properties

Anatomically, the bones of the cranial vault and the mandible have a basic structure similar to many other bones of the skeleton with a strong outer cortex and a cancellous centre. In contrast, most of the bones of the midfacial region of the CFS exhibit significant variations in their thickness and composition. Both the maxillary sinus and certain portions of the temporal bone are comprised only of a thin layer of cortical bone. As such these bones are comparatively fragile and they fragment and comminute easily. The distinct structure of the CFS enables it to withstand impact forces approaching the midface region from below as the mandible absorbs much of the traumatic energy [22]. However, the midface has very low tolerance to impact forces applied from other directions, with nasal bones exhibiting the least resistance. A study by Nahum *et al.* showed that the posterior portion of face fractured with forces between one-fifth and one-third of those required to produce a simple fracture of the mandible [23]. Impact forces directed lateral to the head can lead to zygomatic complex fractures and partial or full dislocation of the midfacial region. Forces applied in a horizontal direction towards the midface can result in comminuted fractures pushing the midface framework against the skull base [24].

1.5 Material Properties

Bone is a composite material composed of an organic matrix which is reinforced with inorganic minerals. The organic part is constituted of 90% collagen, predominantly type I, and the remaining 10% are noncollagen proteins. The inorganic part comprises approximately 65% of the bone structure and consists primarily of hydroxyapatite, in addition to magnesium, potassium, chlorine, iron and carbonate [25-27]. At the macrostructural level bone is classified based on density and porosity into cortical and trabecular bone. In the mature form of adult bone the major portion of cortical and trabecular bone consists of lamellar bone. Lamellar bone has a well organized arrangement of collagen fibres. The orientation of these collagen bundles presents a relationship to the mechanical function of the corresponding bone site [28]. Cortical bone is generally located along the external surfaces of bone trabecular mesh. As well there exist regions in the human skeleton where cortical bone is present as a standalone structure (i.e. *maxillary*

sinuses)[26]. The thickness of the cortical bone in the CFS can vary significantly throughout the midfacial region and cranium (Figure 1-4). Cortical thickness can be measured using CT images, however the ability to measure cortical thickness is challenging in very thin bone regions such as maxillary sinus wall due to the limited resolution of clinical scanners. Trabecular bone exists as an interconnected network of rods and plates (trabeculae). The orientation of the trabecular structure is influenced by the direction of the force applied to the bone.

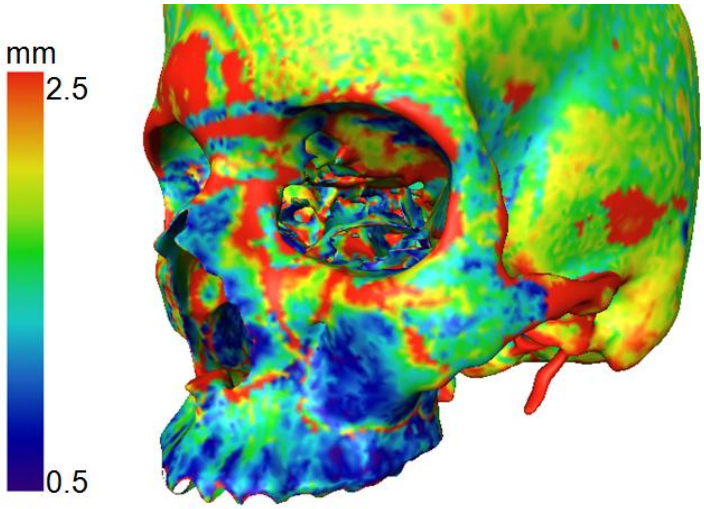

Figure 1-4: Distribution of cortical bone thickness in the CFS

Elastic properties of bone tissue can be measured by applying force to bone specimens for which changes in length can be quantified. The elastic properties of bone can vary based on the anatomical position and the individual. A great number of studies have been conducted to characterize the mechanical properties of both cortical and trabecular bone [29-33]. It has also been shown that the measured mechanical properties of bone can vary depending on the type of mechanical testing employed. The Young's modulus for cortical bone specimens has been found to vary between 7.1 to 28.2 GPa based on tensile tests and between 14.7 and 34.3 GPa based on compression tests[34] . Material properties of craniofacial bone have been measured for the zygoma, maxilla, mandible and cranial vault [35-38]. These studies found that the elastic moduli in the maxilla and zygoma ranged from 9.1GPa to 15.6 GPa and 10.4 to 19.6 GPa[35, 36], respectively.

1.6 Craniofacial Skeleton Biomechanics

To date, there is no one general theory that relates the development, biomechanics and evolution of the skull. To understand the biomechanics of the CFS multiple modelling approaches have been used including physical models, graphical representations, analytic models, computer based simulations, preclinical (*in vitro and in vivo*) models and *in vitro* cadaveric models[39-46]. In many cases, models have focused on isolated regions of skull morphology and their specific contribution to overall function. As such, the CFS has often been treated as a collection of anatomical systems with specific biomechanical problems[40, 47-52]. The application of any of these methods to the study of the biomechanics of the CFS depends on the research question; combinations of these approaches have been used to overcome limitations associated with individual methods [44, 53].

1.6.1 The Evolution of Skull Biomechanics

The foundations of craniofacial biomechanics were first laid in 1953 by Becht through his studies examining the skull, teeth and masticatory muscles in various mammals[2]. His studies linked the morphological aspects of the skull to its mechanical demands based on dietary habits. Around the same time, several theoretical papers were put forward by Tucker [41, 54-56]. In these studies Tucker investigated the relationship between function (mastication activities) and mechanical behaviour and provided a foundation related to much of the basic loading in the CFS. He reported the presence of stresses at muscle attachments and the temporomandibular joint, as well as the generation of stress in the jaw and maxilla due to reaction forces from biting solid food. Tucker proposed two stress categories in the CFS: circumscribed stresses and dispersed stresses. He defined dispersed stresses as one generated in the skull when the maxilla and mandible surfaces are enlarged to spread the load and diffuse it to be resisted locally by the structure. Circumscribed stresses were defined as stresses of high magnitude that were generated within small areas and needed to be transmitted to other regions of the CFS to be resisted and not cause damage. Based on these stress classification, Tucker described initial patterns for the direction and magnitude of stresses in the CFS and established that stress transmission was the primary function of the entire adult skull.

Ten years later, Endo (1965) attempted to characterize the strain patterns produced in the midfacial region by the masseter and temporalis muscles through *in vitro* mechanical testing

conducted on human skulls[57, 58]. In his studies canvas sheets were glued onto the attachments of the muscles to apply forces to the bone surface. Endo reported the presence of various stresses in the midfacial region, which represent the foundation to the current understanding of loading in this region of the CFS. Endo's studies were unique at the time in their use of human skulls rather than animal skulls. However, the findings of both Endo and Tucker were not verified until the late 1980's. In 1987 Buckland-Wright conducted an *in vivo* study in which they measured bone strains on anesthetized cats during simulation of their jaw muscles [7]. They showed that deformations produced by the masseter muscle were higher than those produced by the temporalis muscle. Both tensile and compressive forces were present in the skull during biting, but compressive forces were dominant.

1.6.2 Theories in Craniofacial Biomechanics

Two main structural properties, strength and stiffness, are generally described when studying the mechanics of the CFS. Strength is a measure of a bone's ability to withstand applied forces without failure. Stiffness is a measure of bone's resistance to elastic deformation under load. In developing theories to describe the mechanics of the CFS, many simplifications to the shape of the CFS and loading regimes have been applied. The three main theories that have been used to describe the biomechanics of the CFS are beam theory, buttress theory and functional adaptation theory.

1.6.2.1 Beam Theory

Statics refers to the ability of the skull to transmit loads passing through it where the relative position of all its parts remains constant. The main approach employed by several investigators to study the statics loadings on the skull is based on beam theory. Earlier attempts to understand force transmission and stress concentration using beam theory were conducted by Demes *et al*. and Wolff [59, 60]. The beam theory is based on developing models of beams in various configurations with bending moments from several bite positions to understand the relationship between stress and strength in the CFS (Figure 1-5).

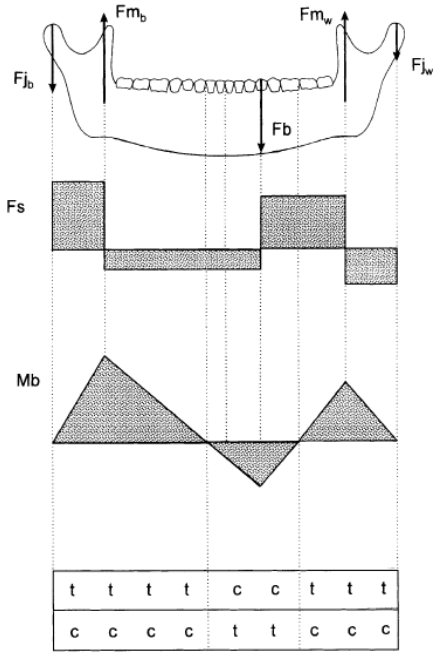

Figure 1-5: Application of beam theory to the mandible
(T.M. Van Eijden. Crit Rev Oral Biol Med (2000), 11(1); pg.123-136. Reprinted with the permission of ©SAGE publications)

The beam theory was also used to understand the biomechanical behaviour of the entire skull. It was applied by simplifying the skull to be a cantilever beam with one free end and one fixed end[40]. Applications of the beam theory to the individual components of the facial region included modeling the superorbital region as beam during incisor biting [57] (Figure 1-6). In this study beam theory was used to understand the bending of the superorbital region in the frontal plane. Based on this it was assumed that strain should be at maximum in the mid sagittal region and it should decrease laterally. Other approaches in analysing full skull biomechanical behaviour modelled the CFS as idealized cylinder[61]. This theoretical analysis using beams tries to quantify the effect of shape on mechanical properties of the structure. Using such analysis to study the CFS does not account for differences in Young's modulus or strength between the different regions of the skull. Moreover, the equations used for beam theory are derived based on assumptions that are not valid for the head structure.

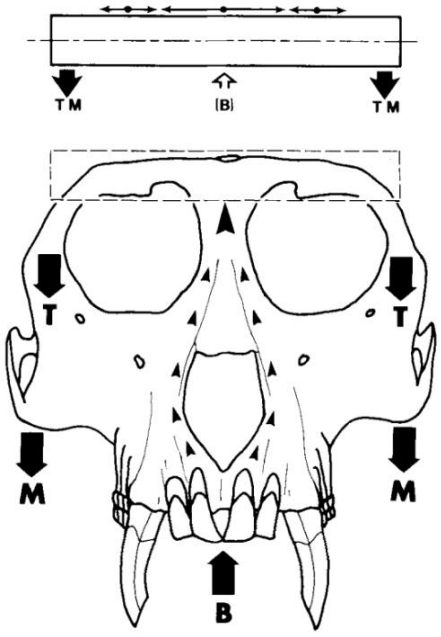

Figure 1-6: Application of beam theory to the superorbital region
(Pascal G. Picq and William L.Hylander (1989). Am J Phys Anthropol, 79(3); pg.393-398. Reprinted with the permission of © John Wiley and Sons)

1.6.2.2 Buttress Theory

The central midfacial face is comprised of the maxilla and the orbito-naso-ethmoidal region. This region of the CFS is comprised of a combination of light weight thin walled cavities and thick bony regions. The buttress theory proposes that the midfacial region is like a framework that is stabilized by horizontal and vertical buttresses (Figure 1-7). These buttresses believed to carry and transmit the forces generated from biting on food while keeping these forces away from other delicate facial bones [2, 24]. It is hypothesized that the midfacial bones convey forces from biting to the rest of the skull through three forceful trajectories (Figure 1-8). The first trajectory runs from the tooth region up through the frontal processes of the maxilla toward the anterior wall of the nasal bone all the way to the glabella region of the frontal bone. The second trajectory runs through the zygomatic buttress to the frontal bone passing through the frontal processes. It also extends to the temporal bone via the zygomatic arch. The third trajectory protract posteriorly along the dorsal maxilla to the sphenoid bone [24]. These trajectories represent regions of thicker bone that provide vertical support from forces generated at the tooth location.

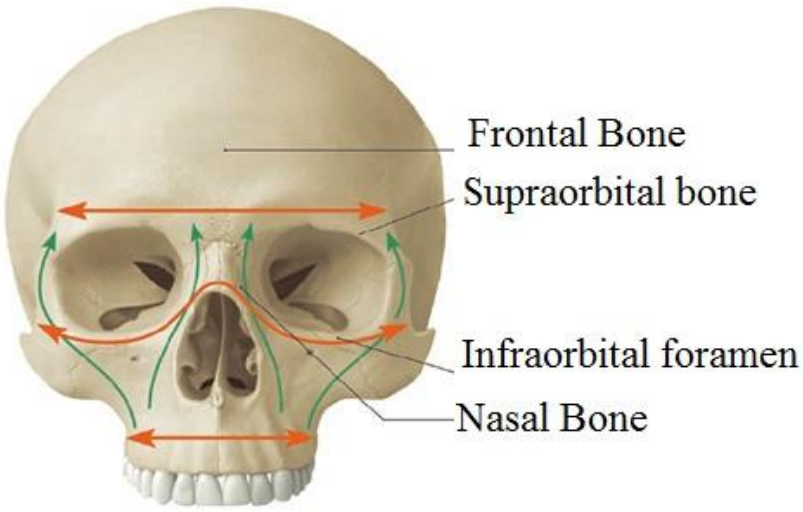

Figure 1-7: Diagram of the transversal buttresses of the midface, represented by the horizontal supraorbital frontal bar, the infraorbital rims and the maxillary process
(Nicolas Hardt and Johannes Kuttenberger (2010). Craniofacial trauma: diagnosis and management (pg. 10). Reprinted with the permission of © Springer)

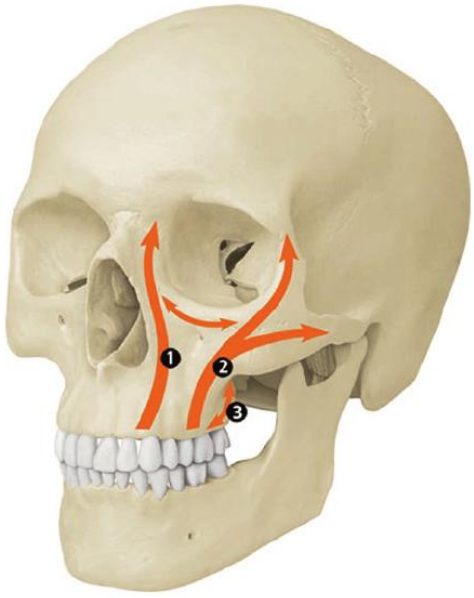

Figure 1-8: Diagram of the vertical maxillary buttresses of the midface. These buttresses represent regions of thicker bone, which provide support for the maxilla in the vertical dimension. 1 Anterior medial naso-maxillary buttress, 2 lateral zygomatico-maxillary buttress, 3 posterior pterygo-maxillary buttress
(Nicolas Hardt and Johannes Kuttenberger (2010). Craniofacial trauma: diagnosis and management (pg. 11). Reprinted with the permission of © Springer)

1.6.2.3 Functional Adaptation Theory

The functional adaptation theory has been proposed to describe the development and mechanics of the CFS stating that "facial bones are optimized for countering masticatory loads, i.e. that they exhibit minimum material and maximum strength for countering cyclical loading regimes"[2, 51]. The majority of the work conducted to develop this theory was based on the adult head skeleton in tetrapods and mammals by looking at the influence of forces on cranial form and feeding mechanisms [24]. However, much of the data collected from such studies cannot be transferred to the human CFS due to significant differences in the morphology and the patency in the sutures. The CFS for such animals is designed for their feeding mechanism which requires movement between the different components to allow for mastication. The human skull is very different than other mammals in two major ways: the short rostrum and the expanded cranium. Having a short rostrum the human skull is optimized to resist more bending strength that can be experienced due to function. For example, the frontal bone was found to be able to withstand 7000N force even though it is not subjected to this magnitude on a regular basis [2]. If bone morphology is a reflection of its function to resist the loads imposed from muscles then why the frontal bone needs to withstand such high load.

1.6.3 Recent Advances in Craniofacial Biomechanics

More sophisticated biomechanical approaches have been used to delineate the forces and strain patterns of the CFS using *in vitro* and *in vivo* methods [48, 51, 62, 63]. The studies by Oyen *et al.* were conducted on monkeys to characterize strain patterns due to mastication by stimulating contractions of the jaw elevator muscles [62, 63]. Similarly *in vivo* studies by Hylander *et al.* and Ross *et al.* were conducted in macaques to measure strains in the midfacial region during mastication [48, 51, 62, 63]. Although the force application in *in vivo* studies represents the most appropriate approach to measure strains in the CFS, the ethical considerations in humans and the limitations in placing multiple strain gauges on the CFS limits investigation of the strain in the full human CFS. The use of cadaver CFS to conduct *in vitro* studies can provide understanding of the mechanics of the CFS, however, the complexity of the loading and muscles limits the investigator ability to obtain comprehensive results.

Computational modeling has also been utilized to quantify the biomechanical behaviour of the CFS[43-45, 53, 64-73]. The development of experimentally validated finite element (FE) models

presents a robust method to generate full field information throughout the CFS under multiple loading configurations. However, due to the complexities in generating these FE models, to date these computationally intensive studies have generally been limited to single specimen specific model [44, 46, 68]. Single specimen results may not be reflective of general strain patterns due to the variety of morphologic differences between individuals. The most recent work combining mechanical testing of skulls and computer modeling have been conducted by Ross *et al*. and Strait *et al*.[48, 69, 71, 74]. In these studies four adult rhesus macaques were used to quantify the strain magnitude and direction using strain gauges during mastication. The data obtained from this study as well as other published data was used to validate an FE model of a macaque cranium during mastication. However, much of the recent work has been devoted to understanding the mechanics of early humans and primates by paleoanthropologist, and relatively few contributions have concentrated on the biomechanical behaviour of the modern human skull.

1.7 Craniofacial Fractures

The delicate and intricate architecture of the CFS makes it more susceptible to complex fractures than other parts of the human skeleton. Studies reported that traffic accidents are the main cause of skull bone fractures followed by sport accidents such as skiing, biking and horse riding [24]. In the study of fractures epidemiology by Neidhardt (2002), it was reported that 41% of skull fractures in patients were due to traffic accidents (18% were due to car accidents, 17% due to bike accidents and 6% due to motorbike accidents). Domestic accidents such as falling resulted in 23% of craniofacial trauma. Sport injuries caused 18% of the injuries while 10% were acquired at work [24]. Violence was found to be the cause of the least number of craniofacial injuries at 8%. The same study by Neidhardt showed that most of the patients suffering from craniofacial fractures are between 16-45 years of age.

The changing pattern in the etiology of craniofacial fractures over the last few decades has resulted in a significant change in the types of fracture most commonly occurring. Superior portion fractures (nasal bone, zygoma and maxilla) are now more common than fractures of the mandible [23]. Prior to this shift in fractures types, the high occurrence of mandible fractures motivated a great number of studies to study the biomechanical behaviour of the mandible using *in vivo* animal studies, *in vitro* cadaveric mechanical testing, mathematical models and finite element models[75-78]. In contrast, little attention was given to studying the mechanical behaviour

of the midfacial region. However, due to the increase in the number of fractures occurring in that area there is a greater need to understand its biomechanical behaviour and fracture patterns.

1.7.1 Types of Fractures

Fracture patterns in the midfacial skeleton can be broadly subdivided into three groups, LeFort I (low-level fracture), LeFort II (subzygomatic fracture) and LeFort III (supra-zygomatc fracture)[24, 79] (Figure 1-9). The bones of the midfacial skeleton are rarely fractured in isolation. This is due to the fact that all the facial and cranial bones, with the exception of the mandible, articulate and interdigitate together through sutures which make it difficult to fracture one bone without disturbing its neighbours. It has been shown that facial fractures commonly occur in adults at articulation sites [80]. For example, the zygomatic bone usually fractures in the region of the frontozygomatic, zygomatico-temporal and zygomatico-maxillary sutures. Although, it is unusual for the mid-facial bones to be fractured individually, they may occasionally be split under extreme violence.

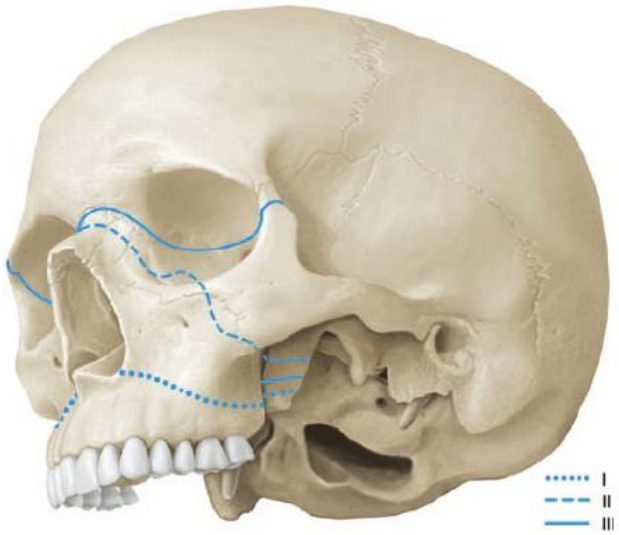

Figure 1-9: Fracture levels LeFort I-III transverse subcranial midface fractures
(Nicolas Hardt and Johannes Kuttenberger (2010). Craniofacial trauma: diagnosis and management (pg. 33). Reprinted with the permission of © Springer)

1.7.2 Mechanisms of Fractures

The bone and soft tissues of the midfacial region are able to absorb the energy from impact forces. However, when these forces exceed the strength of these tissues, a variety of fractures can occur at this region. The forces required to cause fractures in the midface varies from one location to another based on the bone material properties and shape (Figure 1-10). Models have been put forward linking the magnitude of the impact to the fracture patterns in the midfacial region. In these models it is proposed that energy absorption at different locations and depths occur in the midface and it can help to avoid fractures in the other regions of the skull [24].

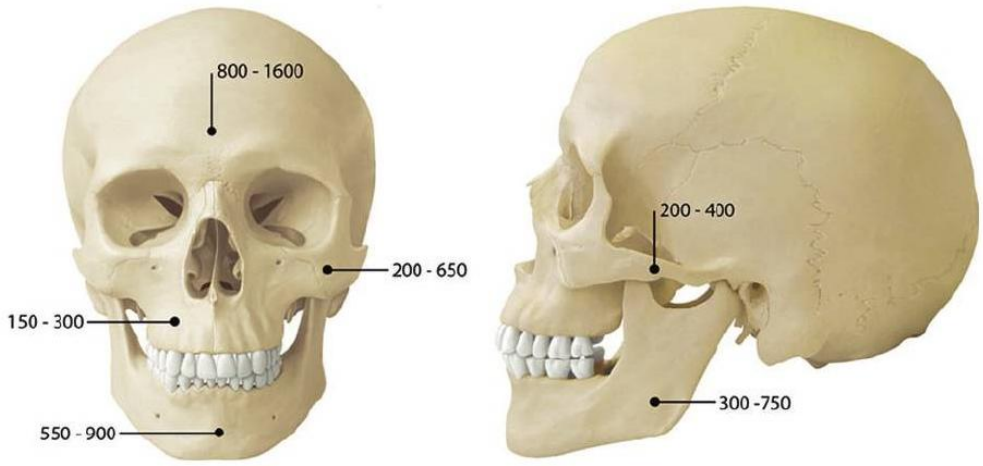

Figure 1-10: Biomechanical Forces (Nm) necessary to cause fractures of the facial skeleton
(Nicolas Hardt and Johannes Kuttenberger (2010). Craniofacial trauma: diagnosis and management (pg. 58). Reprinted with the permission of © Springer)

1.7.3 Treatment

Wires, staples, pins, plates, and screws are hardware used to achieve fixation in the CFS. However, the last two decades have seen major changes in the methods of fixation used for CFS fractures. Surgical techniques have been moving away from delayed closed reduction with internal wires suspension to early open reduction and internal plate fixation (Figure 1-11). More recent advances in fixation methods use biodegradable polymers, glues and adhesives to treat fractures and deformities in the CFS. The principle aim of these devices and techniques is to establish rigid immobilization both to obtain proper, stable anatomic configuration and to

promote rapid healing with less emphasis on providing mechanical stability to resist high levels of applied physiological forces[81, 82].

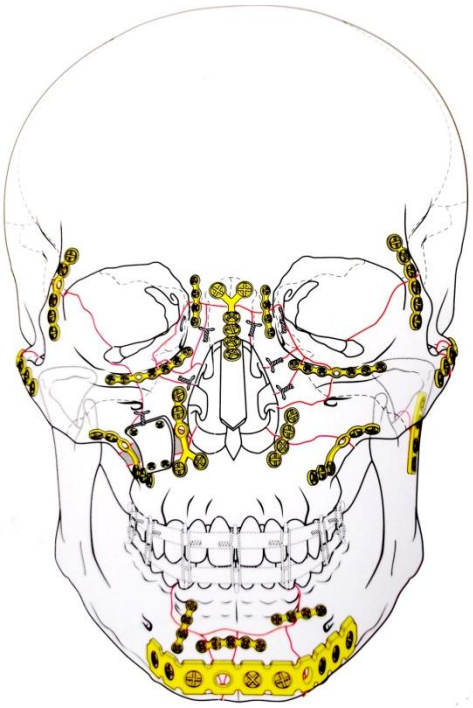

Figure 1-11: Mini-plates and mini-screws for fracture fixation
(Assael L.A and Klotch D.W. et al. (1998). Manual of internal fixation in the cranio-facial skeleton : techniques recommended by the AO/ASIF-Maxillofacial Group, Joachim Prein (Ed.) (pg. 100). Reprinted with the permission of © Springer)

Wire fixation is less common in maxillofacial reconstruction due to the surgical complexity of making a hole in the bone and passing the wire through it. It requires the use of multiple wires with equal tension to provide rigid fixation, as loosening can result in motion and possible nonunion or malpositioning[82]. Wire fixation alone does not provide functionally stable fixation and is associated with many problems such as breakage due to cyclic loading or cut-through the bone. Similarly, staples do not provide sufficient mechanical stability for permanent fixation and often require pre-drilling holes in bones. Thus, pneumatic staplers are more commonly used as a method to rapidly connect bone fragments prior to other fixation methods [82].

The transition from wire osteosynthesis to rigid internal fixation in craniofacial reconstruction using different micro or mini-plates and screw systems is regarded as one of the greatest advances in the field of maxillofacial surgery. The high degree of ductility in these microplate

screw fixation systems permits an optimal adaptation to the thin facial bone and provides three-dimensional stability to the CFS. They are superior compared to other fixation methods in terms of their ability to provide a precise and anatomically exact reconstruction and sustaining functionally important bone sections [24, 82-84]. The screw-holding power is influenced by a combination of intrinsic factors (i.e. outer thread diameter and length) and extrinsic factors (i.e. bone quality and insertion orientation). When used to hold two bone fragments together, screws are commonly inserted perpendicular to the bone axis. However anatomic constraints or surgical conditions (i.e. orientation of the ends of the bone fragments may not be perpendicular to the screw axis) can impact the screw orientation. In such cases, the screw's holding power is decreased, resulting in reduced stability. Anatomic constraints can also limit the number of screws that can be placed on the bone. Thus, screws are often combined with plates to achieve sufficient stability and increased strength of fixation. Plates are typically made of highly flexible titanium so they can be modulated in all three dimensions and ideally adapted to the required demands[24, 82-84]. The main limitation with plate fixation is the larger surgical exposure required and greater profile (thickness) of the plate beneath the soft tissue.

Even though direct fixation using semi-plates and screws has become wide spread and used for stabilization of fractures in the midfacial region of the CFS, the rationale for the number and placement of this orthopaedic hardware to achieve stability is still unknown and guided on the clinician experience. In the treatment of the mandibular fractures, however, the decision about which sites to plate is based on stress distributions and force vectors [81, 85]. Based on research findings, plates are placed strategically so that the force vectors in the bone are used to aid fracture stabilization and promote healing (Figure 1-12). To date, this approach is not used in the stabilization of midfacial fractures. Placement of these devices is not guided by the different forces (tension, pressure, and rotational forces) generated in the facial bones. This can be attributed to the lack of information about the force vectors in midfacial region and the insufficient understanding of craniofacial biomechanics. An understanding of the structure and biomechanics of the maxilla and midface, accompanied by an anatomically orientated therapy, can help surgeons achieve better results in maxillofacial reconstruction.

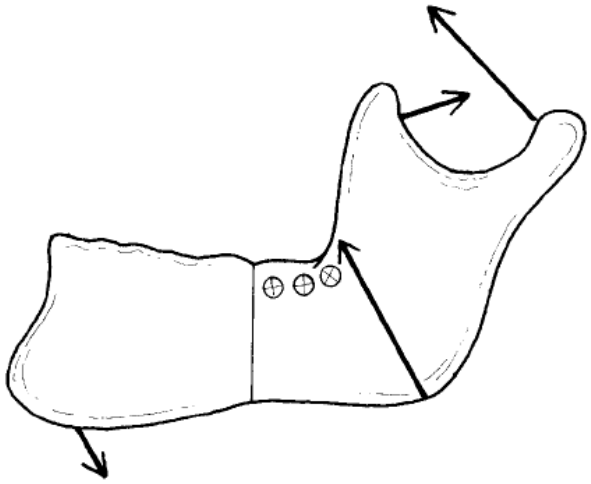

Figure 1-12: Placement of screws in the mandible with muscle and reaction forces acting on the fixation

(Alex M. Greenber (2002). Craniomaxillofacial reconstructive and corrective bone surgery: principles of internal fixation using AO/ASIF technique, Joachim Prein (Ed.) (pg. 105). Reprinted with the permission of © Springer)

The conventional fixation of osteosynthesis plates requires areas of sufficient cortical bone mass to insert screws. This may be difficult to achieve at sites where the boney structures is very thin (i.e. nasoethmoidal and frontal regions) and can cause further fractures due to the force applied to the fragments [86]. In such cases, the conventional microplate screw fixation systems are not possible and alternative fixation techniques are being developed[86-90]. The use of biodegradable implants, glues and adhesive for fracture fixation has potential to overcome many of the problems associated with microplate screw fixation systems. However, to date, substances with adhesive properties for bone gluing purposes are limited due to bad biocompatibility, high infection rates and lack of sufficient adhesive stability [91, 92].

1.7.4 Complications

In spite of the advancement in the different types of technologies and methods of bone fixation in the field of craniomaxillofacial surgery, clinicians continue to experience complications and challenging reconstruction conditions. Several authors reported an overall complication rate among craniofacial procedures between 14% and 22% [79, 93-95]. Complications resulting in functional problems or cosmetic deformity very often require reoperation which can be costly and have a significant negative impact on the patient quality of life[79, 96, 97]. Complications post

craniofacial surgery can be specific to the procedure but some problems can be applicable to all craniofacial procedures such as infection, malunion and nonunion.

Infection is one of the most commonly encountered problem post craniofacial procedures and one of the main causes for removal of maxillofacial internal fixation hardware [98-100]. Infection can be related to many factors such as pre-existing sinus infection which provide a source of contaminating organism and disruption of the normal flow of lymph from fractures in the facial region. Recent studies have shown that hardware removal due to infection was associated with high profile plates [97, 101]. High profile plates are commonly used in the mandible and areas defined as load bearing region within the CFS. Other studies have shown that plates removal is common in these areas [93, 97, 99]. Furthermore, there is evidence to suggest that the more extensive dissection and disruption of surrounding soft tissues required to implant higher profile and more fixation hardware, leads to a greater rate of infection and consequent failure[102] . Such findings raise the questions to whether such high profile plates are needed in these regions and whether excessive plating influences problems and complications associated with craniofacial procedures.

Complications of osteosynthesis in which there is a nonunion or malunion usually results from failure to either adequately reduce disparate fracture fragments or not establishing adequate bone-to-bone contact. This can result in excessive motion between the bone segments and cause tissue rupture in the forming callus or/and hardware failure such as screw pullout and loosening of fixation devices [103]. Ensuring that all forces in the area sufficiently neutralized is essential to achieve adequate stabilization and to minimize the motion between the bone fragments. Mobility of the bone fragments can cause numerous problems such as malocclusion and diplopia[104, 105].

The CFS has relatively little soft tissue to provide coverage to hardware from the outer surface. It is therefore not surprising that palpable/ prominent plates and screws are one of the common complications in craniofacial procedures. The sliding of the overlying soft tissue of the face over the hardware can result in erosion, infection and subsequent exposure of the fixation devices. Large size hardware has a larger tendency toward eroding the overlaying tissue [27, 95, 103, 106]. In the study by Orringer *et al.* about removal of rigid internal fixation devices in craniofacial surgery 34.5% of the patients underwent hardware removal for palpable or prominent plates and screws.

Assumptions and theories made about craniofacial loading and strain patterns have led to clinically significant failure of osteosynthetic fixation devices. These fixation devices need to be placed in anatomically correct position to neutralize all forces acting on the fragments to prevent them from dislocation. However, little information is available about the mechanics of the CFS. Moreover, there is current evidence that hardware fixation of facial fractures is being over-engineered [27, 95, 103, 106, 107]. A lot of the evidence is the rate of hardware removal, hardware profile palpability, pain and cold intolerance, which cause significant morbidity and not only require infrequent hardware removal but ads to cost, morbidity, and drains resources. Designing devices and treatments for the CFS without accounting for the actual complexities of the true mechanical environment continues to cause clinical complications and failures. As such, characterizing the biomechanical environment of the CFS is essential for developing materials and techniques that adequately address its structure and need.

1.8 Experimental Stress and Strain Analysis

There are multiple biomechanical parameters that can be used to characterize the integrity of bone. The basic variables that need to be measured to develop an understanding of the biomechanical behaviour of any structure are force and displacement from which many other variables of interest can be derived. When a load is imposed on a structure, the deformation of the structure can be measured and plotted in a load deformation curve. Much information about the mechanical properties of a structure can be gained by examining this curve. A hypothetical load-deformation curve for a bone sample is shown in Figure 1-13. The initial straight portion of the curve is called the elastic region. This region provides information about the structure capacity for returning to its original shape after the load is removed. Deformation within this region is not permanent and the structure recovers to its original shape. The slope of the curve within the elastic region represents the stiffness of the structure. As loading continue the structure reaches a yield point which represents the elastic limit of the structure [108, 109]. When the load exceeds this limit, the structure exhibits plastic behaviour. Within the plastic region the deformation is permanent and the structure cannot recover to its original dimensions when unloaded. Continuous loading will result in failure which indicated by the ultimate failure point on the deformation curve. The ultimate failure point represents the load and deformation the structure can sustain before breaking. The area under the curve is the energy that the structure can store before it breaks.

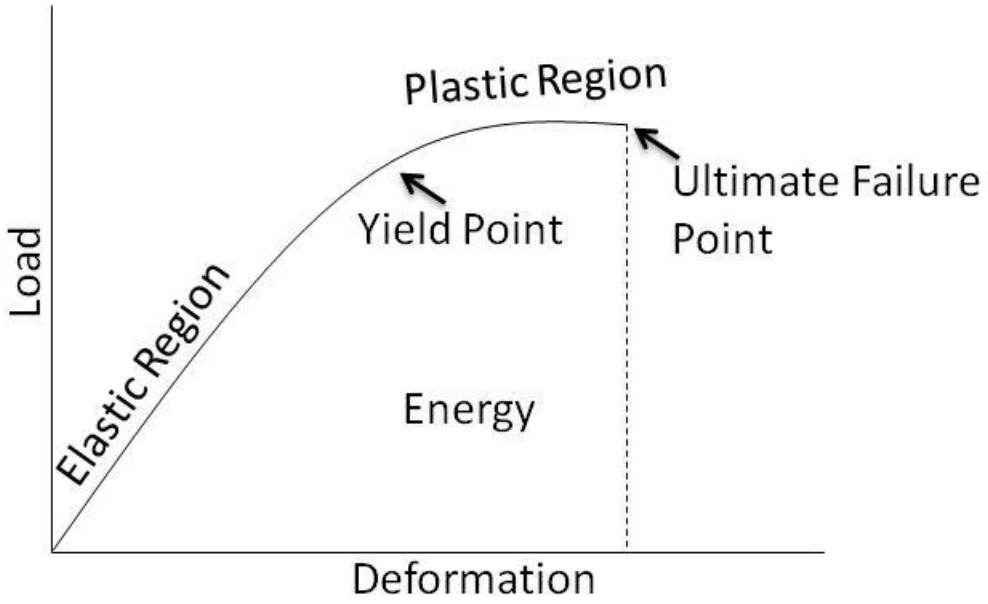

Figure 1-13: Hypothetical load-deformation curve for a bone sample

Characterizing structures in term of their material properties independent of geometry requires standardizations of the size and shape of the test specimens. To remove the geometrical contribution from the measurements, the force applied to the body should be divided by the surface area (i.e. stress) and the deformation should be divided by the original dimensions of the structure (.i.e. strain). This will produce a stress-strain curve from which multiple parameters can be derived such as elastic modulus (slope of elastic region), strain energy (area under the curve), ultimate stress and strain (maximum values). Each of these parameters reflects a different property of bone: elastic modulus is a measure of the intrinsic stiffness of the material and is closely related to mineralization of bone; strain energy is an important measurement of bone fragility and a major index of bone resistance to fracture; ultimate stress and strain reflect the general strength of the bone.

Materials can be divided into two categories (brittle or ductile) based on the degree of yielding exhibited prior to fracture. Ductile material can withstand more deformation under tensile force prior to failure, while brittle material breaks without significant deformation. Biomechanically, bone is regarded as a biphasic composite material, with the mineral as one phase and the collagen as the other. The mineral component is primarily responsible for bone compressive characteristics, whereas the collagen structure determine the tensile behaviour. Generally, bone is

considered brittle material, however, bone exhibits ductile behaviour as it approach the failure point[108-112]

Stress (σ) is a measure of the local intensity of a force in a material and defined as the ratio of the applied force to the structure cross sectional area (unit of stress is N/mm^2). Strain is a measure of the amount of deformation of a body due to applied force. It is a dimensionless unit equaling the change in object length divided by its original length. When a material stretched the strain is positive (tensile strain) and when it is compressed the strain is negative (compressive strain). Strains are classified into two types: Normal and shear strains. Normal strains (ε) refer to the state where change in material dimensions does not change the shape of the object (no change in angles). By contrast, shear strains (γ) cause change in angles but no change in length (Figure 1-14).With respect to the three axes (x,y,z) we have three normal strains (ε_{xx}, ε_{yy}, ε_{zz}) and three shear strains (γ_{xy}, γ_{yz}, γ_{zx}).

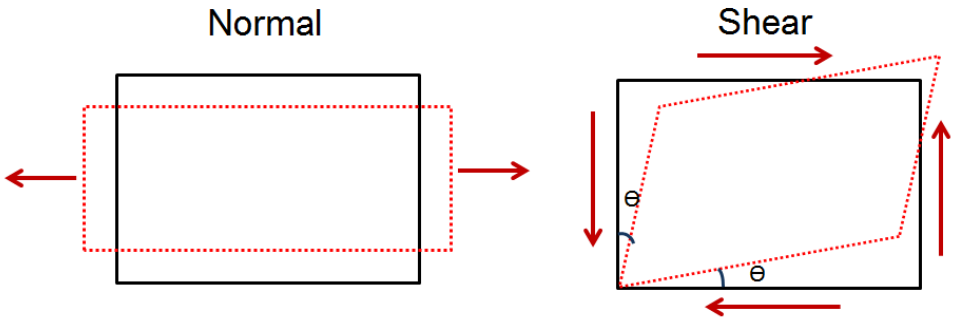

Figure 1-14: Normal and Shear strains

Stress and strain are related by Hooke's Law:

$$Elastic\ modulu\ (E) = \frac{\sigma}{\varepsilon}$$

Similarly the shear strains and shear stresses (τ) are related by the shear modulus (G):

$$Shear\ modulu\ (G) = \frac{\tau}{\gamma}$$

Applying a force to a material results in an extension or contraction in the direction of applied force. However, the transverse direction of the material will undergo the opposite change. For example, when a material is stretched, its cross section area decreases. This behaviour is defined

as Poisson effect or Poisson ratio (ν). Poisson ratio is constant for materials and can be used to relate strains in three directions:

$$\varepsilon_y = \varepsilon_z = -\nu\frac{\varepsilon_x}{\mathrm{E}}$$

Using Hooke's law the normal stresses and strains in all three directions can be defined as:

$$\varepsilon_X = \frac{1}{E}(\sigma_X - \nu(\sigma_Y + \sigma_Z)$$

$$\varepsilon_Y = \frac{1}{E}(\sigma_Y - \nu(\sigma_Z + \sigma_X)$$

$$\varepsilon_Z = \frac{1}{E}(\sigma_Z - \nu(\sigma_X + \sigma_Y)$$

In every material there are planes (principal planes) where the shear strain and stress are zero. The normal stress and strain vectors that are perpendicular to these planes are called principal stresses and strains. The maximum stress or strain is the largest tensile stresses or strains. The minimum principles stress or strains are the largest compressive stresses or strains. The maximum and minimum strains are defined in relation to the angle measured from the orientation of the material at any coordinate axes to its principal axes (Figure 1-15):

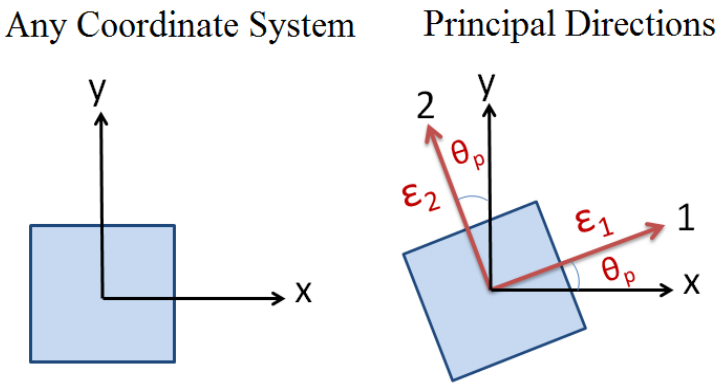

Figure 1-15 : Principal strains and principal angle

$$\varepsilon_{1(max),2(min)} = \frac{\varepsilon_x + \varepsilon_y}{2} \pm \sqrt{(\frac{\varepsilon_x - \varepsilon_y}{2})^2 + {\varepsilon_{xy}}^2}$$

$$tan2\theta_p = \frac{\varepsilon_{xy}}{\varepsilon_x - \varepsilon_y}$$

Where θ_p is the principal angle

The stresses in the three principal planes can be combined to an equivalent stress known as von Mises stress (σ_o). Von Mises stress can be used to determine the failure criterion for ductile materials. If von Mises stress exceeds the yield stress, then the material is considered to be at the failure condition. Since bone behaviour exhibit ductility, von Mises stress can be used as failure criterion for bony structures [112]. The von Mises stress is defined in terms of the principal stresses as follows:

$$\sigma_o = \sqrt{\frac{(\sigma_I - \sigma_I)^2 + (\sigma_{II} - \sigma_{III})^2 + (\sigma_{III} - \sigma_I)^2}{2}}$$

Stress and strain are used to understand how materials behave when subjected to loading. With biological tissues, it should be noted that stress and strain are defined in term of idealized representation of the material as a continuum model. In the case of bone, continuum model refers to considering the bone a perfectly homogenous material by ignoring architectural features or discontinuities in the materials such as vascular channels.

In bone, strain can be measured using strain gauges. Strain gauge is a sensor whose resistance varies with change in applied force. It was first discovered by Lord Kelvin in 1856 by stretching an electrical conductor and observing changes in resistance[113]. The idea of using a sensor to measure strain in structures uses the basic principle that electrically conductive materials posses a strain/resistance relationship. Electrical conductivity refers to the ability of the material to transport electrical charge. The strain/ resistance relationship in such materials is defined as the ratio of relative electrical resistance change of the conductor to the relative change in its length. When these materials are deformed elastically, any dimensional changes will result in change in strain sensitivity.

The resistance of a conductor is defined as:

$$Resistance\ (R) = \frac{Resistivity\ (\rho) \times Length(l)}{Area(A)} - - - - - - - - (1)$$

Strain sensitivity which is also known as Strain Gauge Factor is expressed as:

$$Strain\ Sensitivity(F) = \frac{Change\ in\ reistance(\Delta R) \Big/ Initial\ Resistance(R)}{Change\ in\ length(\Delta l) \Big/ Initial\ Length\ (l)} - - - (2)$$

When a material stretched within its elastic range, for a given change in length there will be an associated reduction in cross sectional area due to Poisson effect. Assuming resistivity is constant and knowing Poisson ratio (ν) was found to be 0.3 for most of resistive materials the sensitivity factor will be:

$$F = 1 + 2\nu\ \approx 2 - - - - - - (3)$$

Materials with a sensitivity factor that is different from 2 in the elastic range are usually highly non-linear making them undesirable for strain gauge construction. Using equations (1) and (2) the strain can be determined if the gauge factor is known and the change in resistance is measured:

$$Strain\ = \frac{(\Delta R) \Big/ (R)}{F} - - - - - (4)$$

Strain gauges are bonded to the structure at the location where the strain is to be determined. Applying force to the structure causes the surface to stretch or contract resulting in the deformation of the strain gauge attached to the surface. In order to register the strain, the strain gauge is connected to an electrical circuit to measure the small changes in the electrical resistance. Strain gauges can be used to measure strain in one direction (unaxial gauge) or three directions (rosette) (Figure 1-16). The rosette strain gauge is primarily made of three unaxials gauges relatively oriented at 30°, 45°, 60°, 90° or 120°. The uniaxial gauge measures strain only

in the direction parallel to its long axes. Measuring strain in three directions using rosette strain gauge allows for calculating the principal strain components at the gauge site.

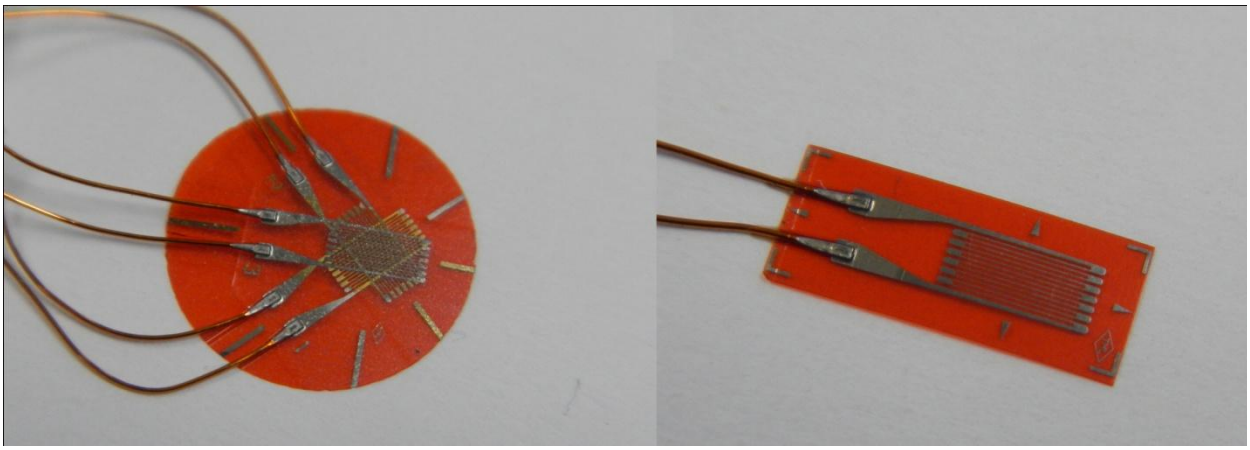

Figure 1-16 : Rosette strain gauge (left) and Uniaxial strain gauge (right)

For the strain gauge in Figure 1-17 the maximum and minimum strains and principle angle can be calculated using the following equation:

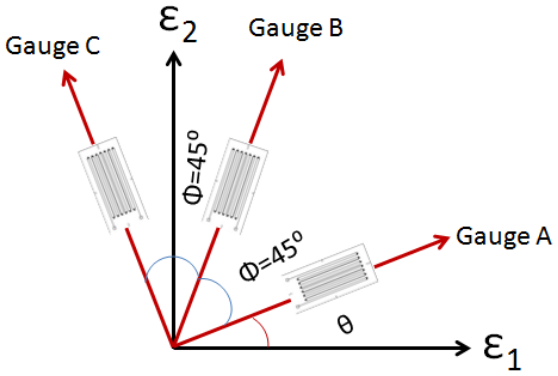

Figure 1-17: Rectangular strain gauge with 45° angle between the strain gauges

$$\varepsilon_{1,2} = \frac{\varepsilon_A + \varepsilon_C}{2} \pm \frac{1}{\sqrt{2}}\sqrt{(\varepsilon_A - \varepsilon_B)^2 + (\varepsilon_B - \varepsilon_C)^2}$$

$$\theta_p = \frac{1}{2} tan^{-1}(\frac{\varepsilon_A - 2\varepsilon_B + \varepsilon_C}{\varepsilon_A - \varepsilon_C})$$

Although strain gauges have been one of the most important experimental tools for understanding loading in bones, errors from the gauge system and its environment can significantly impact the acquired data. The success of the strain gauge measurement technique is highly dependent on the skills of the operator and adherence to recognized practices. Strain gauges are sensitive to forces and any excessive force during application to the bone surface can change the strain gauge factor. Also, since the gauge is attached to the surface using adhesive, insufficient cure or voids can affect strain transmission characteristics. Moreover, harsh and corrosive environment that contain high levels of moisture can weaken the bond between the gauge and surface. Several adhesives and coating materials have been developed to enhance the usability of strain gauges for bone and minimize complications.

1.9 Finite Element Modeling

The finite element method (FEM) is a numerical technique that gives apporixmate solutions for complex problems such as those found in structural mechanics and heat conductions. In principle, the FEM consist of replacing complicated differntial equations for irregular shapes with an extensive system of algebraic equations that represent small geomteric entities that can be solved by a computer. The technique name is derived from the process of dividing the structure into an assembly of elements. These elements are connected to each other with nodes to create an interconnected mesh. The process of dividing the structure into finite number of subregions is called discretization which primairly allows for replacing the complex continum with an infinite number of degrees of freedom by a discrete system with a finite number of degrees of freedom. Over each element, the unknown variables (e.g. temperature or displacement) are approximated using linear or high-order polynomial equations in terms of the geometrical location of the nodes [114, 115].

A knowledge of the material properties and loading conditions is required in structural mechanics problems that aim at finding solutions for stress and strain . Each material has a unique elastic modulues and Poisson ratio that can be assigned to structure elements. Loading forces and mechanical constraints (i.e. regions of immobility) experienced by the structure in real life are refered to as boundary conditions in FE. These boundary conditions are assigned to the

structure to mimic loading expirenced by the structure in real applications. In the discretized structure the material properties of the elements and the loading criteria are assembled into an overall system matrix and load vector. The system matrix is then solved by evaluating the unknown nodal displacements. From displacement many outcomes can be calculated such as strain, stress, principal stress and bending moments. The following example (Figure 1-18) illustrates the use of finite element method:

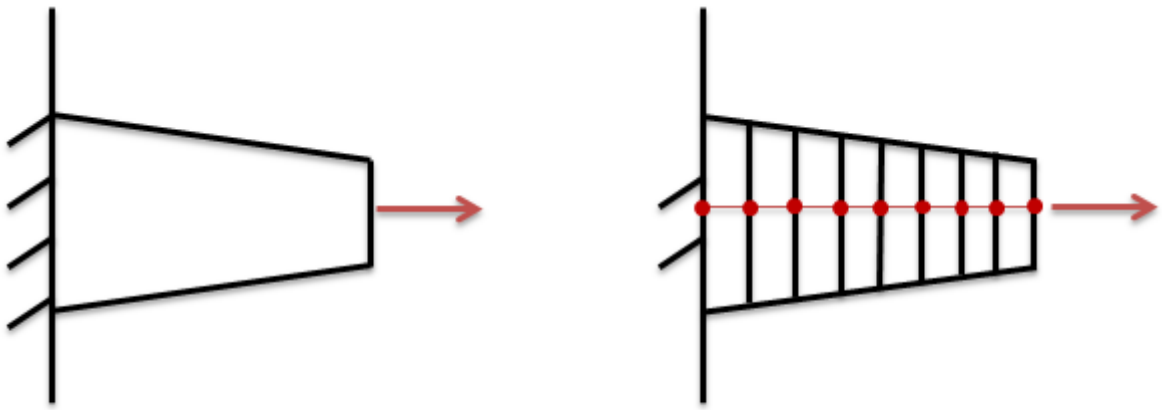

Figure 1-18: Tapered beam represented using the finite element method

A finite element model of the beam can be created by dividing it into 8 smaller sections with 9 nodes. The width of each section is constant across the model but the cross sectional area changes based on the location of the section. By discretizing the structure into elements, it is easier to approximate the changing area of the tapered beam.

The FEM has been widely used to analyze the mechanical behaviour of bone both at the continuum level and at the microstructural level[44, 116-120]. FE modelling of bony structures has been a very useful tool for developing a better understanding of the biomechanics enviroment of the human skeleton. It has the potential for providing a complete characterization of the stress and strain patterns in bony structures under physiological or non-physiological loadings. Validation of FE analysis with experimental data (*in vitro* or *in vivo*) is essential to ensure robust findings. Utilization of the very limited resource of cadaveric specimens for FE model validation, allows investigation of many more questions using the developed model than would be possible based on experimental testing alone. The FE method represents an efficient tool for

predicting the outcome of multiple loading scenarios and for analyzing complex geometry, which occurs *in vivo,* and which normally is difficult to represent with other experimental techniques [121].

To date, several studies have shown that FE models of bony structures can be used reliably to predict failure loads and fracture patterns in the pelvis, femur and scapula[119-123]. FE modeling has been used previously to examine head impact and injury, craniofacial distraction, expansion and growth, and stresses around implants[124-127]. Early attempts to model the CFS were limited by the resolution of the imaging techniques, capabilities of computational technologies and insufficient experimental validation [128]. More recent attempts to model the CFS lack experimentally derived material properties, sensitivity analyses, or validation attempts have been based on single specimen models [129, 130].

1.10 Imaging

1.10.1 Computed Tomography

Computed tomography (CT) is a non-destructive evaluation technique that uses x-ray images to produce 3D volume of an object. A CT system consists of radiation unit which emits x-ray beam to an object placed between the energy source and a data acquisition system. The x-ray unit consists of a tube with variable focal spot sizes. Modern CT scanners have power rating of 20-60KW at voltage of 80-120KV. The data acquisition system consists of a detector which converts the incident x-ray to of varying intensity to electric signals. In conventional CT scanner the patient placed on a table and the tube-detector system rotates 360° around while the patient table moving perpendicular to the rotation plane. In its basic principal the CT images are shadow images generated from the x-ray attenuations. When the x-ray beam passes through the patient each material attenuates the beam differently. At each angle the object is scanned and a new shadow image produced until the object scanned for a 360° rotation. The 2D shadow images are processed and stacked together using computer software based on the orientation of the sample to create 3D volume. Each 2D image consists of small units called pixels. These pixels have varying gray values with brighter pixels representing high attenuations [131-133].

For more than three decades CT has been widely used for diagnostic and quantitative assessment of bone in patients [133]. Improvement of the CT resolution and computational power recently has led to the utilization of CT images in the development of 3D FE models in predicting failure and

fracture patterns for bone structures. CT scan images can be used to provide information about the geometry and morphology of the structure under investigation, as well as its material properties[134]. Structure specific FE models of the CFS can be generated through CT imaging via direct conversion into FE meshes. However, developing such models is limited by geometric complexity and imaging techniques as the accuracy of FE models largely depends on accurate representation of specimen geometry and material properties.

1.10.2 Micro-Computed Tomography

Micro-computed tomography (μCT) scanners employ micro-focus x-ray beam to visualize objects at the microstructural level. The basic working principle and system for μCT and CT are very similar. However, the use of a smaller focal spot allows for higher energy beams and higher image resolution. μCT systems were primarily used for bone imaging studies due to the high contrast between calcified and soft tissues, but they have also been used for soft-tissue imaging. Advances made in μCT imaging systems allow for generating scans with 1 μm resolution for *in vivo* and *in vitro* studies. One major limitation with μCT imaging is the size of the specimen. Any specimens with diameters bigger than 2 cm are hard to image at high resolution [135].

1.11 Motivation

This work was motivated by the findings of Szwedowski *et al.* in the study characterizing the biomechanical behaviour of the CFS using validated FE model. In the Szwedowski *et al*. study a subject-specific finite element model of fresh frozen human CFS was developed successfully and validated against strain measurements from *in vitro* mechanical testing. The model incorporated position dependent cortical bone thickness and trabecular bone materials properties based on CT scan image intensity. Cortical strains were measured from the *in vitro* model under mechanical loading through the masseter and temporalis muscles. The developed FE model was found to have a correlation of 0.73 against experimentally measured *in vitro* strains. Disparities between the calculated and measured strains were found to be greater in thin and complex bone regions (i.e. sinuses). The FE models also exhibited high sensitivity to changes in the material properties and cortical thickness. The model was found to be very sensitive to the assignment of the cortical bone modulus with sensitivites of 0.869 and 0.544 for models with a cortical elastic modulus of 10 GPa and 17 GPa, repectively[116]. Assigning local specimen specific cortical thickness based on

measurment from the CT scan provided the best correlation with *in vitro* mechanical testing data. However, cortical thickness measurment from CT images were found to be limited in very thin structures. This is because the cortical thickness in the CFS is smaller than the resolution of diagnostic CT imaging system.

The FE model developed by Szwedowski *et al.* did not incorporate bony articulations in the CFS which was shown to impact the global stress and strain patterns in animal FE models[72, 136]. The strain gauge placed near the zygomaticotemporal suture in the CFS exhibited low correlation between the FE results and mechanical testing in Szwedowski *et al.* study. This may be attributed to the in accurate representation of the CFS morphology by not including the sutures. The results from Szwedowski *et al.* study showed that the developed model was very sensitive to assumptions regarding the geometry, material properties and cortical thickness and that assigning patient spesific parameters yields a better correlation between FE models and testing data. As such, there is a need to focus on investigating how these parameters impact the models to allow for better correlations between FE models and mechanical testing, before such models can be utilized to better understand craniofacial biomechanics.

1.12 Clinical Need

The irregular shape and thickness of the bones, the presence of multiple articulations, and the variable muscles loads in the CFS create a complex structure with a unique mechanical environment and fracture patterns. However, most existing technologies and treatments in the field of craniomaxillofacial surgery (specifically methods of osteosynthesis) do not account for these structural properties. As such, many of these technologies and techniques have inherent weaknesses and clinical failure continue to occur. Complications in osteosynthesis results in the development of variable cosmetic or functional deformities and often require subsequent re-operation for correction of these problems. These complications and corrective surgeries can negatively impact the quality of life of a patient as well as placing additional strain on medical systems through added costs for surgery, care and rehabilitation.

FE models have shown a great deal of success in predicting the mechanical environment of bony structures, such as long bones and the pelvis[119, 120]. The FE method possesses the potential to develop models which can be used to better understand the mechanics of osteosynthesis based on individual morphology and aid in surgical planning. It also can provide an insight to the

biomechanical behaviour of the natural and restored CFS which is important in defining the mechanical requirements for the repair and reconstruction of thin bone structures. Developing validate FE models will provide the platform to investigate both the healthy and deformed CFS under complex loading.

1.13 Thesis Objectives

The broad objective of this research is to investigate the biomechanical behaviour of thin bone structures in the human CFS by characterizing its strains pattern through the development and analysis of µFE models and mechanical testing. Understanding how large voxel size in clinical CT images impact the bone geometry and material properties used in generating FE models and ultimately their biomechanical behaviour will aid in determining the approches to correct for such inaccuracies. Similarly, investigating the morphology of sutures in the CFS and how they impact load transmission locally can be used to imrpove full head FE models to acheive better correlation with mechanical testing studies. However, information collected from µFE models of thin bone structures and sutures will only reflect the mechanical behaviour locally within the skull. Therfore, mechanical testing on multi-specimens will be conducted to gain an understanding of the strain patterns in presence of different morphologies.

It is hypothesized that high resolution imaging and multi-specimen mechanical testing is required to accurately understand the behaviour of thin bone structures and articulations in the CFS. Once microstructural understanding is developed it can be applied to yield robust models generated from clinical resolution CT imaging. Such models will be used to characterize the global biomechanical behaviour of the CFS.

1.13.1 Specific Aims

1. Compare the accuracy of FE models of thin bone structures within the CFS based on CT and micro-CT data, evaluating the impact of voxel size on geometry and material properties and the effect of these parameters on biomechanical behaviour.
2. Develop a new automated method for quantifying the 3D connectivity of the craniofacial sutures.
3. Characterize the strain patterns in the cranial and craniofacial sutures using FEM.

4. Quantify the bending strength of CFS bone samples containing sutures and samples without suture using three-point bending test.
5. Characterize the strain patterns in the CFS under simple single muscle loading using mechanical testing.

1.13.2 Thesis Outline

This thesis will provide information about the biomechanical behaviour of thin bone structure in the CFS. A combination of mechanical testing, finite element modeling and image processing techniques were used to investigate the bone structure and biomechanical behaviour. The present work is comprised of five studies, which have been published or submitted to peer-reviewed journals.

Chapter 2 investigates the impact of CT and µCT voxel size on the thickness and intensity values of thin bone structures and cortical thickness measurements. The impact of these parameters on strain patterns in thin bone structures through 3D FE modeling were assessed in five thin bone specimens. Each sample scan was downsampled to voxel sizes of 82, 164, 328, and 488 µm and used to generate FE models. The minimum bone thickness, average intensity and maximum principal strain were quantified at each voxel size. This study has been published in the Annals of Biomedical Engineering Journal and co-authored by Dr.Cari Whyne and Dr. Jeffrey Fialkov.

Chapter 3 presents a new technique for quantifying the connectivity of bony projections inside cranial and facial sutures using a combination of skeletonization, thinning algorithms and 3D intensity mapping. The technique was demonstrated in the zygomaticotemporal, zygomaticomaxillary, frontozygomatic, sagittal and coronal sutures through semi-automated analysis and image processing of µCT scans. This study has been published in the Journal of Biomechanics and co-authored by Dr.Cari Whyne, Dr. Jeffrey Fialkov and Dr.Parsa Hojjat.

Chapter 4 investigates how morphological features (number of interdigitations and bony connectivity), direction of loading (parallel, perpendicular and pressure loading), suture material properties (isotropic or transversely isotropic) influence the mechanical behaviour of the suture and surrounding bone using FEM. A total of 37 FE models were developed to evaluate the impact of these parameters on the mechanical behaviour of the bone/suture complex. This study

will be submitted to Journal of Biomechanics and co-authored by Dr. Cari Whyne, Dr. Jeffrey Fialkov and Dr. Diane Wagner.

Chapter 5 investigates the bending strength of suture/bone samples excised from fresh frozen cadaveric heads. The zygomaticotemporal, frontozygomatic, sagittal and coronal sutures from six cadaver heads were tested in three-point bending to failure. The bending strength and number of interdigitations in the suture were quantified for each sample. The correlation between bending strength and number of interdigitations was evaluated using linear regression analysis. This study will be submitted to Journal of Biomechanics and co-authored by Dr. Cari Whyne and Dr. Jeffrey Fialkov.

Chapter 6 investigates the biomechanical behaviour of the midfacial region of the human CFS under muscle loading. Five fresh frozen human cadaveric heads were loaded through either the masseter muscle or the temporalis muscle. The strain magnitude was measured using 8 strain gauges, which were bonded to the bony surface of the midfacial region. The strain magnitude and direction at the different location was used to understand the impact of muscle loading on midfacial mechanics. This study has been submitted to the Journal of Craniofacial Surgery and co-authored by Dr. Eran Regev, Dr. Marteen Beek, Dr. Cari Whyne and Dr. Jeffrey Fialkov.

Finally, chapter 7 presents a general discussion of the main findings in the 5 investigations and considers their strengths and limitations. It also includes future directions and the significance of the current work.

1.14 References

1. Moore KL, Agur AMR, Moore KL, et al. *Essential Clinical Anatomy.* 2nd ed. Philadelphia: Lippincott Williams & Wilkins, 2002.

2. Hall BK, Hanken J. *The Skull.* Chicago: University of Chicago Press, 1993.

3. Dixon AD, Hoyte DAN, Rönning O. *Fundamentals of Craniofacial Growth.* Boca Raton: CRC Press, 1997.

4. Lenton KA, Nacamuli RP, Wan DC, et al. Cranial suture biology. *Curr Top Dev Biol.* 2005;66:287-328.

5. Slater BJ, Lenton KA, Kwan MD, et al. Cranial sutures: A brief review. *Plast Reconstr Surg.* 2008;121:170e-8e.

6. Mao JJ, Wang X, Kopher RA. Biomechanics of craniofacial sutures: Orthopedic implications. *Angle Orthod.* 2003;73:128-135.

7. Buckland-Wright JC. Bone structure and the patterns of force transmission in the cat skull (felis catus). *J Morphol.* 1978;155:35-61.

8. Jaslow CR. Mechanical properties of cranial sutures. *J Biomech.* 1990;23:313-321.

9. Jaslow CR, Biewener AA. Strain patterns in the horncores, cranial bones and sutures of goats (capra hircus) during impact loading. *J Zool.* 1995;235:193-210. Available from: http://dx.doi.org/10.1111/j.1469-7998.1995.tb05137.x.

10. Herring SW, Teng S. Strain in the braincase and its sutures during function. *Am J Phys Anthropol.* 2000;112:575-593.

11. Byron CD, Borke J, Yu J, et al. Effects of increased muscle mass on mouse sagittal suture morphology and mechanics. *Anat Rec A Discov Mol Cell Evol Biol.* 2004;279:676-684.

12. Rayfield EJ. Cranial mechanics and feeding in tyrannosaurus rex. *Proc Biol Sci.* 2004;271:1451-1459.

13. Rayfield EJ. Using finite-element analysis to investigate suture morphology: A case study using large carnivorous dinosaurs. *Anat Rec A Discov Mol Cell Evol Biol.* 2005;283:349-365.

14. PRITCHARD JJ, SCOTT JH, GIRGIS FG. The structure and development of cranial and facial sutures. *J Anat.* 1956;90:73-86.

15. Rafferty KL, Herring SW, Marshall CD. Biomechanics of the rostrum and the role of facial sutures. *J Morphol.* 2003;257:33-44.

16. Enlow DH. *Facial Growth.* 3rd -- ed. Philadelphia: Saunders, 1990.

17. Israel H. Continuing growth in the human cranial skeleton. *Arch Oral Biol.* 1968;13:133-137.

18. Israel H. Continuing growth in sella turcica with age. *Am J Roentgenol Radium Ther Nucl Med.* 1970;108:516-527.

19. Israel H. The dichotomous pattern of craniofacial expansion during aging. *Am J Phys Anthropol.* 1977;47:47-51.

20. Nordin M, Frankel VH. *Basic Biomechanics of the Musculoskeletal System.* 3rd ed. Philadelphia: Lippincott Williams & Wilkins, 2001.

21. Rogers SL. *The Human Skull: Its Mechanics, Measurements, and Variations.* Springfield, Ill.: Thomas, 1984.

22. Nahum AM. The biomechanics of maxillofacial trauma. *Clin Plast Surg.* 1975;2:59-64.

23. Banks P, Brown A. *Fractures of the Facial Skeleton.* Oxford ; Boston: Wright, 2001.

24. Hardt N, Kuttenberger J, ebrary I. Craniofacial trauma. 2010:278. Available from: http://link.library.utoronto.ca/eir/EIRdetail.cfm?Resources__ID=1157113&T=F.

25. Bilezikian JP, Raisz LG, Martin TJ. Principles of bone biology. 2008:1900. Available from: http://myaccess.library.utoronto.ca/login?url=http://www.sciencedirect.com/science/book/9780123738844.

26. Khurana JS, ebrary I. Bone pathology. 2009:416. Available from: http://link.library.utoronto.ca/eir/EIRdetail.cfm?Resources__ID=976701&T=F.

27. Prein J, Arbeitsgemeinschaft für Osteosynthesefragen. *Manual of Internal Fixation in the Cranio-Facial Skeleton: Techniques Recommended by the AOASIF-Maxillofacial Group.* Berlin ; New York: Springer, 1998.

28. Weiner S, Traub W, Wagner HD. Lamellar bone: Structure-function relations. *J Struct Biol.* 1999;126:241-255.

29. Carter DR, Spengler DM. Mechanical properties and composition of cortical bone. *Clin Orthop Relat Res.* 1978;(135):192-217.

30. Guo X. Mechanical properties of cortical bone and cancellous bone tissue. In: Cowin SC, ed. *Bone Mechanics Handbook.* 2nd ed. Boca Raton: CRC Press, 2001:1-23.

31. Reilly DT, Burstein AH. Review article. the mechanical properties of cortical bone. *J Bone Joint Surg Am.* 1974;56:1001-1022.

32. Reilly DT, Burstein AH, Frankel VH. The elastic modulus for bone. *J Biomech.* 1974;7:271-275.

33. Mow VC, Huiskes R. Basic orthopaedic biomechanics & mechano-biology. 2005. Available from:

http://myaccess.library.utoronto.ca/login?url=http://ovidsp.ovid.com/ovidweb.cgi?T=JS&NEWS=n&CSC=Y&PAGE=booktext&D=books&AN=01382443.

34. An YH, Draughn RA. *Mechanical Testing of Bone and the Bone-Implant Interface.* Boca Raton: CRC Press, 2000.

35. Peterson J, Wang Q, Dechow PC. Material properties of the dentate maxilla. *Anat Rec A Discov Mol Cell Evol Biol.* 2006;288:962-972.

36. Peterson J, Dechow PC. Material properties of the human cranial vault and zygoma. *Anat Rec A Discov Mol Cell Evol Biol.* 2003;274:785-797.

37. Schwartz-Dabney CL, Dechow PC. Variations in cortical material properties throughout the human dentate mandible. *Am J Phys Anthropol.* 2003;120:252-277.

38. Dechow PC, Nail GA, Schwartz-Dabney CL, et al. Elastic properties of human supraorbital and mandibular bone. *Am J Phys Anthropol.* 1993;90:291-306.

39. Bock WJ, Kummer B. The avian mandible as a structural girder. *J Biomech.* 1968;1:89-96.

40. Thomason JJ, Russell AP. Mechanical factors in the evolution of the mammalian secondary palate: A theoretical analysis. *J Morphol.* 1986;189:199-213.

41. Tucker R. Studies in functional and analytical craniology .3. the breviarcuate skull and its analysis. *Aust J Zool.* 1954;2:399-&.

42. Tucker R. Studies in functional and analytical craniology .6. strains and the direction of certain vectors in the breviarcuate skull. *Aust J Zool.* 1954;2:427-&.

43. Curtis N. Craniofacial biomechanics: An overview of recent multibody modelling studies. *J Anat.* 2011;218:16-25.

44. Szwedowski TD, Whyne CM, Fialkov JA. Toward characterization of craniofacial biomechanics. *J Craniofac Surg.* 2010;21:202-207.

45. Wang Q, Wright BW, Smith A, et al. Mechanical impact of incisor loading on the primate midfacial skeleton and its relevance to human evolution. *Anat Rec (Hoboken).* 2010;293:607-617.

46. Provatidis C, Georgiopoulos B, Kotinas A, et al. In vitro validated finite element method model for a human skull and related craniofacial effects during rapid maxillary expansion. *Proc Inst Mech Eng H.* 2006;220:897-907.

47. Demes B. Biomechanics of the primate skull base. *Adv Anat Embryol Cell Biol.* 1985;94:1-59.

48. Ross CF, Berthaume MA, Dechow PC, et al. In vivo bone strain and finite-element modeling of the craniofacial haft in catarrhine primates. *J Anat.* 2011;218:112-141.

49. Barry CP, Ryan WJ, Stassen LF. Anatomical study of factors contributing to zygomatic complex fracture instability in human cadavers. *Plast Reconstr Surg.* 2007;120:1743; author reply 1743.

50. Kasrai L, Hearn T, Gur E, et al. A biomechanical analysis of the orbitozygomatic complex in human cadavers: Examination of load sharing and failure patterns following fixation with titanium and bioresorbable plating systems. *J Craniofac Surg.* 1999;10:237-243.

51. Hylander WL, Johnson KR. In vivo bone strain patterns in the zygomatic arch of macaques and the significance of these patterns for functional interpretations of craniofacial form. *Am J Phys Anthropol.* 1997;102:203-232.

52. Herring SW, Teng S, Huang X, et al. Patterns of bone strain in the zygomatic arch. *Anat Rec.* 1996;246:446-457.

53. Ross CF, Hylander WL. In vivo and in vitro bone strain in the owl monkey circumorbital region and the function of the postorbital septum. *Am J Phys Anthropol.* 1996;101:183-215.

54. Tucker R. Studies in functional and analytical craniology .1. the elements of analysis. *Aust J Zool.* 1954;2:381-390.

55. Tucker R. Studies in functional and analytical craniology .2. the functional classification of mammalian skulls. *Aust J Zool.* 1954;2:391-&.

56. Tucker R. Studies in functional and analytical craniology .4. more extreme forms of the breviarcuate skull. *Aust J Zool.* 1954;2:412-&.

57. Endo B. Experimental studies on the mechanical significance of the form of the human facial skeleton. *J Fac Sci Univ Tokyo.* 1966;3:1-106.

58. Endo B. Distribution of stress and strain produced in the human facial skeleton by the masticatory force *J Anthrop Soc Nippon.* 1965;73:123-136.

59. WOLFF J. A theoretical approach to solve the chin problem. *FOOD ACQUISITION PRO.* 1984:391-405.

60. Bilsborough A, Chivers DJ, Wood BA, et al. *Food Acquisition and Processing in Primates.* New York: Plenum Press, 1984.

61. Greaves WS. The mammalian postorbital bar as a torsion-resisting helical strut. *J Zool.* 1985;207:125-136.

62. Oyen OJ, Tsay TP. A biomechanical analysis of craniofacial form and bite force. *Am J Orthod Dentofacial Orthop.* 1991;99:298-309.

63. Oyen OJ, Melugin MB, Indresano AT. Strain gauge analysis of the frontozygomatic region of the zygomatic complex. *J Oral Maxillofac Surg.* 1996;54:1092-5; discussion 1095-6.

64. Hylander WL, Picq PG, Johnson KR. Masticatory-stress hypotheses and the supraorbital region of primates. *Am J Phys Anthropol.* 1991;86:1-36.

65. Ravosa MJ, Johnson KR, Hylander WL. Strain in the galago facial skull. *J Morphol.* 2000;245:51-66.

66. Ross CF, Metzger KA. Bone strain gradients and optimization in vertebrate skulls. *Ann Anat.* 2004;186:387-396.

67. Ross CF. In vivo function of the craniofacial haft: The interorbital "pillar". *Am J Phys Anthropol.* 2001;116:108-139.

68. Szwedowski TD, Fialkov F, Whyne C. Sensitivity analysis of a validated subject-specific finite element model of the human craniofacial skeleton . *Proceedings of the Institution of Mechanical Engineers Part H, Journal of engineering in medicine.* 2010;224:1-10.

69. Strait DS, Wang Q, Dechow PC, et al. Modeling elastic properties in finite-element analysis: How much precision is needed to produce an accurate model? *Anat Rec A Discov Mol Cell Evol Biol.* 2005;283:275-287.

70. Strait DS, Wang Q, Dechow PC, et al. Modeling elastic properties in finite-element analysis: How much precision is needed to produce an accurate model? *Anat Rec A Discov Mol Cell Evol Biol.* 2005;283:275-287.

71. Strait DS, Weber GW, Neubauer S, et al. The feeding biomechanics and dietary ecology of australopithecus africanus. *Proc Natl Acad Sci U S A.* 2009;106:2124-2129.

72. Wang Q, Smith AL, Strait DS, et al. The global impact of sutures assessed in a finite element model of a macaque cranium. *Anat Rec (Hoboken).* 2010;293:1477-1491.

73. Chalk J, Richmond BG, Ross CF, et al. A finite element analysis of masticatory stress hypotheses. *Am J Phys Anthropol.* 2011;145:1-10.

74. Ross CF, Patel BA, Slice DE, et al. Modeling masticatory muscle force in finite element analysis: Sensitivity analysis using principal coordinates analysis. *Anat Rec A Discov Mol Cell Evol Biol.* 2005;283:288-299.

75. Hylander WL, Johnson KR, Crompton AW. Loading patterns and jaw movements during mastication in macaca fascicularis: A bone-strain, electromyographic, and cineradiographic analysis. *Am J Phys Anthropol.* 1987;72:287-314.

76. Mongini F, Preti G, Calderale PM, et al. Experimental strain analysis on the mandibular condyle under various conditions. *Med Biol Eng Comput.* 1981;19:521-523.

77. Hylander WL. Stress and strain in the mandibular symphysis of primates: A test of competing hypotheses. *Am J Phys Anthropol.* 1984;64:1-46.

78. Tanaka E, Tanne K, Sakuda M. A three-dimensional finite element model of the mandible including the TMJ and its application to stress analysis in the TMJ during clenching. *Med Eng Phys.* 1994;16:316-322.

79. Thaller SR, Garri JI, Bradley JP. Craniofacial surgery. 2008:395. Available from: http://myaccess.library.utoronto.ca/login?url=http://site.ebrary.com/lib/utoronto/Top?id=10209842.

80. Jaslow CR. Mechanical properties of cranial sutures. *J Biomech.* 1990;23:313-321.

81. Rudderman RH, Mullen RL. Biomechanics of the facial skeleton. *Clin Plast Surg.* 1992;19:11-29.

82. Greenberg AM, Prein J. *Craniomaxillofacial Reconstructive and Corrective Bone Surgery: Principles of Internal Fixation using AOASIF Technique.* New York: Springer, 2002.

83. Wolfe SA, Baker S. *Facial Fractures.* New York; New York: Thieme Medical Publishers ;$aStuttgart; Georg Thieme Verlag, 1993.

84. Terry BC, Härle F, Härle F, et al. *Atlas of Craniomaxillofacial Osteosynthesis: Microplates, Miniplates, and Screws.* 2nd ed. Stuttgart ; New York: Thieme, 2009.

85. van Eijden TM. Three-dimensional analyses of human bite-force magnitude and moment. *Arch Oral Biol.* 1991;36:535-539.

86. Smeets R, Marx R, Kolk A, et al. In vitro study of adhesive polymethylmethacrylate bone cement bonding to cortical bone in maxillofacial surgery. *J Oral Maxillofac Surg.* 2010;68:3028-3033.

87. Bos RR, Boering G, Rozema FR, et al. Resorbable poly(L-lactide) plates and screws for the fixation of zygomatic fractures. *J Oral Maxillofac Surg.* 1987;45:751-753.

88. Bergsma EJ, Rozema FR, Bos RR, et al. Foreign body reactions to resorbable poly(L-lactide) bone plates and screws used for the fixation of unstable zygomatic fractures. *J Oral Maxillofac Surg.* 1993;51:666-670.

89. Endres K, Marx R, Tinschert J, et al. A new adhesive technique for internal fixation in midfacial surgery. *Biomed Eng Online.* 2008;7:16.

90. Cutright DE, Hunsuck EE, Beasley JD. Fracture reduction using a biodegradable material, polylactic acid. *J Oral Surg.* 1971;29:393-397.

91. Donkerwolcke M, Burny F, Muster D. Tissues and bone adhesives--historical aspects. *Biomaterials.* 1998;19:1461-1466.

92. Heiss C, Hahn N, Wenisch S, et al. The tissue response to an alkylene bis(dilactoyl)-methacrylate bone adhesive. *Biomaterials.* 2005;26:1389-1396.

93. Bakathir AA, Margasahayam MV, Al-Ismaily MI. Removal of bone plates in patients with maxillofacial trauma: A retrospective study. *Oral Surg Oral Med Oral Pathol Oral Radiol Endod.* 2008;105:e32-7.

94. Rauso R, Tartaro G, Stea S, et al. Plates removal in orthognathic surgery and facial fractures: When and why. *J Craniofac Surg.* 2011;22:252-254.

95. Goodrich JT. Craniofacial surgery: Complications and their prevention. *Semin Pediatr Neurol.* 2004;11:288-300.

96. Jack JM, Stewart DH, Rinker BD, et al. Modern surgical treatment of complex facial fractures: A 6-year review. *J Craniofac Surg.* 2005;16:726-731.

97. Bhatt V, Chhabra P, Dover MS. Removal of miniplates in maxillofacial surgery: A follow-up study. *J Oral Maxillofac Surg.* 2005;63:756-760.

98. Perry M. Maxillofacial trauma--developments, innovations and controversies. *Injury.* 2009;40:1252-1259.

99. Francel TJ, Birely BC, Ringelman PR, et al. The fate of plates and screws after facial fracture reconstruction. *Plast Reconstr Surg.* 1992;90:568-573.

100. Fialkov JA, Holy C, Forrest CR, et al. Postoperative infections in craniofacial reconstructive procedures. *J Craniofac Surg.* 2001;12:362-368.

101. Thoren H, Snall J, Kormi E, et al. Symptomatic plate removal after treatment of facial fractures. *J Craniomaxillofac Surg.* 2010;38:505-510.

102. Regev E, Shiff JS, Kiss A, et al. Internal fixation of mandibular angle fractures: A meta-analysis. *Plast Reconstr Surg.* 2010;125:1753-1760.

103. Orringer JS, Barcelona V, Buchman SR. Reasons for removal of rigid internal fixation devices in craniofacial surgery. *J Craniofac Surg.* 1998;9:40-44.

104. Murthy AS, Lehman JA,Jr. Symptomatic plate removal in maxillofacial trauma: A review of 76 cases. *Ann Plast Surg.* 2005;55:603-607.

105. Girotto JA, MacKenzie E, Fowler C, et al. Long-term physical impairment and functional outcomes after complex facial fractures. *Plast Reconstr Surg.* 2001;108:312-327.

106. Jack JM, Stewart DH, Rinker BD, et al. Modern surgical treatment of complex facial fractures: A 6-year review. *J Craniofac Surg.* 2005;16:726-731.

107. Regev E, Shiff JS, Kiss A, et al. Internal fixation of mandibular angle fractures: A meta-analysis. *Plast Reconstr Surg.* 2010;125:1753-1760.

108. Nigg BM, Herzog W. *Biomechanics of the Musculo-Skeletal System.* 3rd ed. Chichester, West Sussex, England ; Hoboken NJ: John Wiley & Sons, 2007.

109. Dvir Z. *Clinical Biomechanics.* New York: Churchill Livingstone, 2000.

110. Mow VC, Huiskes R. Basic orthopaedic biomechanics & mechano-biology. 2005. Available from: http://myaccess.library.utoronto.ca/login?url=http://ovidsp.ovid.com/ovidweb.cgi?T=JS&NEWS=n&CSC=Y&PAGE=booktext&D=books&AN=01382443.

111. Hattori T, Niwa S, Perren SM, et al. *Biomechanics in Orthopedics.* Tokyo ; New York: Springer-Verlag, 1992.

112. Nalla RK, Kinney JH, Ritchie RO. Mechanistic fracture criteria for the failure of human cortical bone. *Nat Mater.* 2003;2:164-168.

113. Window AL. *Strain Gauge Technology.* 2nd ed. London ; New York: Elsevier Applied Science, 1992.

114. Ottosen NS, Petersson H. *Introduction to the Finite Element Method.* New York: Prentice Hall, 1992.

115. Szabo BA, Babuška I. Introduction to finite element analysis. 2011:364. Available from: http://myaccess.library.utoronto.ca/login?url=http://onlinelibrary.wiley.com/book/10.1002/9781119993834.

116. Szwedowski TD, Fialkov F, & Whyne C. Sensitivity analysis of a validated subject-specific finite element model of the human craniofacial skeleton. *Proc Inst Mech Eng [H]*. 2010.

117. Jasinoski SC, Reddy BD, Louw KK, et al. Mechanics of cranial sutures using the finite element method. *J Biomech.* 2010;43:3104-3111.

118. Hardisty MR. *Strain Measurement in Vertebral Bodies by Image Registration.* , 2006.

119. Ramos A, Simoes JA. Tetrahedral versus hexahedral finite elements in numerical modelling of the proximal femur. *Med Eng Phys.* 2006;28:916-924.

120. Anderson AE, Peters CL, Tuttle BD, et al. Subject-specific finite element model of the pelvis: Development, validation and sensitivity studies. *J Biomech Eng.* 2005;127:364-373.

121. Lotz JC, Cheal EJ, Hayes WC. Fracture prediction for the proximal femur using finite element models: Part I--linear analysis. *J Biomech Eng.* 1991;113:353-360.

122. Anderson AE, Peters CL, Tuttle BD, et al. Subject-specific finite element model of the pelvis: Development, validation and sensitivity studies. *J Biomech Eng.* 2005;127:364-373.

123. Gupta S, van der Helm FC, Sterk JC, et al. Development and experimental validation of a three-dimensional finite element model of the human scapula. *Proc Inst Mech Eng [H]*. 2004;218:127-142.

124. Akca K, Cehreli MC, Iplikcioglu H. A comparison of three-dimensional finite element stress analysis with in vitro strain gauge measurements on dental implants. *Int J Prosthodont.* 2002;15:115-121.

125. Cattaneo PM, Dalstra M, Frich LH. A three-dimensional finite element model from computed tomography data: A semi-automated method. *Proc Inst Mech Eng [H]*. 2001;215:203-213.

126. Iseri H, Tekkaya AE, Oztan O, et al. Biomechanical effects of rapid maxillary expansion on the craniofacial skeleton, studied by the finite element method. *Eur J Orthod.* 1998;20:347-356.

127. Jafari A, Shetty KS, Kumar M. Study of stress distribution and displacement of various craniofacial structures following application of transverse orthopedic forces--a three-dimensional FEM study. *Angle Orthod.* 2003;73:12-20.

128. Miyasaka-Hiraga J, Tanne K, Nakamura S. Finite element analysis for stresses in the craniofacial sutures produced by maxillary protraction forces applied at the upper canines. *Br J Orthod.* 1994;21:343-348.

129. Ecker RD, Endo T, Wetjen NM, et al. Diagnosis and treatment of vertebral column metastases. *Mayo Clin Proc.* 2005;80:1177-1186.

130. Gross MD, Arbel G, Hershkovitz I. Three-dimensional finite element analysis of the facial skeleton on simulated occlusal loading. *J Oral Rehabil.* 2001;28:684-694.

131. Hsieh J. *Computed Tomography: Principles, Design, Artifacts, and Recent Advances.* Vol PM114. Bellingham, WA: Spie, 2003.

132. Hsieh J, Society of Photo-optical Instrumentation Engineers. Computed tomography. 2009;PM188:556. Available from: http://link.library.utoronto.ca/eir/EIRdetail.cfm?Resources__ID=1152256&T=F.

133. McKinnis LN. *Fundamentals of Musculoskeletal Imaging.* 3rd ed. Philadelphia: F.A. Davis Company, 2010.

134. Zannoni C, Mantovani R, Viceconti M. Material properties assignment to finite element models of bone structures: A new method. *Med Eng Phys.* 1998;20:735-740.

135. Stock SR. *MicroComputed Tomography: Methodology and Applications.* Boca Raton: CRC Press, 2009.

136. Moazen M, Curtis N, O'Higgins P, et al. Assessment of the role of sutures in a lizard skull: A computer modelling study. *Proc Biol Sci.* 2009;276:39-46.

CHAPTER 2
The Impact of Voxel Size-Based Inaccuracies on the Mechanical Behaviour of Thin Bone Structures

2.1 Abstract

Computed tomography (CT)-based measures of skeletal geometry and material properties have been widely used to develop finite element (FE) models of bony structures. However, in the case of thin bone structures, the ability to develop FE models with accurate geometry derived from clinical CT data presents a challenge due to the thinness of the bone and the limited resolution of the imaging devices. The purpose of this study was to quantify the impact of voxel size on the thickness and intensity values of thin bone structure measurements and to assess the effect of voxel size on strains through FE modeling. Cortical bone thickness and material properties in five thin bone specimens were quantified at voxel sizes ranging from 16.4μm to 488μm. The measurements derived from large voxel size scans showed large increases in cortical thickness (61.9-252.2%) and large decreases in scan intensity (12.9-49.5%). Maximum principal strains from FE models generated using scans at 488μm were decreased as compared to strains generated at 16.4μm voxel size (8.6-64.2%). A higher level of significance was found in comparing intensity (R=-0.78, p=0.0001) vs. Thickness (R=-0.65, p=0.005) to strain measurements. These findings have implications in developing methods to generate accurate FE models to predict the biomechanical behaviour of thin bone structures.

2.2 Introduction

For more than three decades, computed tomography (CT) has been widely used in the diagnosis of bone diseases and the quantitative assessment of response to therapy[1-3]. Improvement of CT geometric resolution and computational power has led to more widespread utilization of CT images in the development of 3D finite element (FE) models to predict failure and fracture patterns in bones[4, 5]. The ability of CT scans to provide information about the morphology and material properties of bone tissues has allowed for more accurate characterization of the biomechanical behaviour of bone structures using patient-specific FE analysis[6-9]. Patient-specific FE models can be generated through geometric segmentation followed by highly automated meshing schemes or via direct conversion of CT voxels into FE elements. However, the quality of such models is limited by the geometric complexity of the structure, the meshing technique employed, and the voxel size of the CT images.

Computed tomography-based measures of skeletal geometry and material properties are highly dependent on the voxel size and spatial resolution of the image acquisition[10, 11]. In the case of thin bone structures, the ability to develop a FE model with an accurate geometry derived from clinical CT data presents a challenge because the thickness of the bone (or the thickness of the cortical shell) may be of the same order or less than the voxel size of the CT scanner. This further affects the values of the CT numbers obtained from the scan (due to partial volume effects) resulting in inaccurate material property assignments. Geometry and material property assignments are directly related to the stress and strain distributions calculated in bone structures using the FE method[4, 12]. Therefore, it is of a great importance to accurately derive heterogeneous material properties distributions from image intensity data and to properly map them onto

accurate geometric reconstructions to yield robust patient specific FE models of thin bone structures.

There are three main factors that contribute to the inability to obtain accurate thin bone or cortical shell thickness and intensity measurements from CT images. The first factor is the finite size of the x-ray beam. When imaging a structure that is smaller than the finite size of the radiation beam, the structure will be recorded with a reduced value proportional to its size in the x-ray beam. As a result, any object smaller than the beam size appears broadened or blurred in the CT scan[12]. Decreasing the size of the radiation beam to capture very thin structures using a clinical CT scanner can only be achieved by increasing the radiation output or scanning time. Both of these solutions would increase the radiation dose, and as such would not be clinically feasible. The second factor that can cause serious measurement error is partial volume effects that occur when a structure covers only part of a pixel. Since a given pixel in an image can only take on a single intensity value, the intensity at that pixel will be represented as an average of the various material densities covering that pixel. This produces a decrease in the CT numbers assigned to edge elements and blurring of thin bone structures resulting in an inaccurate representation of both material properties and geometry. This partial volume effect occurs in all structures but has a higher impact on the representation of thin bone structures due to the greater proportion of edge elements. The third factor that can affect the accuracy of CT scans is the image reconstruction algorithm (e.g. filtered back projection, or chord based reconstruction techniques). As well the interpolation methods (cubic, sinc, etc.) involved in regridding the data to a rectilinear volume impact on the resolution and SNR in the resultant image[11]. Considering these limitations, developing robust models representing the mechanical behaviour of thin bone structures is challenging and may depend upon the utilization of new methods to correct for inaccuracies in both geometry and material property assignments.

The inaccuracy of CT measurements, particularly thickness and CT number measured in Hounsfield Units (HU), of thin structures has been noted by several authors[13-17]. A study by Hangartner *et al.* showed an overestimation of thickness and underestimation of CT number if a structure thickness was below 2 mm (based on a pixel size of 0.3 mm)[14] . For structures like the vertebrae, the thickness of the cortical shell has been reported to be overestimated by a factor of at least two due to image blurring from low-resolution scanning[16]. However, little has been reported about the effect of these inaccuracies (overestimation or underestimation in thickness and intensity) on the biomechanical behaviour predicted using FE models[5].

Voxel size is important in defining anatomic structures using CT. Small voxel images have improved spatial resolution. Resolution is defined as the ability to distinguish two small high contrast objects located a small distance apart in an image and is dependent on the system and its parameters (i.e., voxel size, focal spot size, *etc.*). The voxel size is the basic element of the volume and is generally 1.5 to 2 times smaller than the resolution. A smaller voxel size is associated to a high-resolution image allowing a more accurate representation of geometry and material properties. This study aims to quantify the effect of voxel size on geometry and material property determination in thin bone structures and the resultant effect on mechanical behaviour. It is hypothesized that clinical CT images' voxel size result in large overestimations of the thickness of thin bones and concurrent decreases in image intensity profiles resulting in an inaccurate representation of strain patterns in thin bone FE models. CT and μCT imaging were used to quantify the impact of voxel size on the thickness and intensity values of thin bone structures and cortical thickness measurements and to assess the effect of voxel size on strain patterns in thin bone structures through 3D FE modeling.

2.3 Methods

Computed tomography scans were acquired for a cadaveric head and pelvis at a 0.488 x 0.488 mm pixel size (Lightspeed Plus, GE, Fairfield, CT). Before scanning, radiopaque fiducial markers were affixed to the craniofacial skeleton (CFS) and pelvis to provide a 3D coordinate system for subsequent data processing. The exact position of the bone specimens to be excised was determined based on the cortical thickness of the structures in the CT scan images. Five bone specimens approximately (1.5cmx1.5cmx (0.5-1) cm) were excised from the CFS and pelvis (nasal bone, anterior maxillary sinus wall, zygomatic body, zygomatic arch, and acetabulum, Figure 2-1). These five bone specimens represent variations in thickness and composition to allow for investigation of the effect of voxel size on thin cortical bone alone, thin cortical shell adjacent to trabecular bone, and thicker cortical bone. The anterior maxillary sinus wall and zygomatic body specimens were μCT scanned using the Skyscan 1172 with a 4.1 μm isotropic voxel size (Skyscan 1172, Kontich, Belgium). These two specimens were scanned at the highest available voxel size (4.1 μm) to determine the minimum voxel size that does not alter the geometry or intensity of the structure. Based on an initial analysis, no changes in bone thickness or intensity were observed between scans for specimens at 4.1 μm and 16.4 μm (refer to appendix A for pilot study results). Thus, all the specimens were μCT scanned with an isotropic voxel size of 16.4 μm using the GE Explore Locus μCT scanner (Explore Locus, GE, Fairfield, CT).

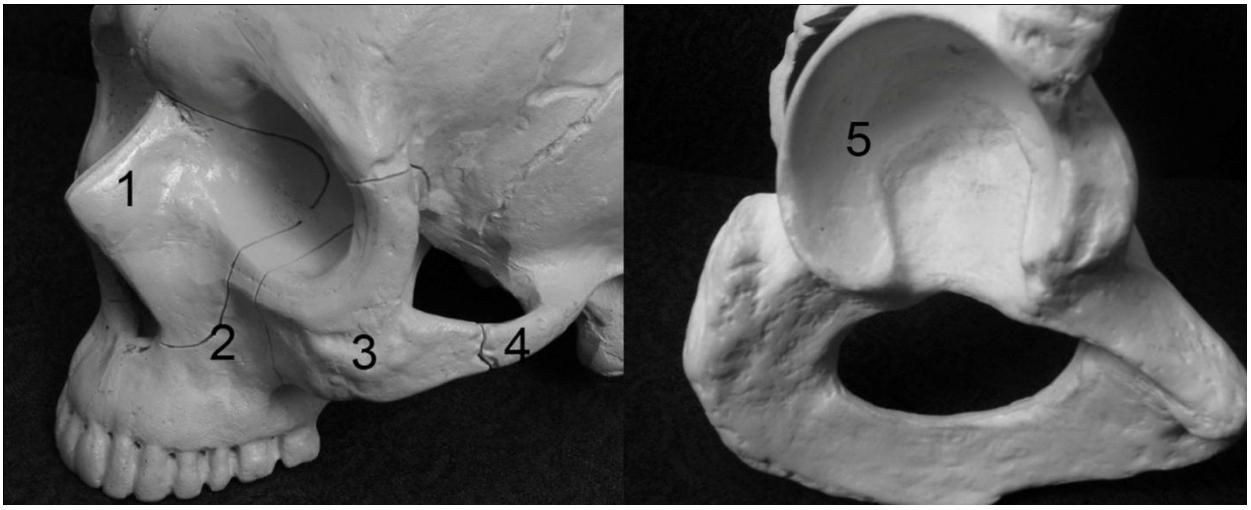

Figure 2-1: Mode representations of the specimens excised from the craniofacial skeleton 1) Nasal bone 2) Anterior maxillary sinus 3) Zygomatic body 4) zygomatic arch. And specimen excised from the pelvis 5) acetabulum

After scanning, the raw images were downsampled to voxel sizes of 82 μm, 164 μm, 328 μm, and 488 μm to evaluate the effect of image voxel size on bone thickness and intensity profile (Figure 2-2). The downsampling technique was performed using the image processing software Amira 5.2 (AmiraDEV5.2, Visage Imaging Inc., San Diego, CA). The software has a built-in resampling function that employs a Lanczos filter to change the voxel size of images. The lanczos filter is one of the most appropriate filters for resampling the scans because it is based on a sinc function and prevents aliasing. The largest image voxel size of 488 μm was chosen to be similar to those of the clinical CT scanners available in our hospital. To ensure that re-sampled scans resulted in a similar image to the clinical CT, the average thickness of the structures in the downsampled scans (at 488 μm) was quantitatively compared to clinical CT scans at the same voxel size. The scans at the five voxel sizes were segmented to identify the boundaries of the bone using intensity-based threshold criteria. A global threshold based on the image voxel size was used to segment the images. The initial global threshold values were chosen using the 50%

relative threshold technique[15]. The intensity at full width half maximum was automatically determined from a histogram of the bone intensity across the cortical layer for each scan and used as an initial guess for the segmentation. However, the segmentation was modified manually by visual inspection to remove internal holes (due to vascular canals) to ensure the segmentation is solid with no holes to facilitate the FE meshing and analysis of the 3D models (refer to appendix B for detailed methods).

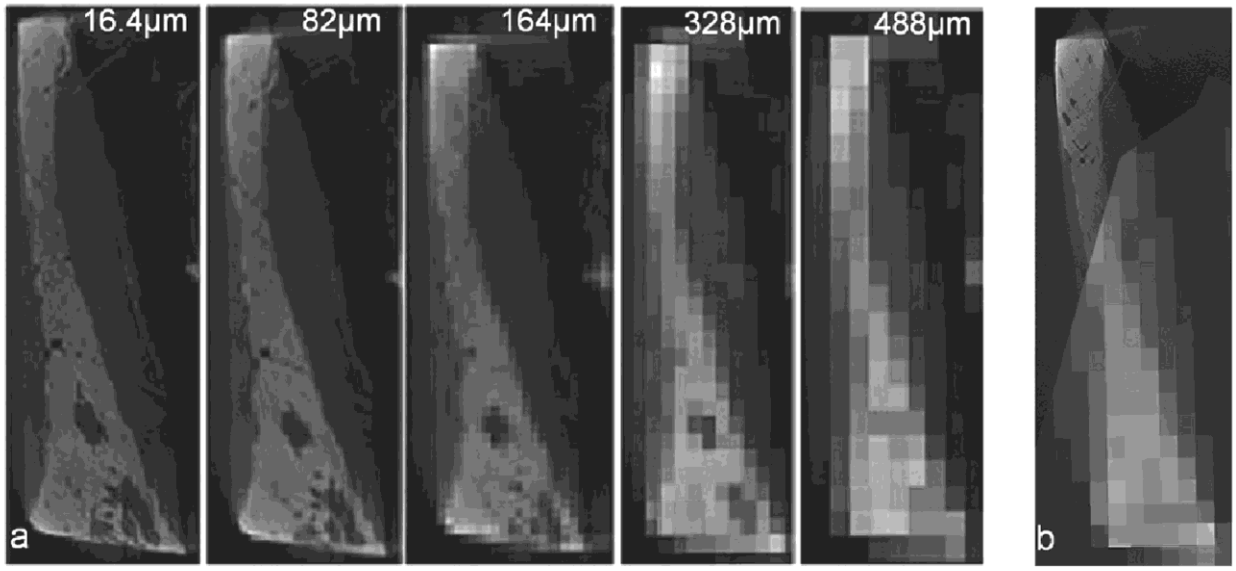

Figure 2-2: a) Anterior maxillary sinus wall scans at voxel sizes from 16.4µm to 488µm. The greyscale represents the intensity of the bone (HU) which is applied to the FE mesh using BONEMAT at each voxel size. b) Scan at16.4µm (*upper section*) overlaid onto the same scan at a voxel size of 488 µm (*lower section*) demonstrating the extent of geometric and intensity based changes due to downsampling of the image

Bone segmentations were used to generate 3D surfaces and to automatically construct ten-node tetrahedral FE meshes at voxel sizes ranging from 16.4 µm to 488 µm (Figure 2-3). The Bonemat algorithm was incorporated into the imaging software AmiraDev 5.2 and used to assign element specific material properties[7]. First, the average CT scan intensity of the voxels was mapped onto

the elements that were within the domain of the voxels. Then, the intensities were converted to the apparent density using an empirical calibration curve. Finally, the relation $E=2017.3\rho^{2.46}$ was used to transform the apparent densities into a heterogeneous distribution of elastic moduli in the FE model[4].

Figure 2-3: Finite Element model of the anterior maxillary sinus wall at voxel size 16.4µm

Measurements of the minimum and average thickness were implemented using a stepwise normal distance measurement tool developed in AmiraDEV5.2. The measurements were made by translating along the inward normal of each 3D surface, until the position was outside the segmentation of the cortical bone. Bone thickness and intensity profiles were quantified at each resolution using full 3D surfaces (Figure 2-4). The intensity was quantified for the cortical bone segmentation using an intensity histogram. The 3D FE meshes were generated from scans at different voxel sizes. All specimens were loaded under a distributed axial compressive force of 10N applied to the top surface of each bone specimen and fixed at the bottom surface. The FE

models were solved with (Abaqus 6.9-1) to produce the stress and strain distributions over the entire model. The number of elements for the FE models for each specimen at the five different voxel sizes was set to be similar to minimize differences due to mesh refinement. Maximum principal strain values were used in this study for comparing the biomechanical behaviour of the models at the five different voxel sizes. Linear regression analysis was performed to show an association between change in maximum principle strain with change in minimum thickness and average intensity. Significance was assumed at $p<0.05$ and all statistical analysis was performed using SPSS software (SPSS Inc, Chicago, IL).

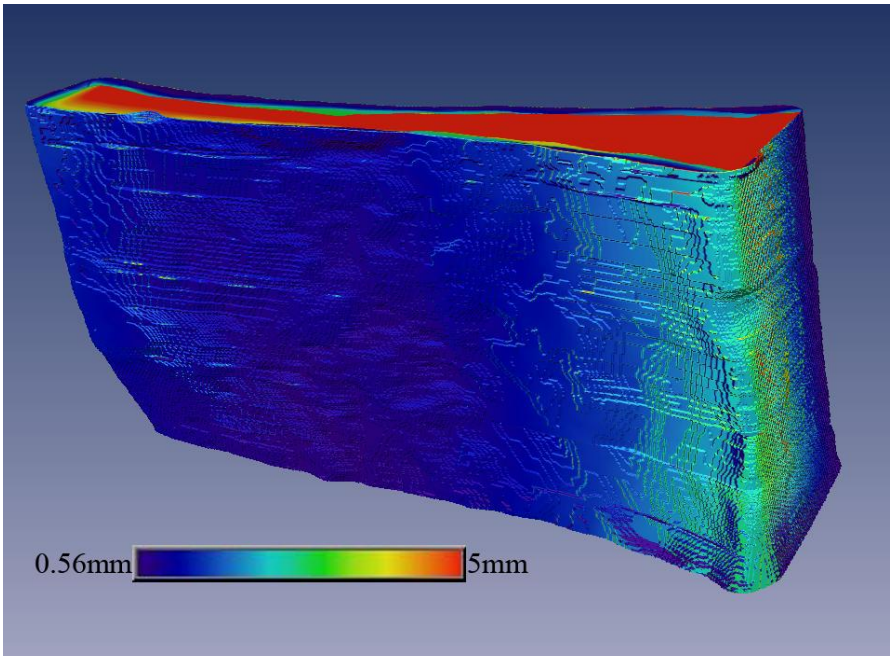

Figure 2-4: Distribution of bone thickness in the anterior maxillary sinus wall (3D surface)

2.4 Results

The minimum measured thickness and average intensity at each voxel size were measured for each of the five bone specimens (Table 2-1 and Figure 2-5). The average measured cortical

thickness of the 5 specimens ranged from 0.35mm (nasal bone) to 2.48mm (zygomatic arch). Downsampling to voxel size of 488μm resulted in large increases in the minimum measured cortical bone thickness (61.9% to 252.2%) and large decreases in overall (average) scan intensity (12.9% to 49.5%). FE models were successfully generated and analyzed at all voxel sizes (25 models in total). Maximum principal strains calculated using FE models generated from scans at the largest voxel sizes (488μm) were decreased (8.6%-64.2%) as compared to strains measured from FE models generated from the smallest voxel size image data (16.4μm) (Table 2-2). Large changes in maximum strain were found to occur as voxel size increased from 164 μm - 488 μm, with both intensity and geometry significantly related to strain (R=-0.78, p=0.0001 and R=-0.65, p=0.005, respectively).

Table 2-1: Minimum bone thickness and average intensity at 16.4 to 488 μm. Percent change represents the increase in minimum thickness (MIN. Thickness in mm), or decrease in average intensity (AVG. Intensity in Hounsfield units) when comparing the smallest to the largest voxel size analyses.

		Voxel Size					
Specimen		**16.4(μm)**	**82(μm)**	**164(μm)**	**328(μm)**	**488(μm)**	**% change**
Sinus Wall	MIN.Thickness	0.56	0.67	0.88	1.01	1.22	116.5
	AVG. Intensity	13051	12722	12446	11310	10612	-18.7
Nasal Bone	MIN.Thickness	0.19	0.23	0.31	0.48	0.69	252.2
	AVG. Intensity	1723	1713	1435	1097	870	-49.5
Zygomatic Arch (cortical shell)	MIN.Thickness	1.27	1.35	1.54	1.80	2.05	61.9
	AVG. Intensity	23957	23792.1	23455.8	22180	20668	-13.7
Zygomatic Body (cortical shell)	MIN.Thickness	1.26	1.31	1.57	1.80	2.06	63.1
	AVG. Intensity	13873	13568	13307	12428	11958	-13.8
Acetabulum (cortical shell)	MIN.Thickness	1.09	1.19	1.43	1.76	1.88	71.9
	AVG. Intensity	1633.1	1619	1575.6	1542	1422.8	-12.9

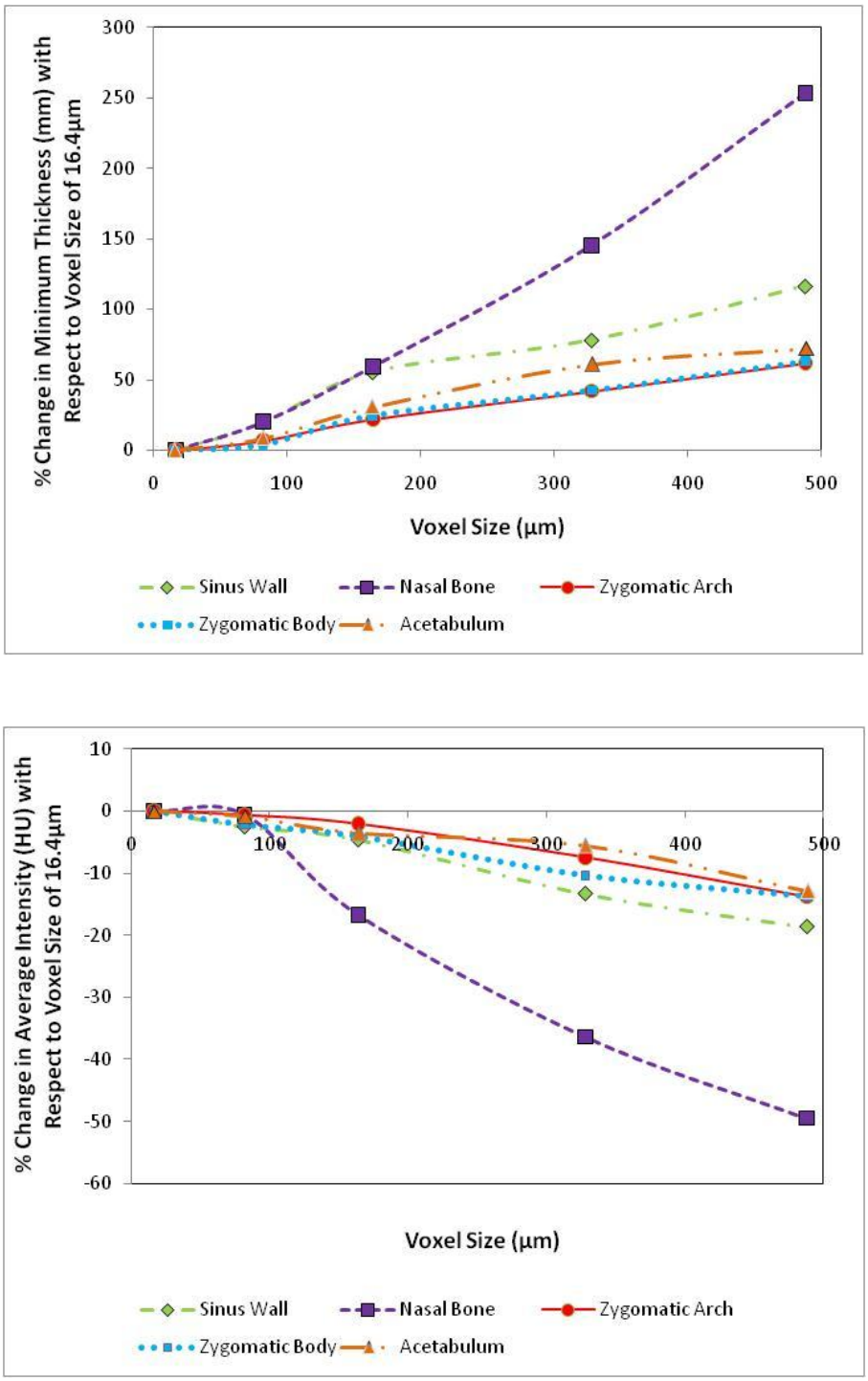

Figure 2-5: Curves representing % change in minimum cortical thickness (*top graph*) and average intensity (*bottom graph*) with change in voxel size.

Table 2-2: Maximum principal strains for the five bone structures generated through FE modeling at voxel sizes from 16.4µm to 488 µm and the changes in strain between the smallest and highest voxel sizes.

	Maximum Principal Strain (με)					
Specimen	**16.4 µm**	**82 µm**	**164 µm**	**328 µm**	**488 µm**	**%change**
Nasal Bone	1.64E-03	1.48E-03	1.35E-03	9.02E-04	5.88E-04	-64.23
Sinus Wall	1.80E-04	1.53E-04	1.44E-04	1.30E-04	8.40E-05	-53.26
Acetabulum	7.37E-04	7.35E-04	6.99E-04	6.84E-04	5.29E-04	-28.26
Zygomatic Body	3.36E-05	3.12E-05	3.09E-05	2.82E-05	2.64E-05	-21.53
Zygomatic Arch	2.66E-05	2.60E-05	2.59E-05	2.53E-05	2.43E-05	-8.60

2.5 Discussion

This study quantified the effect of voxel size on geometry and material property determination in thin bone structures and the resultant effect on their mechanical behaviour. Our results confirm previously reported overestimation of CT cortical bone width measurements and accompanying underestimation of intensity[14, 16, 18]. It further demonstrated that voxel size has a large effect on simulated biomechanical behaviour, with large voxel size resulting in greatly reduced maximum principal strains. Previous studies have shown that using clinical CT scanners, CT numbers and bone morphology cannot be measured accurately for a thickness less than 2-2.5mm (pixel size 0.3mm)[14]. Therefore, it is not surprising that the thin bony structures in the CFS and pelvis (as analyzed in this study) are influenced by voxel size, and their morphology is inaccurately represented in clinical CT scans. Yet, the need for understanding the effect of these inaccuracies on the biomechanical behaviour of thin regions is growing as FE modeling is being more widely used to characterize strain patterns in thin bone structures.

A voxel size of 16.4 µm was found to be sufficient in the analyzed specimens to yield image data with equal thickness and intensity values as scans acquired at 4.1 µm. Processing scans at a voxel size of 4.1 µm requires increased computational power and analysis time; as this smaller voxel

size did not impact the thickness or intensity measurements, future analysis conducted at 16.4 μm should be sufficient to model thin human cortical bone structures.

Our results confirmed that images with large voxel sizes had a higher impact on overestimating bone thickness in thinner specimens with the nasal bone (average thickness 0.35mm) suffering from the most progressive thickness overestimation (252.2%). The thickest bone specimen (cortical shell of the zygomatic arch: average thickness 2.48mm) suffered from the least overestimation of measured thickness (61.9%). The increase in bone thickness with the increase in voxel size is attributed to the averaging of the various intensities covering the area of each voxel. When downsampling a scan, the area represented by each voxel in the downsampled image increases to include the materials contained in multiple voxels in the higher resolution image. Due to edge effect, this can results in a decrease in the CT numbers and blurring making the thin bone structures appear thicker in the μCT image. In the thinner bone specimens the percentage of surface voxels with mixed intensities (bone and none bone) to the total number of voxels in the structure is higher than in thicker bone specimens. As such, this blurring has a higher relative impact on the average intensity and measured thickness of thin bone structures. Qualitatively, as the voxel size increased a concurrent loss of curvature was also identified in the specimens, changing the geometry of the bone structure. This was most pronounced in the highly curved structure of the zygomatic arch. The large voxel size images also resulted in more jagged edges, which represent a major limitation in developing accurate FE models of thin bone structures.

Radial profiles through the cortical bone using a single slice demonstrated the influence of partial volume effect on thickness and intensity. In thin specimens, the sharp edges of the intensity profiles turned into sloping edges with a sharp decrease in the peak CT values as voxel size

increased to 488 μm (Figure 2-6a). Thicker bone specimens were not as influenced by partial volume effect and their radial profiles at 488 μm still resembled the original profiles shape (Figure 2-6b). Moreover, when evaluating bone thickness based on the width of the intensity distribution across the thickness of the section at 50% of maximum intensity (the full width at half maximum value), the overestimation was higher in thinner specimens (Figure 2-7). This was similar to the overestimations in thickness observed by direct 3D measurements (Table 2-1).

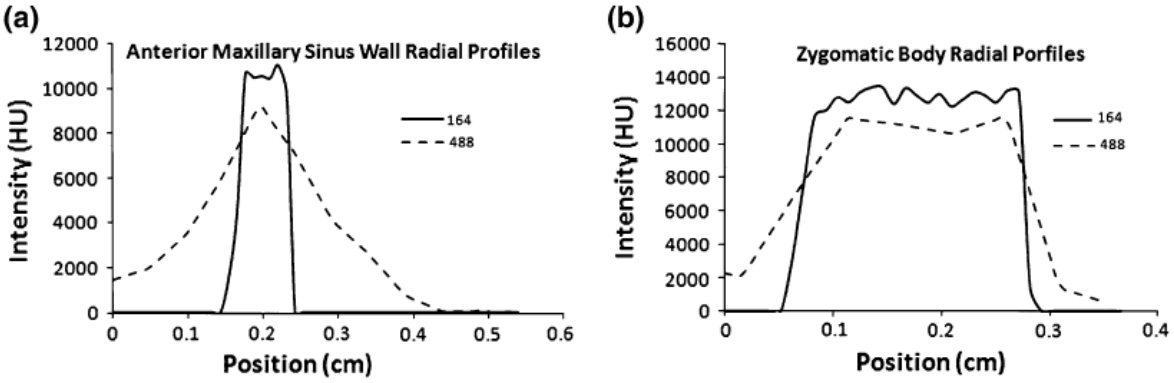

Figure 2-6: Radial Profiles of average intensity through a CT slice of the anterior maxillary sinus wall (a) and the zygomatic body (b) showing the effect of partial volume effect on voxel intensity and geometry.

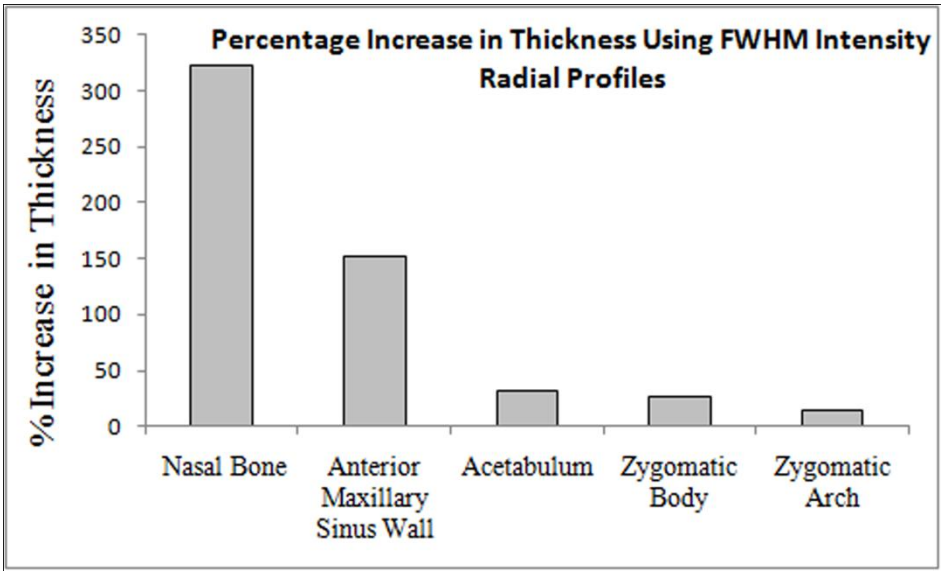

Figure 2-7: Percentage increase from 16.4μm to 488 μm in thickness of the five specimens based on the width of the intensity distribution across the thickness of the section at 50% of maximum intensity (the full width at half maximum value) of the intensity profile.

Underestimations in the intensity numbers due to increased voxel size were directly translated into underestimation of bone density, which was used to derive the elastic modulus of the bone in the FE models. Since the biomechanical behaviour of a linear elastic structure is directly related to its material properties, the bone specimens' strain patterns were inaccurately represented in the FE models with material properties generated using scans with 488 μm voxel sizes. The maximum principal strain decreased in all FE models (Figure 2-8) with the increase of the voxel size (with maximum principal strain decreasing by more than 60% at the largest voxel size, 488 μm, in the thinnest specimen). However, the decrease in the maximum principal strain was not linear between the developed FE models at the different voxel sizes. In all five specimens it was observed that large changes in maximum strain were found to occur as voxel size increased from 164 μm - 488 μm. Similarly, higher changes in intensity and thickness were observed in this voxel size range. The fact that voxel size range with higher changes in thickness

and intensity corresponded to the same voxel size range with larger changes in maximum strain provides further evidence that these changes in strain are due to changes in geometry and Young's modulus.

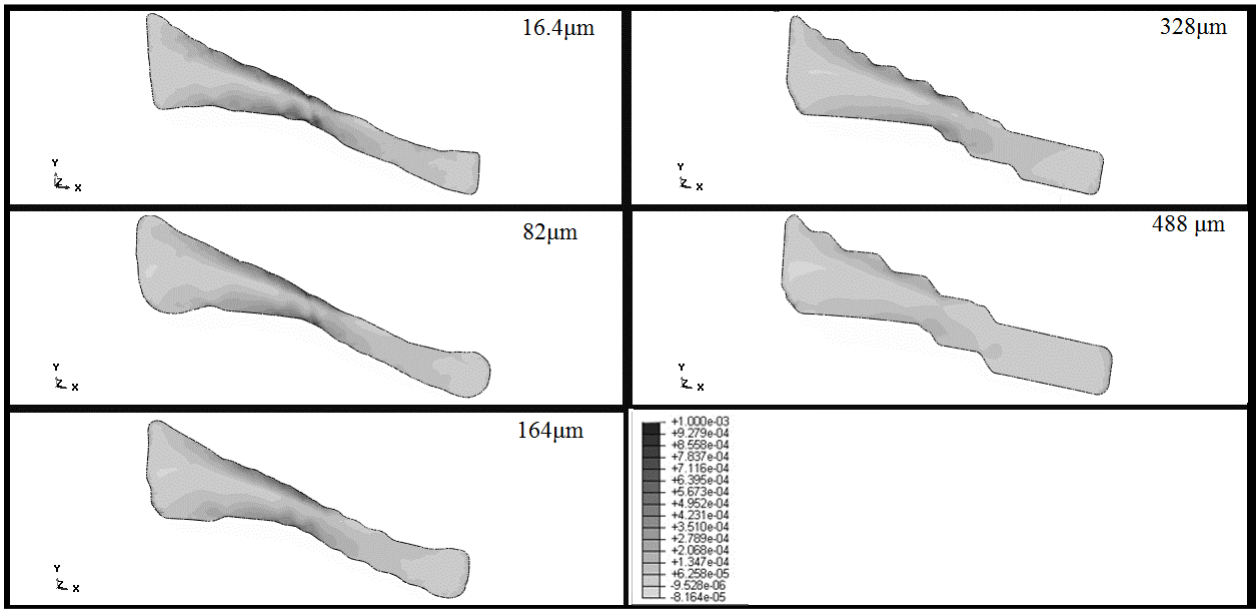

Figure 2-8: Cross sections representing maximum principal strains distribution for the anterior maxillary sinus wall specimen at the five voxel sizes.

The statistical analysis showed that higher level of significance was found when comparing intensity to strain (R=-0.78, *p*=0.0001) vs. thickness to strain (R=-0.65, *p*=0.005). These findings indicate that variations in geometry may not be the major cause of changes in strain in µFE models, but rather the material property (elastic modulus) assignment based on the µCT intensity data may have a more profound effect on strain. Such knowledge is important when developing new methods or algorithms to correct degraded images with large voxel sizes that will be used for structural analysis.

These findings are also important in considering the development of accurate FE models of thin bone structures, such as the CFS and pelvis. Previous studies have shown lower correlations between FE models strains and strains measured during mechanical testing in thin vs. thicker regions in the craniofacial skeleton[19]. Identifying how voxel size affects the strains generated by FE models at these regions is important to develop more accurate patient specific models.

Two limitations in the methods used in this study should be noted. First, the threshold selection was critical for defining the bone boundaries at each voxel size to yield accurate measures of width. In applying a fixed threshold, based on the smallest voxel size scan, segmentation of the bones at larger voxel sizes was compromised as the artificial boundary lines cut away bone from the edges. This resulted in segmentations which did not include the entire bony structure as visible on the images at each voxel size. Since this study aimed at understanding the inaccuracies due to overestimation in geometry, a semi-automated intensity-based thresholding method was instead used independently at each voxel size to identify the boundary of the bones (AmiraDEV 5.2). The global threshold with varying values depending on the image voxel size allowed for capturing the overestimation in thickness, which happens when segmenting blurred images. However, this approach was limited in that the selection of the global threshold and segmentation approach was critical resulting in some systematic errors. Moreover, in this study, the bone specimens were cleaned of all tissues and placed in liquid prior to imaging to allow for well-defined boundaries and ease of segmentation. Application of techniques to compensate for large voxel size imaging in a clinical scenario may face additional challenges due to reduced contrast arising from the presence of soft tissue structures adjacent to bone.

A second limitation of this study is related to the level of noise in the downsampled images. Our downsampled images generated from high-resolution μCT scans have less noise than images

acquired using clinical CT at a similar voxel size and as such do not fully represent an equivalent image quality. Our results demonstrated that even with the absence of increased noise in the downsampled images, the strain magnitude was not as accurate in the FE models generated from images with larger voxel sizes. Clinical scans would demonstrate further degradation of the image quality due to increased noise, likely resulting in even higher differences in strain values calculated from CT generated FE models.

Clearly, measurements of thickness and intensity of thin bone based on clinical CT imaging present a challenge when used to develop FE models. Our results showed that cortical bone with a thickness up to 2.48mm, alone or adjacent to trabecular bone, cannot accurately be represented using direct conversion of clinical CT image data to FE models. Inaccuracies in the predicted strain values result in inaccurate information about bone quality and volume that are important parameters for studying and developing design criteria for the treatment of conditions and injuries of the human skeleton. Standard CT scans currently in clinical use (even those with pixel size on the order of 0.5 to 1mm), can result in blurring and may represent a limitation in obtaining accurate information about the morphology, material properties, and mechanical behaviour of thin bone regions of the human skeleton. Small voxel size micro imaging is able to accurately represent thin bone geometry and thickness; however, such imaging may be limited in its clinical relevance or application to larger structures (i.e. the full CFS or pelvis). Future work is required to better understand the relative impact of morphologic and material inaccuracies on biomechanical behaviour of thin bone structures and to develop methods for improving the ability of clinical resolution CT-based models to accurately represent the structure and behaviour of thin bone.

2.6 References

1. Hangartner TN, Overton TR. Quantitative measurement of bone density using gamma-ray computed tomography. *J Comput Assist Tomogr.* 1982;6:1156-1162.

2. Hounsfield GN. Computerized transverse axial scanning (tomography): Part I. description of system. 1973. *Br J Radiol.* 1995;68:H166-72.

3. Mora S, Goodman WG, Loro ML, et al. Age-related changes in cortical and cancellous vertebral bone density in girls: Assessment with quantitative CT. *AJR Am J Roentgenol.* 1994;162:405-409.

4. Anderson AE, Peters CL, Tuttle BD, et al. Subject-specific finite element model of the pelvis: Development, validation and sensitivity studies. *J Biomech Eng.* 2005;127:364-373.

5. Huiskes R, Hollister SJ. From structure to process, from organ to cell: Recent developments of FE-analysis in orthopaedic biomechanics. *J Biomech Eng.* 1993;115:520-527.

6. Chen G, Schmutz B, Epari D, et al. A new approach for assigning bone material properties from CT images into finite element models. *J Biomech.* 2010;43:1011-1015.

7. Helgason B, Taddei F, Palsson H, et al. A modified method for assigning material properties to FE models of bones. *Med Eng Phys.* 2008;30:444-453.

8. Taddei F, Pancanti A, Viceconti M. An improved method for the automatic mapping of computed tomography numbers onto finite element models. *Med Eng Phys.* 2004;26:61-69.

9. Zannoni C, Mantovani R, Viceconti M. Material properties assignment to finite element models of bone structures: A new method. *Med Eng Phys.* 1998;20:735-740.

10. Newman DL, Dougherty G, al Obaid A, et al. Limitations of clinical CT in assessing cortical thickness and density. *Phys Med Biol.* 1998;43:619-626.

11. Newton TH, Potts DG. *Radiology of the Skull and Brain. Edited by Thomas H. Newton [and] D. Gordon Potts.* Saint Louis: Mosby, 1971.

12. Taddei F, Pancanti A, Viceconti M. An improved method for the automatic mapping of computed tomography numbers onto finite element models. *Med Eng Phys.* 2004;26:61-69.

13. Hangartner TN. Thresholding technique for accurate analysis of density and geometry in QCT, pQCT and microCT images. *J Musculoskelet Neuronal Interact.* 2007;7:9-16.

14. Hangartner TN, Gilsanz V. Evaluation of cortical bone by computed tomography. *J Bone Miner Res.* 1996;11:1518-1525.

15. Prevrhal S, Engelke K, Kalender WA. Accuracy limits for the determination of cortical width and density: The influence of object size and CT imaging parameters. *Phys Med Biol.* 1999;44:751-764.

16. Silva MJ, Wang C, Keaveny TM, et al. Direct and computed tomography thickness measurements of the human, lumbar vertebral shell and endplate. *Bone.* 1994;15:409-414.

17. Treece GM, Gee AH, Mayhew PM, et al. High resolution cortical bone thickness measurement from clinical CT data. *Med Image Anal.* 2010;14:276-290.

18. Hangartner TN. Thresholding technique for accurate analysis of density and geometry in QCT, pQCT and microCT images. *J Musculoskelet Neuronal Interact.* 2007;7:9-16.

19. Szwedowski TD, Fialkov F, & Whyne C. Sensitivity analysis of a validated subject-specific finite element model of the human craniofacial skeleton. *Proc Inst Mech Eng [H]*. 2010.

2.7 Appendix A

Pilot Study Data:

The sinus wall and zygomatic body specimens were μCT scanned using the Skyscan 1172 with a 4.1 μm isotropic voxel size. These two specimens were scanned at the highest available voxel size (4.1 μm) to determine the minimum voxel size that does not alter the geometry or intensity of the structure. No changes in bone thickness were found when the scan was downsampled from 4.1 μm to 16.4 μm. Minimal changes were observed in the intensity (less than 0.5% decrease) between scans for specimens at 4.1 μm and 16.4 μm. Thus, all the specimens were μCT scanned with an isotropic voxel size of 16.4 μm for the first study.

Table A: Minimum bone thickness and average intensity at 4.1 μm to 16.4 μm

Sample	Voxel Size (μm)	Avg. Intensity Hounsfield units	Minimum cortical thickness (mm)
Sinus Wall	4.1	13104	0.56
Sinus Wall	16.4	13051	0.56
% change		-0.4	0
Zygomatic Arch	4.1	23984	1.27
Zygomatic Arch	16.4	23957	1.27
% change		-0.1	0

2.8 Appendix B

Standard operating procedure:

Detailed description of cortical bone thickness, average intensity and maximum principle strain quantification:

1. Excise bone samples from the craniofacial skeleton
1. Micro-CT the samples at a resolution of 14μm (GE Explore Locus, General Electric Company)
2. Load the micro-CT scan in AmiraDev Imaging software
3. Using a Lanczos filter downsample the scan to voxel sizes of 82 μm, 164 μm, 328 μm, and 488 μm
4. Always use the original scan to obtain the downsampled scans
5. Using the segmentation module in Amira segment the target bone to create a label field. A label field is segmentation of the bone in the scan
6. Using the label field generate a 3D surface of the structure
7. To quantify bone intensity, generate a histogram based on the label field. This will produce an intensity histogram for the selected region in the segmentation and will ignore any other materials in the scan.
8. Record the average intensity for the bone
9. The 3D surface and segmentation are needed to quantify the cortical bone thickness
10. Connect the 3D distance measurement tool (SurfDist) in Amira to both the scan and segmentation
11. The SurfDis tool uses the segmentation to find the normal distance between the sample surfaces. Record the minimum distance between the surfaces
12. In Amira generate a 3D mesh using the bone surface. This will generate a mesh with 4-node tetrahedral elements
13. Using the bonemat method map the material properties to the model by converting the Intensity to density to Young's modulus. Use the following equation $E=2017.3\rho^{2.46}$
14. Save the model in an input file (*.inp)
15. Open the model in Abaqus/CAE and change the model mesh to 10-node tetrahedral elements
16. Assign the boundary conditions to the mesh:

a. The load should be applied as a compressive load (x direction)
b. The opposite surface should be fully constrained in the same direction as the load (x direction), one point in the center of the surface should be constrained in all directions (x,y, z) and one line of nodes should be constrained in the direction perpendicular to the loading direction (y direction).

17. Check the quality of the mesh
18. Run the model using the supercomputing facility
19. In Abaqus viewer quantify the maximum principle strain
20. Repeat the previous steps for scans at each voxel size

CHAPTER 3
A Technique for the Quantification of the 3D Connectivity of Thin Articulations in Bony Sutures

3.1 Abstract

The anatomy and development of cranial and facial sutures have been studied in detail using histological sections, 2D radiographs and more recently CT imaging. However, little attention has been paid to evaluating and quantifying the connectivity of these thin cortical bone articulations. More recent technological advances such as micro-CT imaging has the potential to be used to provide quantitative measurements of 3D connectivity in bony articulations. This study presents a new technique for quantifying the connectivity of bony projections inside cranial and facial sutures using a combination of skeletonization, thinning algorithms and 3D intensity mapping. The technique is demonstrated in five sutures through semi-automated analysis and image processing of μCT scans. In the sagittal, coronal and frontozygomatic sutures an average bone connectivity of 6.6% to 11.6% was found with multiple bony projections providing an interlocking structure between adjacent bones. Much higher bone connectivity was present in the zygomaticotemporal and zygomaticomaxillary sutures (22.7% to 37.4%) with few bony projections. This method combining μCT scanning and image processing techniques was successfully used to quantify the connectivity of thin bone articulations and allowed detailed assessment of sutural fusion in 3D. The wider application of this technique may allow quantification of connectivity in other structures, in particular fracture healing of long bones.

3.2 Introduction

Sutures are articulations in which the margins of adjacent bones are united by fibrous or bony tissue. They function to hold the bones of the skull together while allowing movement between cranial bones during childbirth. They also act as sites of bone growth and as mechanical stress absorbers. Articulations in thin bone structures in the human skeleton are understood to be fully fused by adulthood, with some structures achieving fusion up to the seventh decade[1]. However, when suture growth is not appropriately regulated, sutures can fuse prematurely (craniosynostosis**)** resulting in craniofacial deformities[2]. Current clinical orthopaedic devices in use to modify skull growth and deformities apply forces to generate microscale bone strain in order to alter sutural growth patterns. Thus, characterizing the biomechanical behaviour of cranial and facial sutures is important for understanding how mechanical stimuli modulate sutural growth.

The development, patency and structure of sutures in the craniofacial skeleton (CFS) and cranial vault have been studied in detail[3-6]. Yet most of these studies were carried out in the early 1920's until the early 1980's. As such, they were largely based on results of gross inspection of external and internal surfaces, histological sections and 2D radiographs. Although the analytical methods used in these studies provided qualitative information about the fusion of the sutures, they did not provide quantitative measurements of their connectivity. More recently other methods of investigation have been used to study suture structure and development, including conventional CT, µCT and scanning electron microscopy[3, 7].

High resolution 3D medical imaging techniques such as micro-computed tomography have the potential to be used for studying the development of facial and cranial sutures. The interdigitation of adult sutures has been recognized by several investigators[1]. However, the degree of connectivity through the full thickness of the suture has never been quantified. µCT can be utilized to quantify the connectivity of the bony projections, extensions which arise from the opposing edges of the bones on both sides of the suture (Figure 3-1).This could advance the mechanical understanding of the closure of cranial and facial sutures at different ages and under different pathologies.

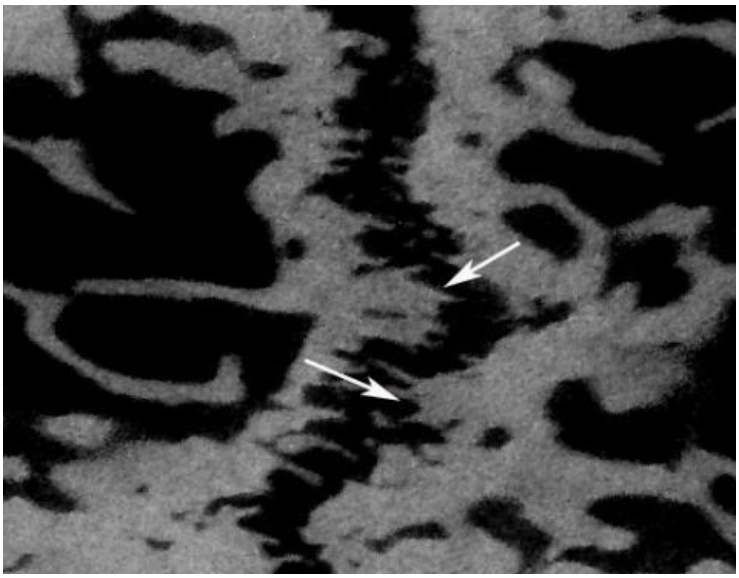

Figure 3-1: Irregular edges of the adjacent bones forming the suture gap due to multiple bony projections (White arrows).

To date, quantifying bone connectivity in 3D has been focused in studying cancellous bone architecture and little attention has been paid to thin, primarily cortical bone articulations. Methods of quantifying bone connectivity have been expressed in simple 2D approaches such as histological sections or 3D mathematical models using the Euler characteristics[8]. A study by Sherick *et al.* to quantify 3D connectivity in the coronal suture employed the Euler number approach[9]. However, this mathematical approach is mainly used for evaluating cancellous bone structure and is based on the assumption that a mesh is one fully connected structure without any isolated parts[10], which is not valid for the suture. A study by Korbmacher *et al*. quantified connectivity in the midpalatal suture by calculating the ratio of the length of obliterated suture to the total suture length, but utilized single 2D CT slices in three orthogonal planes [11].

The objective of this study was to develop a new and robust semi-automated method for quantifying the connectivity of cortical bone in 3D using µCT imaging through a combination of skeletonization, thinning algorithms and 3D intensity maps. We hypothesize that it is possible to quantify the degree of connectivity across thin bone articulations through the development of highly automated 3D image analysis techniques. This novel method may not only have

implications for research on the development and nature of CFS, but also may be a useful tool in the investigation and assessment of fracture healing.

3.3 Methods

The zygomaticotemporal (19x13x3mm), zygomaticomaxillary (6x13x8mm), frontozygomatic (6x13x8mm), coronal (1x14x7mm) and sagittal (16x17x5mm) sutures were excised from a preserved cadaveric head (seventh decade of age) obtained from the Department of Anatomy at the University of Toronto. These five sutures were selected for this study as they are accessible, of convenient size for analysis and represent various regions in the CFS. The sutures were µCT scanned at a resolution of 14 µm (GE Explore Locus, General Electric Company). An unsharp masking filter and a Lanczos filter were used to sharpen the bone boundaries and improve the quality of the images. The filtered µCT scans were segmented using intensity based threshold criteria to identify the boundaries of the bone and suture gap. The resulting segmentation required manual user improvement in order to fill holes that were not captured by the segmentation mainly in the suture region. Manual intervention required to improve the segmentation was performed using Amira's interactive segmentation tool.

Using the skeletalization Module in AmiraDEV 4.1, the suture segmentations were converted to a Large Disk Data object. It should be noted that the suture segmentation includes both the bone and connective tissue present between the adjacent bones. A 3D distance map for each voxel in the suture segmentation was produced by measuring the distances between each voxel and the nearest object boundary. The results of the distance map were used to quantify the average width of each suture. An automated thinning algorithm which incorporates both the segmentation and the 3D distance map was used to extract the centerlines of the structure contained in the segmentation (Figure 3-2). The output of the thinning algorithm was used to generate a 3D surface of the suture central plane. A bone intensity distribution map was generated for each suture scanned by converting the intensity values from the µCT scan (within the suture gap) into scalar field. Since the surface is generated based on the scan, the nodes connecting the surface triangles have the same coordinates as the voxels at the same location in the 3D slices. Thus, the values of the intensity from the scalar filed were assigned to the nodes on the 3D surface generated from the thinning algorithm output (refer to appendix C for a detailed standard operating procedure).

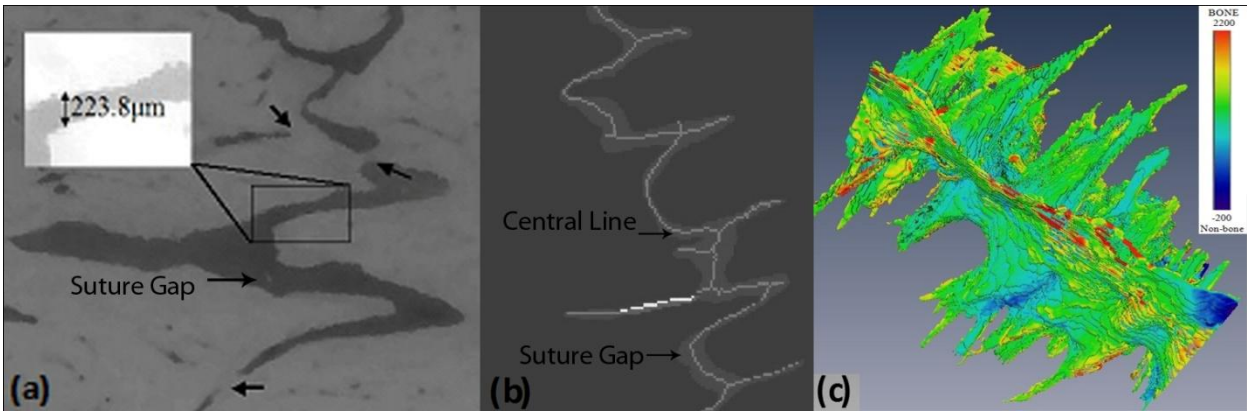

Figure 3-2: a) µCT scan of the coronal suture with bony connections across the suture gap (black arrows) and the suture gap width. b) The centerlines of the structure contained in the coronal suture segmentation. c) 3D connectivity map for the coronal suture (white is bone bridging the suture gap and black is connective tissue)

The percentage connectivity across each suture was quantified by determining the number of surface nodes that corresponded to bone intensity and the number of nodes that corresponded to non-bone intensity. Bony projections which did not meet the opposing edge of the suture were not reflected in the connectivity percentage. The percentage connectivity only reflected the bony bridges across the suture gap . Finally, the presence of internal bony projections was qualitatively determined from the segmentations of the sutures.

3.4 Results

The sagittal, coronal, frontozygomatic, zygomaticomaxillary and zygomaticotemporal µCT scans showed that the sutures remained partially open up to the seventh decade of age. The µCT scan of the specimens also showed that the thin bone sections in the frontozygomatic, coronal and sagittal suture regions were not highly fused and bony projections connected the cranial or facial bones. However, higher connectivity with few bony projections (Figure 3-3) was present in the zygomaticotemporal and zygomaticomaxillary sutures (Table 3-1). No histological correlates were used to validate the findings as histology allows for only 2D planar connectivity measurements in contrast to the 3D data generated through the µCT analysis. Matching µCT data to an exact histological section is hard to achieve due to variation in orientation and slice thickness.

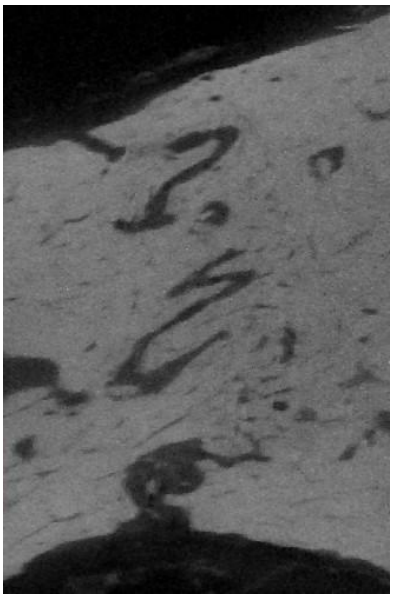

Figure 3-3: Zygomaticotemporal suture with high connectivity between the adjacent bones forming the suture gap

Table 3-1: Data for suture average width, connectivity and bony projections in the five sutures

Sutures	Suture Average Width (μm)	Average Percentage Connectivity %	Bony Projections Presence
Sagittal	367	6.6	High
Coronal	286	11.6	High
Frontozygomatic	443	10.3	Medium
Zygomaticotemporal	240	37.4	Small
Zygomaticomaxillary	361	22.7	Small

3.5 Discussion

A semi-automated method combining skeletonization, thinning algorithms and 3D intensity maps was used to quantify the connectivity in thin bone articulations in 3D. It provided a quantitative measure of the degree of fusion in the cranial and facial sutures as well as a 3D connectivity map. This method overcomes many of the limitations associated with existing approaches for quantifying bone connectivity. In the Euler number approach, connectivity highly

depends on the number of cavities in the segmentation. Also this approach is based on the continuity assumption that the bone network in the structure is fully connected and that every marrow cavity is fully surrounded with bone. The technique used by Korbmacher *et al.* quantified connectivity in CT slices in three planes, however this method does not provide full 3D volumetric representation of the suture connectivity[11]. In contrast, the method presented in this paper does not require the continuity assumption and quantifies connectivity through the full 3D volume of the suture. It further provides 3D connectivity maps showing the location of the bony bridges in the suture gap and uses automatically determined centerlines removing potential bias due to inter/intra observer error.

Based on the results of this study it was observed that the sagittal, coronal and frontozygomatic sutures had multiple bony projections providing an interlocking structure between adjacent bones with an average bone connectivity of 6.6% to 11.6%. However, few bony projections were present in the zygomaticotemporal and zygomaticomaxillary sutures with much higher bone connectivity between the adjacent bones (22.7% to 37.4%). This inverse relationship between the percentage connectivity of the adjacent bones of the suture and the number of bony projections is not a contradiction but rather consistent with existing literature about mechanisms in which bones achieve mechanical stability while transmitting loads[12]. The results indicate two ways in which sutures may achieve closure and mechanical stability: fusion by laying bone to connect adjacent surfaces and interdigitation by forming bony projections.

Using a global threshold value to segment the scan can result in an overestimation or underestimation in the number of voxels representing bone within the suture gap. This can result in an increase or decrease in the degree of connectivity within the suture. For this study time consuming manual intervention using Amira's interactive segmentation tool was performed to correct for any segmentation errors. However, incorporating more automated segmentation methods and known density phantoms can be used to overcome this limitation in future analysis.

The present study aimed to develop a new method to quantify the connectivity of thin bone articulations. Five sutures from a single cadaver head were used as a proof of principle to demonstrate the developed method. This method can be applied to quantify connectivity in sutures at different ages and multiple locations in the human skeleton. Future biomechanical

evaluation will be necessary to quantify the impact of different patterns of connectivity in sutures on strength, stiffness and fracture risk in the CFS.

The quantification of the connectivity of thin bone structures may be significant in developing accurate structural models of the CFS (i.e. finite element modeling) and may prove important in understanding strain transmission and fracture modes across bones adjacent to sutures. This technique can also be utilized for quantifying differences in connectivity between healthy and abnormal sutures. Furthermore, the method presented for thin bone connectivity analysis may be applied to a wide variety of cortical and cancellous bone, such as the 3D assessment of bony connectivity in fracture healing and bone regeneration in the presence of isolated islands of bone in the surrounding marrow space.

3.6 References

1. Rice DP. Developmental anatomy of craniofacial sutures. *Front Oral Biol.* 2008;12:1-21.

2. Mao JJ, Wang X, Kopher RA. Biomechanics of craniofacial sutures: Orthopedic implications. *Angle Orthod.* 2003;73:128-135.

3. Furuya Y, Edwards MS, Alpers CE, et al. Computerized tomography of cranial sutures. part 1: Comparison of suture anatomy in children and adults. *J Neurosurg.* 1984;61:53-58.

4. Kokich VG. Age changes in the human frontozygomatic suture from 20 to 95 years. *Am J Orthod.* 1976;69:411-430.

5. Latham RA, Burston WR. The postnatal pattern of growth at the sutures of the human skull. an histological survey. *Dent Pract Dent Rec.* 1966;17:61-67.

6. T. Wingate Todd, D. W. Lyon Jr. Cranial suture closure. its progress and age relationship. part II. - ectocranial closure in adult males of white stock. *Am J Phys Anthropol.* 1925;8:23-45.

7. Anderson PJ, Netherway DJ, David DJ, et al. Scanning electron microscope and micro-CT evaluation of cranial sutures in health and disease. *J Craniofac Surg.* 2006;17:909-919.

8. Feldkamp LA, Goldstein SA, Parfitt AM, et al. The direct examination of three-dimensional bone architecture in vitro by computed tomography. *J Bone Miner Res.* 1989;4:3-11.

9. Sherick DG, Buchman SR, Goulet RW, et al. A new technique for the quantitative analysis of cranial suture biology. *Cleft Palate Craniofac J.* 2000;37:5-11.

10. Odgaard A, Gundersen HJ. Quantification of connectivity in cancellous bone, with special emphasis on 3-D reconstructions. *Bone.* 1993;14:173-182.

11. Korbmacher H, Schilling A, Puschel K, et al. Age-dependent three-dimensional microcomputed tomography analysis of the human midpalatal suture. *J Orofac Orthop.* 2007;68:364-376.

12. Herring SW. Mechanical influences on suture development and patency. *Front Oral Biol.* 2008;12:41-56.

3.7 Appendix C

Standard operating procedure:

1. Take the head out of the freezer and place it in the fridge for 24 hours
2. Scan the head using a clinical CT scanner at a voxel size of 0.488mm (Light speed VCT GE Medical Systems)
3. Dissect the head from all soft tissues
4. Determine the suture samples to be excised and using a pencil draw the sample outlines (The sagittal, coronal, frontozygomatic, zygomaticomaxillary and zygomaticotemporal)
5. Using a dremel, cut the bone samples
6. Place each sample in a plastic bag and label it with the suture name and head ID
7. Micro-CT the suture samples at a resolution of 14 µm (GE Explore Locus, General Electric Company)
8. Load the scans in AmiraDev (AmiraDEV 4.1) imaging software
9. Convert the scan into, 'large disk data,' format
10. Crop the scans size to obtain similar sizes for all samples
11. Using the labeling module segment the suture gap. First you segment the non-bone area then segment the bony regions
12. Use arithmetic to add the two regions together so the segmentation contain all the material in the suture gap
13. Manually fix the segmentation to ensure all bony bridges are segmented
14. Using the Distance Map and thinning algorithms in AmiraDev Skeletonization package, find the center line for the segmentation
15. For detailed application of these two algorithms refer to AmiraDev software documentations
16. Step 13 will produce a plane that represent the center of the suture segmentation
17. Map the material intensity for each point on the plane based on the µCT scan values
18. Quantify the number of points on the plane that has intensity equivalent of bone
19. Quantify the number of points on the plane that has intensity equivalent of non-bone
20. Calculate the percentage connectivity defined as the number of points with bone intensity divided by the number of points with no bone intensity
21. To visualize the points of connectivity in the suture, generate a surface using the output of step 17

22. The following is an illustration of the previous steps

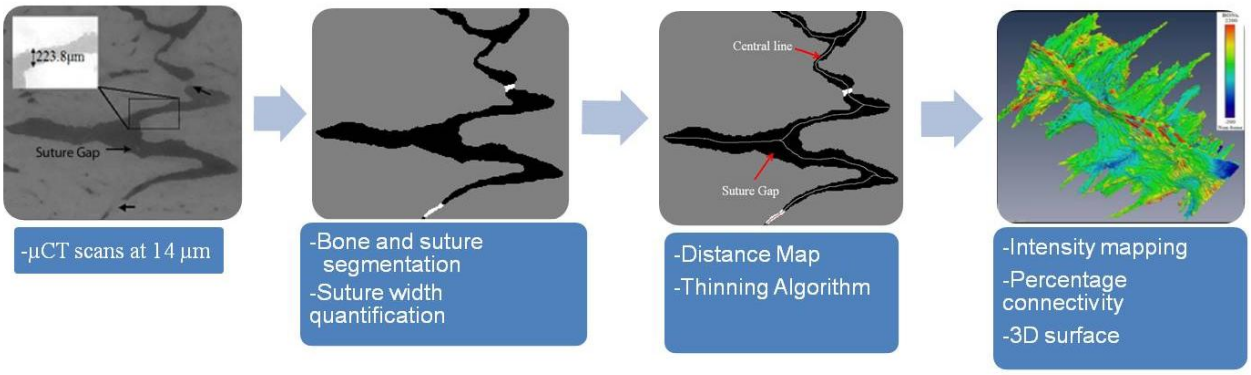

CHAPTER 4
Characterization of Craniofacial Sutures Using the Finite Element Method

4.1 Abstract

Characterizing the biomechanical behaviour of sutures in the human craniofacial skeleton (CFS) is essential to understanding the global impact of these articulations on load transmission. There are limited studies aimed at characterizing the biomechanical behaviour of suture due to the complexity of their interdigitated morphology, the multidirectional loading they are exposed to and the lack of well-defined suture material properties. This study aimed to quantify the impact of morphological features (number of interdigitations and bony connectivity), direction of loading (parallel, perpendicular and pressure loading) and suture material properties (isotropic or transversely isotropic) on the mechanical behaviour of sutures and surrounding bone in the CFS. Thirty-six idealized finite element models were developed to parametrically evaluate the impact of loading conditions. One additional specimen-specific finite elements model was developed based on suture morphology obtained from μCT scans to represent the morphological complexity inherent to sutures. Outcome variables of strain energy and von Mises stress were evaluated to characterize the sutures' biomechanical behavior. Loading direction was found to impact the relationship between strain energy and Interdigitation Index and yielded varied patterns of von Mises stress in both the suture and surrounding bone. Adding bone connectivity reduced suture strain energy and altered the von Mises stress distribution. Incorporating transversely isotropic material properties was found to reduce strain energy, but had little impact on stress patterns. High-resolution μCT scanning of the suture revealed a complex morphology with areas of high and low interdigitations. The specimen specific suture model results were reflective of strain energy absorption and von Mises stress distribution patterns consistent with the simplified FE model results. Suture mechanical behaviour is impacted by morphologic factors (interdigitation and connectivity), which may be optimized for regional loading within the CFS.

4.2 Introduction

Sutures are articulations in which bones and connective tissues meet to form fibrous joints in the craniofacial skeleton (CFS). The bones that make up the suture are generally of intramembranous origin and grow by ossification at the suture margin[1]. They function to hold the bones of the skull together while allowing for mechanical stress transmission and deformation (i.e. distortion during childbirth, cyclic loading from muscle activity, forces from therapeutic mechanical devices and traumatic impacts)[2]. The primary function of sutures in the CFS changes with age. In postnatal stages and early development, the sutures provide high flexibility to allow for enlargement of the head around the developing organs. Calvarial sutures undergo most of their growth during these early stages of development, whereas facial sutures are most active during adolescence. In adulthood, sutures are believed to function primarily as shock absorbers to dissipate stresses transmitted through the skull [3-11].

Sutures can be classified into three types based on their morphology: 1) flat or butt-ended sutures 2) overlapping sutures with rough or ridged contact surface and 3) interdigitating sutures with interlocking bony processes. However, in some cases sutural morphology cannot be simply classified into one category as boundaries between sutural walls can include a combination of bony processes and small round surfaces[1, 11]. Suture morphology changes from a simple butt joint in early life (which must stay patent to function) to a joint with differing degrees of interdigitation and interlocking projections in adulthood[1]. The underlying causes of suture fusion in healthy adults or in craniosynostosis patients remain unclear but are thought to be related to mechanical, genetic and hormonal factors [12, 13]. Under normal conditions, sutures in the human skeleton have been reported to be fully fused by late adulthood[1]. However, recent advances in micro-computed tomography have shown that sutures remain partially open even beyond the seventh decade with the degree of connectivity across the suture gap varying in different CFS sutures[14]. The study by Maloul *et al*. showed that sutures in the upper section of the cranium had multiple bony projections providing an interlocking structure between adjacent bones. In contrast, few bony projections were present in the zygomaticotemporal and zygomaticomaxillary sutures with much higher bone connectivity. Based on these findings suture morphology cannot be limited to the shape of the adjacent bones but must include the degree of bony bridging across the suture gap.

The human CFS is subjected to three main types of loading. Quasi-static tensile loading due to the growth of internal organs occurs mainly during the first two decades of life. Cyclic loading is applied through muscle contraction and bite force during mastication and can result in both compressive and tensile forces [6, 15-17]. Impact loading can also occur at high magnitudes and rates of loading (i.e. due to falls, fighting, foreign objects, motor vehicle accidents *etc*.). The sutures impact the mechanical response of the skull to loading by modulating the load transmitted between adjacent bones – this can include direct load transmission, reorientation of loading and damping [3, 8, 18-21]. Large variations in suture morphologies (shape, complexity and stiffness) and fiber arrangements, have led to speculation that sutures may adapt to their environment[12]. Studies have shown that suture morphology can be linked to compression, tensile or bending loading[6, 22, 23], but controversy remains as to how suture morphology impact the global function of the adult CFS during loading. The multifaceted morphologies seen in some sutures may relate to the complex loading experienced when subjected to masticatory forces.

The role of sutures in adult skull has been investigated by many researchers. *In vivo* and *in vitro* experimental studies have been carried out to understand the global impact of sutures and their role in transmitting mechanical stress. Experimental strain gauge studies and computational modeling (finite element (FE) and multibody dynamic analyses) have been used to evaluate the mechanical behaviour of sutures in the CFS [6, 18, 24-26]. FE modelling has been successful in developing a better understanding of the biomechanics of the human skeleton, with the potential to providing a complete characterization of the stress and strain patterns under physiological or non-physiological loadings [16, 17, 26-30]. However, FE modeling of the CFS sutures requires assignment of appropriate morphology, material properties and loading conditions (i.e. connectivity, fiber arrangements, directions of loading) to yield results reflective of the physiologic behaviour.

In spite of efforts to understand the global functional and mechanical properties of the CFS, little attention has been directed at understanding the mechanical consequences of variation in suture morphology (i.e. number of interdigitations and connectivity) and direction of loading (i.e. perpendicular or parallel to the suture) at the individual suture level [5, 6, 10, 18, 23, 31-34]. In order to understand the global impact of sutures on the overall strain pattern of the CFS it is important to characterize individual suture mechanics (with various morphologies) in response to different loading scenarios. This study aims to investigate how morphological features (number of

interdigitations and bony connectivity), direction of loading (parallel, perpendicular and pressure loading), suture material properties (isotropic or transversely isotropic) influence the mechanical behaviour of the suture and surrounding bone. It is hypothesized that the design of a single suture is adapted for regional functional specialization within the CFS.

4.3 Materials and Methods

Idealized finite element models of the bone-suture-bone complex were developed in Abaqus CAE (Simulia,USA) using 3D tetrahedral elements (300K-400K elements). The dimensions of the full complex were 9mm (width) x 20mm (height) x 3mm (depth) with a 0.2mm suture width. Differing suture morphologies were modeled by varying the number of interdigitations. The interdigitation index (I.I.), defined as the ratio between the entire length of the suture divided by the straight distance between the suture adjacent bony surfaces[23], was modeled as low (I.I.=2.3), moderate (I.I.=3.4) and complex (I.I.=4.3).

In all FE models the bone was treated as an isotropic material as per Jasinoski *et al*. study (Young's modulus E=6GPa, Poisson's ratio v=0.27)[35]. In the literature there is a considerable variation in the reported values of Young's modulus and Poisson's ratio for cranial and facial sutures with Young's modulus values ranging from 1.16 to 610 MPa [36-38]. In this study an average value was used as per Jasinoski *et al.* study. The sutures were assigned isotropic material properties (E=50MPa v=0.30) or transverse isotropic material properties (E_1=80MPa , E_2= 20 MPa, E_3=20MPa, v_{12}=0.4, v_{13}=0.1, v_{23}=0.4, G_{12}=20MPa, G_{13}=26.6MPa and G_{23}=20MPa) [35]. The higher Young's modulus is aligned with the direction of the fibre with the smaller Young's modulus in the other two directions.

Two bone-suture complexes (coronal and zygomaticotemporal) were excised from a fresh frozen human CFS (85years of age) obtained from the Department of Anatomy at the University of Toronto, decalcified in formic acid and embedded in paraffin wax. The sutures were sectioned in the sagittal plane and stained using Hematoxylin and Eosin (H&E). The orientation of the fibres in the transversely isotropic materials model was determined based on the histological sections, which demonstrated fibres arranged in straight lines between adjacent surfaces at a 40 degree offset angle (Figure 4-1 and Figure 4-2). Other studies used fibre orientation based on observations made by Rafferty *et al.* in miniature pigs[23] . To account for connectivity in the

suture gap, the bone surfaces were bridged with bony connections that represented 17% connectivity for each of the three interdigitations indexes (Maloul *et al.*)[14].

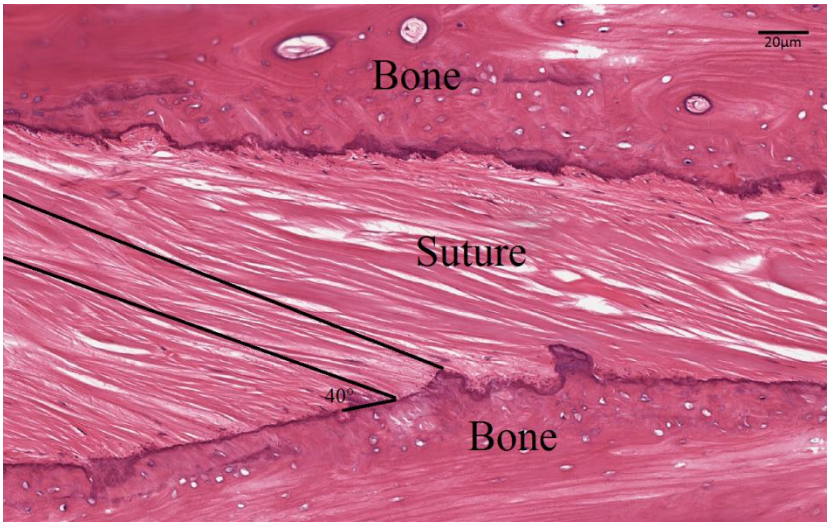

Figure 4-1: Fibre arrangement inside the suture in histology section

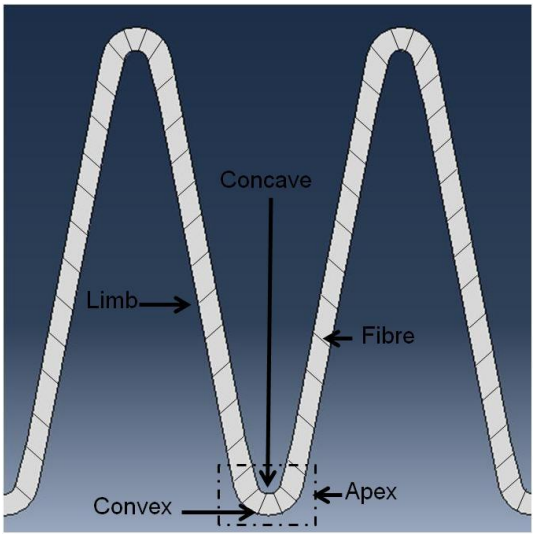

Figure 4-2: Fibre orientation within the limbs and apices of the suture

Each FE model was loaded with a static uniform load of 20N in three separate configurations (Figure 4-3): 1. Parallel - a tensile load applied to the upper surface of the bone (parallel to the suture) while lower edge was constrained, 2. Perpendicular - load applied to the left side surface of the complex (perpendicular to the suture) with the right edge fully constrained in the same

direction as the loading and one center point constrained in all directions and 3. Pressure -loading applied as a full surface pressure to represent impact loading.

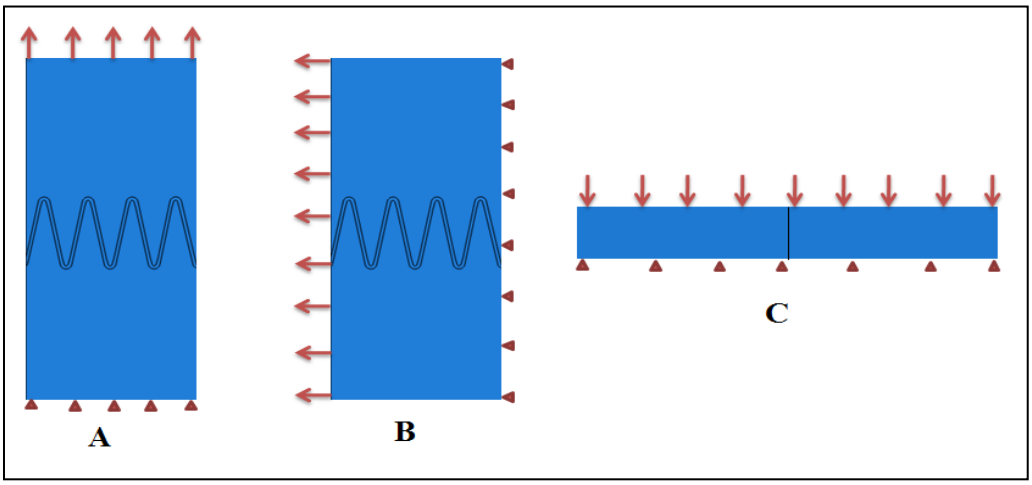

Figure 4-3: Three different loading directions simulated in Abaqus/CAE: A) parallel, B) perpendicular and C) pressure

A section of the coronal suture was excised from a fresh frozen cadaver head and µCT scanned at a resolution of 14 µm (GE Explore Locus, General Electric Company). The µCT scan was segmented in AmiraDEV 5.2 imaging software using intensity based threshold criteria to identify the boundaries of the bone/suture and generate FE model (900K elements). The FE model was assigned isotropic material properties for bone and sutures as in the simplified FE models. The model was loaded in parallel, perpendicular and pressure (separately) to investigate the mechanical behaviour of the suture with real morphology (refer to appendix D for a detailed standard operating procedure).

Overall a total of 36 idealized FE models and one µCT based model were analyzed (Table 4-1). Outcome variables of strain energy (SE) and von Mises stress were evaluated for each model to understand the role of suture structure in transmitting loads. Since the volume of the suture changes depending on the number of interdigitations, the strain energy cannot be directly compared. Thus, the strain energy values were adjusted to control for differences between the models in volume. Following Dumont *et al.* (2009), the scaled strain energy was calculated as[39]:

$$Scaled\ SE\ for\ model\ \ B = \left(\frac{Volume\ of\ model\ B}{Volumeof\ model\ A}\right)^{\frac{1}{3}} \left(\frac{Force\ applied\ to\ B}{Force\ applied\ \ to\ A}\right)^{2}\ SE\ of\ model\ B$$

Table 4-1: A total of 37 FE models were developed using different material properties and suture morphology

Isotropic Suture Material			Transversely Isotropic Suture Material			Isotropic Suture Material with Connectivity			Transversely Isotropic Material with Connectivity		
Perpendicular	Parallel	Pressure	Perpendicular	Parallel	Pressure	Perpendicular	Parallel	Pressure	Perpendicular	Parallel	Pressure
I.I.=2.3			I.I.=2.3			I.I.=2.3			I.I.=2.3		
I.I.=3.4			I.I.=3.4			I.I.=3.4			I.I.=3.4		
I.I.=4.3			I.I.=4.3			I.I.=4.3			I.I.=4.3		
µCT based models			-			-			-		

4.4 Results

The effect of load direction: The highest overall strain energies in the bone/suture complex, bone and suture were found under parallel loading. The lowest strain energy was found under perpendicular loading for the bone/suture complex and bone, however strain energy in the suture was minimized under pressure loading. For all loading directions areas of highest stress were located at the interdigitation apices in both the sutures and bones, with lower stresses occurring along the limbs (Figure 4-4). These results were consistent independent of the suture material definitions and the I.I.

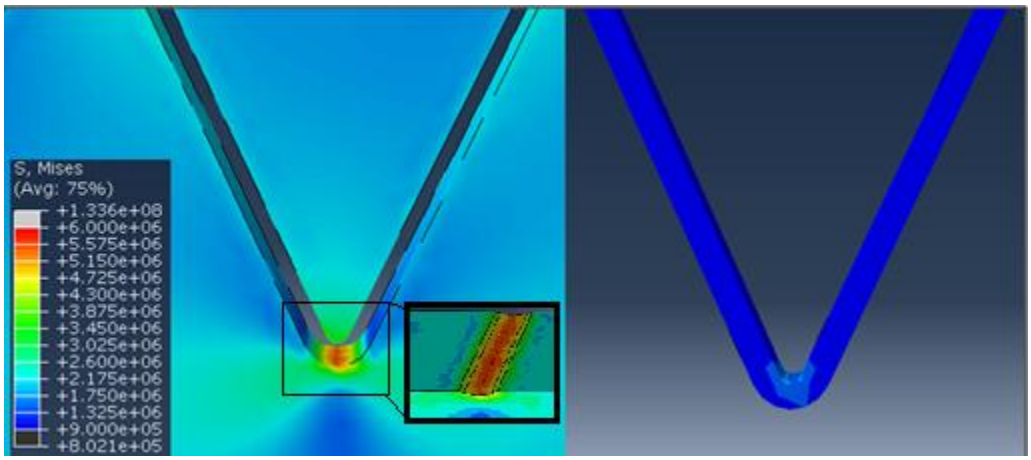

Figure 4-4: Stress plots (in Pa) of the limbs and apices of the interdigitations for bone (*left*) and suture (*right*) in response to parallel loading.

The effect of interdigitation index: Under parallel loading the strain energies of the bone/suture complex and the sutures were inversely related to I.I. In contrast, the strain energy in the bone, increased with I.I. (Figure 4-5A). In perpendicular and pressure loading, suture, bone and bone/suture complex strain energy increased with higher levels of interdigitation (Figure 4-5B and C). The changes in strain energy with interdigitation level were much smaller under pressure loading in comparison to parallel and perpendicular load scenarios. Under parallel and pressure loading the increase in I.I. reduced bone stress along the convex surfaces of the apices, corresponding to an increase in the stress along the limbs of the sutures (Figure 4-6). In contrast, bone stress was reduced along the limbs with increased I.I. for perpendicular loading. For all loading cases increases in I.I. reduced the overall suture stress, both at the apices and along the limbs (Figure 4-7).

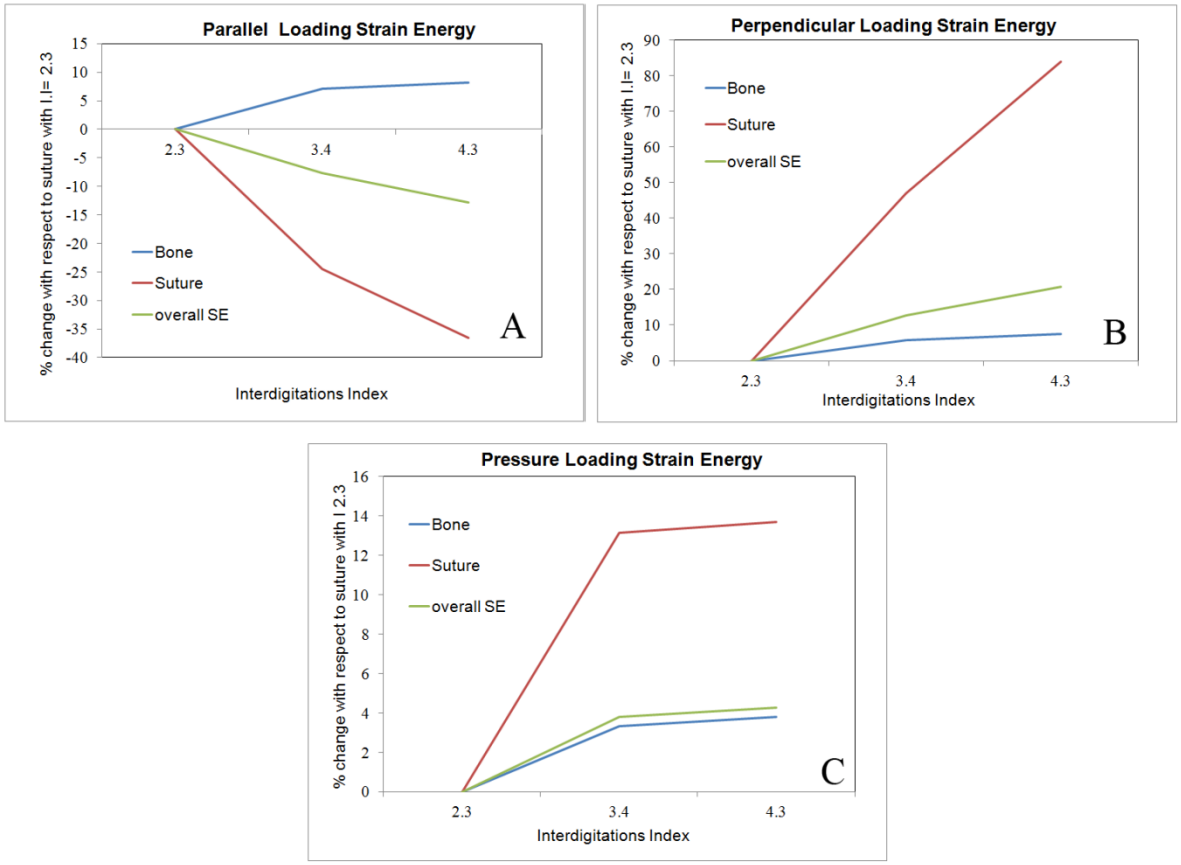

Figure 4-5: The effect of I.I. on the strain energy in bone, suture and bone/suture complex (total structure strain energy) in response to parallel, perpendicular and pressure loading. This was calculated as the percentage difference between strain energy in low interdigitated suture and the other two cases of interdigitations.

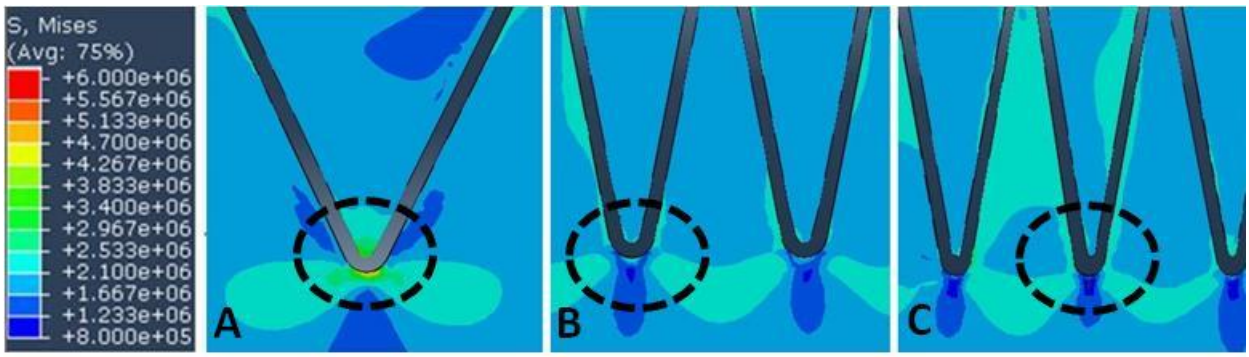

Figure 4-6: Plots of bone stress (in Pa) in the interdigitation apices and limbs for (A) low I.I., (B) moderate I.I. and (C) complex I.I. in response to parallel loading.

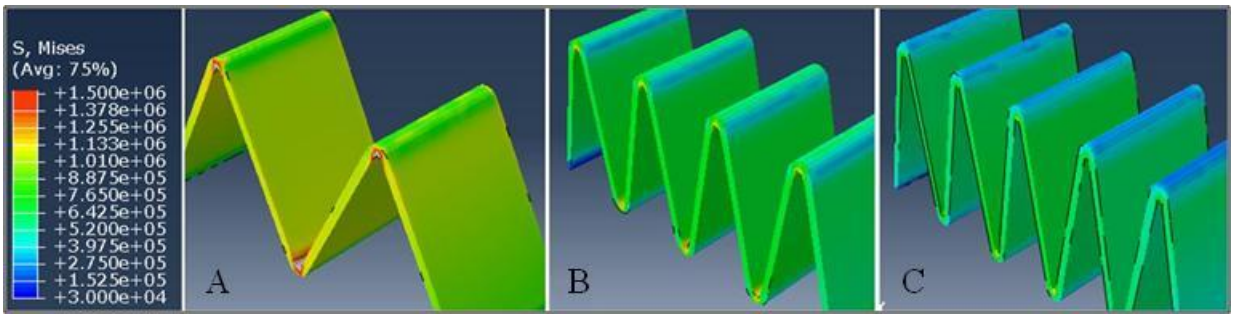

Figure 4-7: Plots of suture stress (in Pa) in the interdigitation apices and limbs for (A) low I.I., (B) moderate I.I. and (C) complex I.I. in response to parallel loading.

The effect of suture material property assignment: Changing the suture material properties from isotropic to transversely isotropic decreased the strain energy within the suture in all cases. Only minimal effects were seen in the bone strain energy due to changes in suture material definition (slight decrease). Correspondingly, strain energy was reduced in the overall bone/suture complex (Table 4-2). Changing the suture material properties did not alter the distribution of the stress in the bone or suture.

Table 4-2: Percentage change in strain energy (calculated as (SE for transversely isotropic model-SE for Isotropic model)/ SE for isotropic model) for suture, bone and overall bone/suture complex averaged for I.I in response to three loading directions.

	% change in Strain Energy averaged for I.I.		
	Suture	Bone	Overall
Parallel	-14	-0.9	-6
perpendicular	-20	-2	-7
Pressure	-3	-0.8	-1

The effect of connectivity: Adding bone connectivity across the suture caused large reductions in strain energy in the suture in all cases (Table 4-3). The impact of connectivity on the bone was dependent on the applied loading, with increases in strain energy under parallel loading vs. decreases in strain energy under perpendicular and pressure loading. Furthermore, there was no effect of I.I. when connectivity was present. In the overall bone/suture complex, the overall strain energy was reduced. Adding connectivity significantly altered the stress patterns in the suture and bone (Figure 4-8). Stress was highly decreased in the suture and regions of high stress were concentrated in the bony bridges.

Table 4-3: Percentage change in strain energy (calculated as (SE for model with connectivity-SE for model without connectivity)/ SE for model without connectivity) for suture, bone and overall bone/suture complex averaged for I.I in response to three loading directions (Isotropic : Iso. , transversely isotropic :Tiso.)

% change in Strain Energy averaged for I.I.						
	Suture		Bone		Overall	
	Iso.	Tiso.	Iso.	Tiso.	Iso.	Tiso.
Parallel	-95	-94	9	9	-33	-29
perpendicular	-63	-55	-5	-4	-18	-12
Pressure	-67	-66	-4	-3	-7	-6

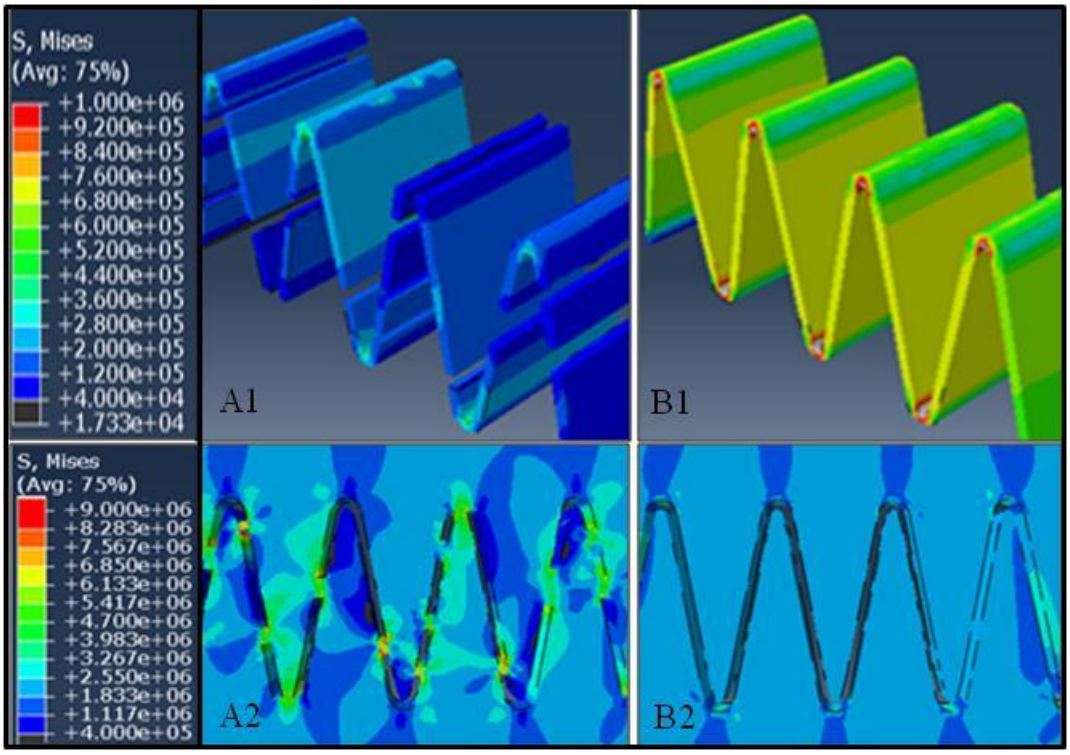

Figure 4-8: Plots of suture stress (in Pa) under parallel loading in the interdigitation apices and limbs in a complex suture with connectivity (A1) and without connectivity (B1) and bone stress in a complex suture with connectivity (A2) and without connectivity (B2)

µCT based FE models: The µCT scan of the suture revealed a complex morphology that was not apparent from a surface view. The suture was relatively butt ended near the ectocranial surface and highly interdigitated endocranially (Figure 4-9). For the whole bone/suture complex, parallel loading yielded the highest strain energies and perpendicular loading yielded the lowest strain energies, as in the idealized models. The suture strain energy for the ectocranial and endocranial sides were analyzed independently and found to be consistent with the trends exhibited in the idealized FE models for cases representing high and low levels of interdigitation (Table 4-4). Similar patterns to the idealized models, with high stresses found at the apices, were present in the specimen specific µCT based FE model (Figure 4-10).

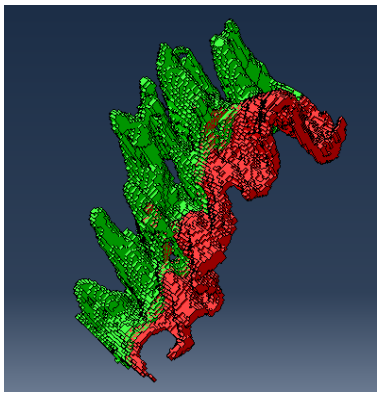

Figure 4-9: 3D representation of the internal morphology of the coronal suture with high interdigitation (green) and low interdigitation (red).

Table 4-4: Strain Energy in the suture and bone (divided into two sides based on the interdigitations) in the µCT based FE models in response to the three loading cases.

	Total Strain Energy (N.m)			
	Suture		Bone	
	Low I.I.	High I.I.	Low I.I.	High I.I.
Parallel	4.2×10^{-4}	1.6×10^{-4}	9.3×10^{-4}	1.5×10^{-3}
perpendicular	3.3×10^{-5}	8.2×10^{-5}	6.1×10^{-4}	6.6×10^{-4}
Pressure	4.7×10^{-5}	1.8×10^{-4}	6.5×10^{-4}	1.1×10^{-3}

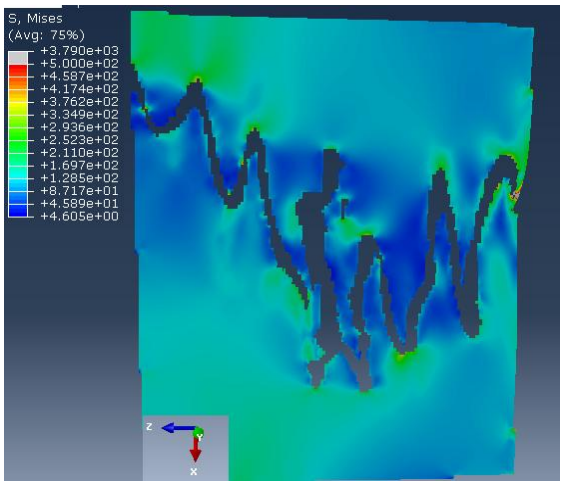

Figure 4-10: Plot of bone stress (in MPa) (endocranial side) in the interdigitation apices and limbs in the µCT based FE in response to loading parallel compressive loading.

4.5 Discussion

The effect of load direction

Sutures in the skull experience loading due to internal (i.e. mastication) and external (i.e. trauma) factors. Physiologically, sutures experience complex loading in multiple directions yet little information is available describing their loading environment. In this study the FE models were analyzed in three configurations to gain a better understanding of the response of sutures to varied loading directions. The FE models of the bone/suture complex absorbed the most strain energy when loaded parallel to the suture. This type of loading corresponds to the most common loads experienced by the sutures in the CFS resulting from bite force. As such, these findings support previous hypotheses that sutures in the adult skull are primarily optimised to withstand loading due to function[40-45] .While the mechanical behaviour of individual sutures has been evaluated by several investigators under parallel loading [35, 46-48], no previous studies have modeled suture loading in other directions (perpendicular or pressure), as presented herein. Modeling the loading on sutures in various directions is important as sutures in the CFS experience complex multi-direction loading due to mastication.

The effect of interdigitation index

Higher strain energy in a structure indicates a greater ability to absorb shock. When loading parallel to the suture, the results showed that energy absorption in the suture, as well as the overall complex, decreased with increasing I.I. These findings are consistent with previous results reported by Jasinoski *et al.* (2002). Jasinoski *et al.* reported disagreement between their modeling results and the experimental findings of Jaslow *et al*. (1990), however, the discrepancy between the two studies can be attributed to the load application to the suture[4, 35]. Our results showed that the relationship between the suture, bone and overall complex strain energy and I.I. is dependent on the direction of loading, which is consistent with the work of Jasinoski *et al.* in modeling parallel loading strain energy trends. Our findings related to strain energy under pressure loading are consistent with the experimental work of Jaslow *et al*., conducted in three-point bending. Thus, attention should be given to loading direction when comparing results to previous studies aiming at characterizing the mechanical behaviour of the sutures in the CFS.

A higher I.I. may optimize the bone/suture complex to withstand perpendicular or pressure loading (representative of the direction experienced during impact loading). To better understand these results a closer look at the morphology and loading experienced by the suture based on their location in the CFS is required. Fractures in the cranium mainly occur due to trauma, which is represented by pressure loading in this study. Thus, it is fair to assume that the cranial sutures should be adapted to withstand such loading by having a high I.I. This idea is supported by the findings of Maloul *et al*. and Rice, which showed that cranial sutures have high numbers of interdigitations [1, 14]. In adults, the cranium is made of thick bones whose primary function is to protect the brain thus requiring high forces to fracture; high I.I. complements this function.

In contrast, while impact loading can be experienced by facial sutures, Maloul *et al*. reported the presence of few interdigitations in the facial sutures[14]. Yet, since facial sutures primarily experience parallel loading from bite force, their structure may be optimized to bear load in that direction with a lower I.I. This is consistent with Nahum *et al*. work that have shown that most of the bones of the midfacial region of the CFS are comparatively fragile, fragmenting and comminuting easily from impact force while able to withstand high parallel forces from bite force[49, 50]. A low I.I. improves load transmission (by increasing the absorption of strain energy)

under parallel loading. These findings emphasize the idea that midfacial suture morphology may be optimized for load transmission during mastication.

Increase in I.I. reduced bone Von Mises stress near the convex of the apices under parallel loading, which corresponded to an increase in the stress along the limbs of the suture. These patterns of stress can be attributed to the formation of more interdigitations, which relieve the peak stresses in the bone around the suture due to the increase in the surface area available to transmit the force from the bone boundaries to the suture. Similar trends in stresses were briefly reported by Jasinoski *et al.*(2010), Zhang *et al.* (2002), Borke *et al.* (2003), and Yu *et al.* (2004)[35, 46-48], in 2D FE models. In both perpendicular and pressure loadings, the distribution of stresses was not as impacted by I.I., as the majority of the loading is carried by the bone.

The effect of suture material property assignment

Transversely isotropic models with a 40º tension-resistant fibre arrangement (Figure 4-2) for the suture had lower strain energy than isotropic materials. This is consistent with Jasinoski *et al.* results, which showed that the inclusion of fibres (oriented at 15 º or 75 º) reduced strain energy. The fibre orientation assignment in Jasinoski *et al.* was a simplification of the complex arrangements in miniature pigs reported by Rafferty *et al.* (1999)[23]. In this study, histological sections of sutures from human cadaveric heads used to determine fibre orientation demonstrated similar arrangements (although differing in average angles). However, the agreement in the findings by this study and Jasinoski *et al.* confirm that differences in the fibre angle have little impact on strain energy trends. It should be noted that Jasinoski *et al.* results only represent parallel loading while in this study the decrease in strain energy from assigning transversely isotropic materials properties was exhibited in all 3 loading directions. This suggests that there is no functional advantage of this tension-resistant fibre arrangement in the suture in the adult skull under the conditions investigated in this study but could possibly be related to other loads experienced (i.e. during developmental stages).

The effect of connectivity

The decrease in the suture strain energy due to bony bridging was expected. The bony connections transmit the force between the bone boundaries and reduce the force transmitted to the suture. This behaviour was exhibited under all loading directions but had the greatest impact

in parallel loading. This larger reduction in strain energy can be attributed to the nature of force transmission under parallel loading, with the entire suture volume contributing evenly to absorb strain energy. Surprisingly, increase in bone strain energy occurred only in parallel loading with minimal decrease in perpendicular and pressure loading. Closer investigation of the strain energy in bony bridging revealed higher strain energies distributed evenly through all bony bridges in response to parallel loading. In contrast, in perpendicular loading, strain energy was elevated as distance from the bony bridges to the loading surface decreased. Similar findings occurred under pressure loading where strain energies in the bony bridges were highest in areas of maximum deformation.

µCT based FE models

The combined suture morphology of high and low interdigitations in the µCT based models yielded results reflective of strain energy absorption consistent with the simplified FE model results. In the case of parallel loading the highly interdigitated side absorbed less energy than the less interdigitated side, while in cases of perpendicular and pressure loading highly the interdigitated side absorbed more energy. Furthermore, the uneven and very irregular shape of the various interdigitations did not appear to alter the biomechanical behaviour. This µCT based model represents the more complex morphology of the sutures in the CFS under various loading conditions. However, the consistency in the findings between the idealized models and µCT based model suggest that although morphological differences (i.e. interdigitation index and connectivity) can impact the biomechanical behaviour of sutures, the distribution of these parameters within individual sutures may not be critical to strain energy measures.

In this study all sutures were modeled with a single Young's modulus and Poisson's ratio, based on the limited material property data from the literature[36-38]. Differences which may exist in suture material properties due to location or age, may alter the magnitude of the suture response, but will have minimal impact on the patterns of strain energy described (based on the large difference between the moduli of suture material and bone). As well, the analysis of sutures was greatly simplified by assuming material behaviour to be the same in tension and compression. However, the compressive and tensile strengths of many biologic materials are very different. For example, collagen fibres in the suture will provide only tensile strength to the material. This assumption results in identical strain energy and von Mises stress magnitude in the structure under tensile and compressive loading[51]. Similarly, the simplified suture morphology and

loading can provide an insight into the suture mechanics but do not represent complex loading experienced by individual sutures *in vivo*. It is not possible based on idealized simple FE models to make comprehensive conclusions describing the mechanical behaviour of sutures under complex loading. While the geometrically complex μCT based model supports the idealized findings, it too does not account for the material property assumptions as described above[51].

Overall, the results of this study demonstrate that suture morphology may be optimized to allow the skull to respond to different loading directions. Suture mechanical behaviour is impacted by morphologic factors (interdigitation and connectivity) that can alter their role in reducing the total strain energy absorbed under load. The morphology of each individual suture may be adapted for regional functional specialization within the CFS. Future work investigating additional specimen specific suture morphology and complex loading behaviour is needed to further elucidate the role of sutures in the adult CFS.

4.6 References

1. Rice DP. Developmental anatomy of craniofacial sutures. *Front Oral Biol.* 2008;12:1-21.

2. Mao JJ, Wang X, Kopher RA. Biomechanics of craniofacial sutures: Orthopedic implications. *Angle Orthod.* 2003;73:128-135.

3. Buckland-Wright JC. Bone structure and the patterns of force transmission in the cat skull (felis catus). *J Morphol.* 1978;155:35-61.

4. Jaslow CR. Mechanical properties of cranial sutures. *J Biomech.* 1990;23:313-321.

5. Jaslow CR, Biewener AA. Strain patterns in the horncores, cranial bones and sutures of goats (capra hircus) during impact loading. *J Zool.* 1995;235:193-210. Available from: http://dx.doi.org/10.1111/j.1469-7998.1995.tb05137.x.

6. Herring SW, Teng S. Strain in the braincase and its sutures during function. *Am J Phys Anthropol.* 2000;112:575-593.

7. Byron CD, Borke J, Yu J, et al. Effects of increased muscle mass on mouse sagittal suture morphology and mechanics. *Anat Rec A Discov Mol Cell Evol Biol.* 2004;279:676-684.

8. Rayfield EJ. Cranial mechanics and feeding in tyrannosaurus rex. *Proc Biol Sci.* 2004;271:1451-1459.

9. PRITCHARD JJ, SCOTT JH, GIRGIS FG. The structure and development of cranial and facial sutures. *J Anat.* 1956;90:73-86.

10. Rafferty KL, Herring SW, Marshall CD. Biomechanics of the rostrum and the role of facial sutures. *J Morphol.* 2003;257:33-44.

11. Rayfield EJ. Using finite-element analysis to investigate suture morphology: A case study using large carnivorous dinosaurs. *Anat Rec A Discov Mol Cell Evol Biol.* 2005;283:349-365.

12. Herring SW. Mechanical influences on suture development and patency. *Front Oral Biol.* 2008;12:41-56.

13. Persson M, Magnusson BC, Thilander B. Sutural closure in rabbit and man: A morphological and histochemical study. *J Anat.* 1978;125:313-321.

14. Maloul A, Fialkov J, Hojjat SP, et al. A technique for the quantification of the 3D connectivity of thin articulations in bony sutures. *J Biomech.* 2010;43:1227-1230.

15. Tomasz Daniel Szwedowski. Development and validation of a subject-specific finite element model of the human craniofacial skeleton. 2007.

16. Szwedowski TD, Whyne CM, Fialkov JA. Toward characterization of craniofacial biomechanics. *J Craniofac Surg.* 2010;21:202-207.

17. Szwedowski TD, Fialkov F, Whyne C. Sensitivity analysis of a validated subject-specific finite element model of the human craniofacial skeleton . *Proceedings of the Institution of Mechanical Engineers Part H, Journal of engineering in medicine.* 2010;224:1-10.

18. Behrents RG, Carlson DS, Abdelnour T. In vivo analysis of bone strain about the sagittal suture in macaca mulatta during masticatory movements. *J Dent Res.* 1978;57:904-908.

19. Hylander WL, Johnson KR, Crompton AW. Loading patterns and jaw movements during mastication in macaca fascicularis: A bone-strain, electromyographic, and cineradiographic analysis. *Am J Phys Anthropol.* 1987;72:287-314.

20. Herring SW, Teng S, Huang X, et al. Patterns of bone strain in the zygomatic arch. *Anat Rec.* 1996;246:446-457.

21. Rayfield EJ, Norman DB, Horner CC, et al. Cranial design and function in a large theropod dinosaur. *Nature.* 2001;409:1033-1037.

22. Herring SW, Rafferty KL, Liu ZJ, et al. Jaw muscles and the skull in mammals: The biomechanics of mastication. *Comp Biochem Physiol A Mol Integr Physiol.* 2001;131:207-219.

23. Rafferty KL, Herring SW. Craniofacial sutures: Morphology, growth, and in vivo masticatory strains. *J Morphol.* 1999;242:167-179.

24. Popowics TE, Herring SW. Load transmission in the nasofrontal suture of the pig, sus scrofa. *J Biomech.* 2007;40:837-844.

25. Rayfield EJ. Using finite-element analysis to investigate suture morphology: A case study using large carnivorous dinosaurs. *Anat Rec A Discov Mol Cell Evol Biol.* 2005;283:349-365.

26. Wang Q, Smith AL, Strait DS, et al. The global impact of sutures assessed in a finite element model of a macaque cranium. *Anat Rec (Hoboken).* 2010;293:1477-1491.

27. Dumont ER, Piccirillo J, Grosse IR. Finite-element analysis of biting behavior and bone stress in the facial skeletons of bats. *Anat Rec A Discov Mol Cell Evol Biol.* 2005;283:319-330.

28. Ross CF, Patel BA, Slice DE, et al. Modeling masticatory muscle force in finite element analysis: Sensitivity analysis using principal coordinates analysis. *Anat Rec A Discov Mol Cell Evol Biol.* 2005;283:288-299.

29. Chalk J, Richmond BG, Ross CF, et al. A finite element analysis of masticatory stress hypotheses. *Am J Phys Anthropol.* 2011;145:1-10.

30. Curtis N, Kupczik K, O'higgins P, et al. Predicting skull loading: Applying multibody dynamics analysis to a macaque skull. *Anat Rec (Hoboken).* 2008;291:491-501.

31. Smith KK, Hylander WL. Strain gauge measurement of mesokinetic movement in the lizard varanus exanthematicus. *J Exp Biol.* 1985;114:53-70.

32. Herring SW, Mucci RJ. In vivo strain in cranial sutures: The zygomatic arch. *J Morphol.* 1991;207:225-239.

33. Rafferty KL, Herring SW, Artese F. Three-dimensional loading and growth of the zygomatic arch. *J Exp Biol.* 2000;203:2093-2104.

34. Sun Z, Lee E, Herring SW. Cranial sutures and bones: Growth and fusion in relation to masticatory strain. *Anat Rec A Discov Mol Cell Evol Biol.* 2004;276:150-161.

35. Jasinoski SC, Reddy BD, Louw KK, et al. Mechanics of cranial sutures using the finite element method. *J Biomech.* 2010;43:3104-3111.

36. Margulies SS, Thibault KL. Infant skull and suture properties: Measurements and implications for mechanisms of pediatric brain injury. *J Biomech Eng.* 2000;122:364-371.

37. Radhakrishnan P, Mao JJ. Nanomechanical properties of facial sutures and sutural mineralization front. *J Dent Res.* 2004;83:470-475.

38. Coats B, Margulies SS. Material properties of human infant skull and suture at high rates. *J Neurotrauma.* 2006;23:1222-1232.

39. Dumont ER, Grosse IR, Slater GJ. Requirements for comparing the performance of finite element models of biological structures. *J Theor Biol.* 2009;256:96-103.

40. Tucker R. Studies in functional and analytical craniology .1. the elements of analysis. *Aust J Zool.* 1954;2:381-390.

41. Tucker R. Studies in functional and analytical craniology .2. the functional classification of mammalian skulls. *Aust J Zool.* 1954;2:391-&.

42. Tucker R. Studies in functional and analytical craniology .3. the breviarcuate skull and its analysis. *Aust J Zool.* 1954;2:399-&.

43. Tucker R. Studies in functional and analytical craniology .4. more extreme forms of the breviarcuate skull. *Aust J Zool.* 1954;2:412-&.

44. Tucker R. Studies in functional and analytical craniology .5. the functional metamorphoses of the carnivorous skull. *Aust J Zool.* 1954;2:418-426.

45. Tucker R. Studies in functional and analytical craniology .6. strains and the direction of certain vectors in the breviarcuate skull. *Aust J Zool.* 1954;2:427-&.

46. Zhang G, Borke J, Yu J. Mechanical environment and cranial suture wavy pattern. *Georgia Life Sciences Summit,Atlanta.* 2002.

47. Borke J, Zhang G, Yu J, et al. Mechanical environment and suture complexity. *Journal of Dental Research.* 2003;82:A1505.

48. Yu J, Borke J, Zhang G.Brief synopsis of cranial sutures: Optimization by adaptation *Seminars in Pediatric Neurology.* 2004;11:249.

49. Nahum AM. The biomechanics of maxillofacial trauma. *Clin Plast Surg.* 1975;2:59-64.

50. Hoffman HT, Krause CJ. Traumatic injuries to the frontal sinus. In: Fonseca RJ, Walker RV, eds. *Oral and Maxillofacial Trauma.* Vol 1. Philadelphia: Saunders, 1991:576-99.

51. Armenàkas AE. *Advanced Mechanics of Materials and Applied Elasticity.* Boca Raton, FL: Taylor & Francis, 2006.

4.7 Appendix D

Standard operating procedure:

1. In Abaqus/CAE software generate the idealized FE models based on the following geometry: 9mm (width) x 20mm (height) x 3mm (depth) with a 0.2mm suture width
2. To assign different interdigitations to each model use the width of the sample divided by the length of the desired suture to determine the interdigitation index (I.I.)
3. Make three models with following I.I. values : 2.3, 3.4 and 4.3
4. Assign material properties for bone (Young's modulus E=6GPa, Poisson's ratio v=0.27) and for suture (E=50MPa v=0.30)
5. Generate a mesh using 10-node tetrahedral elements
6. Check the quality of the mesh to ensure no bad elements or singularity exist in the mesh
7. Assign a 20N tensile force in a direction parallel to the suture (x direction)
8. Constrain the opposite surface of the bone/suture sample in same direction as the load (x direction)
9. Constrain one point in the middle of the opposing surface (as in step 8) in all directions (x,y,z)
10. Constrain a line in the middle of the opposing surface (as in step 8) in the y direction
11. Save the model as an *.inp file and run on the supercomputing facility computers
12. Obtain the username and password to access the supercomputing server from your supervisor
13. Go back to step seven and assign the force in a direction perpendicular to the suture (y direction)
14. On the opposing surface to the loading surface constrain the bone/suture sample in same direction as the load (y direction)
15. Constrain one point in the middle of the opposing surface (as in step 14) in all directions (x,y,z)
16. Constrain a line in the middle of the opposing surface (as in step 14) in the x direction
17. Save the model as an *.inp file and run on the supercomputing facility computers
18. Go back to step seven and assign the force in as a pressure loading (z direction)
19. On the opposing surface to the loading surface constrain one edge in same direction as the load (z direction)
20. Constrain one edge of the opposing surface (as in step 19) in x and z direction

21. Constrain one edge of the opposing surface (as in step 19) in the y direction

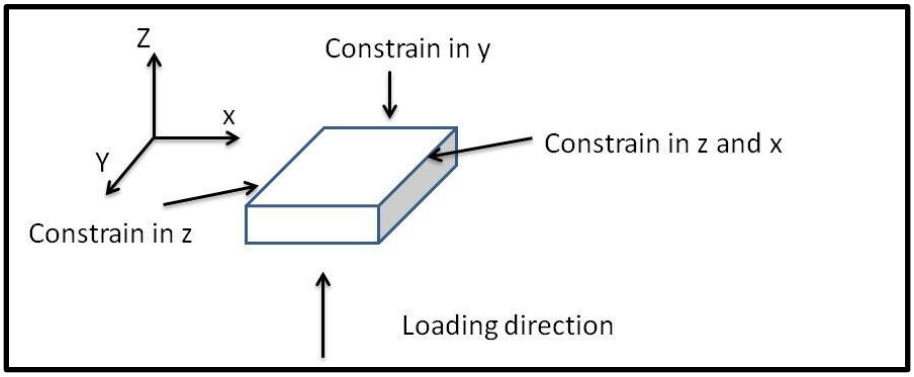

22. Save the model as an *.inp file and run on the Supercomputing Facility computers
23. To generate models with or transverse isotropic material properties (E_1=80MPa , E_2= 20 MPa, E_3=20MPa, v_{12}=0.4, v_{13}=0.1, v_{23}=0.4, G_{12}=20MPa, G_{13}=26.6MPa and G_{23}=20MPa) go back to step 4 and assign the new material properties
24. Make sure the high E value is in the same direction as the fiber connecting the bone surfaces
25. Change material properties for all the models under different loading directions and with the three I.I.
26. To add connectivity to the models go back to step one and modify the model drawing by adding connections across the suture gap. The connectivity should be 17% of the volume of the suture
27. In the material assignment module in Abaqus assign bone material properties to these bony connections
28. Repeat steps 5-21 to generate models with connectivity and isotropic material properties to the sutures
29. Change the suture material properties to transverse isotropic material as in step 23 to generate models with connectivity and transverse isotropic material properties to the sutures

µCT based models

1. Excise bone sample containing sutures from the heads
2. Micro-CT scan the samples at a 14µm resolution (GE Explore Locus, General Electric Company)
3. Load the scan in AmiraDev software
4. Segment the bone and suture boundaries using the segmentation module
5. Generate a surface from the segmentation
6. Use the surface to generate a 3D mesh using the bone surface. This will generate a mesh with 4-node tetrahedral elements
7. Save the model as *.inp file
8. Open the model in Abaqus/CAE
9. Change the mesh to 10-node tetrahedral elements
10. Assign material properties to the model the same way as in the idealized model
11. Assign loads to the model in all three directions with same constrains as in the idealized model
12. Save the models as *.inp and run them on the Supercomputing server

Analyzing the models

1. Open Abaqus viewer to do post processing
2. In Abaqus quantify the strain energy in bone area, suture area and suture/bone complex for all models
3. Output the value of strain energy for each section in each model into a text file
4. In Abaqus generate von Mises stress patterns for all models
5. Make an excel file with strain energy values for all the models
6. Scale the strain energy values based on the following equation to account for differences in volume due to changes in I.I.

$$Scaled\ SE\ for\ model\ \ B = \left(\frac{Volume\ of\ model\ B}{Volumeof\ model\ A}\right)^{\frac{1}{3}} \left(\frac{Force\ applied\ to\ B}{Force\ applied\ \ to\ A}\right)^{2} SE\ of\ model\ B$$

CHAPTER 5
Characterization of the Bending Strength of Craniofacial Sutures

5.1 Abstract

The complex, thin and irregular bones of the human craniofacial skeleton (CFS) are connected together through bony articulations and connective tissues. These articulations are known as sutures and are commonly divided into two groups, facial and cranial sutures, based on their location in the CFS. CFS sutures can exhibit highly variable degrees of interdigitation and complexity and are believed to play a role in accommodating the mechanical demands of the skull. This study aimed to evaluate the mechanical behaviour of CFS bone samples with and without sutures and to determine the effect of sutural interdigitations on mechanical strength. Sagittal, coronal, frontozygomatic and zygomaticotemporal sutures along with adjacent bone samples not containing sutures were excised from six fresh-frozen cadaveric heads. The interdigitation of the sutures was quantified through μCT based analysis. Three-point bending to failure was performed on a total of 29 samples. The bending strength of bone samples without sutures demonstrated a non-significant increase of 14% as compared to samples containing sutures (P=0.2). The bending strength of bones containing sutures was positively correlated to the sutural interdigitation index (R= 0.701, P =0.002). The higher interdigitation indices found in human cranial vs. facial sutures may be present to resist bending loads as a functional requirement in protecting the brain.

5.2 Introduction

The delicate and intricate architecture of the craniofacial skeleton (CFS) makes it more susceptible to fractures than other parts of the human skeleton[1]. The frequency of head injuries and complications in craniomaxillofacial surgery has inspired numerous studies to characterize the biomechanical behaviour of the CFS[2-9]. However, much of this work has focused on analyzing the CFS as a continuous structure without accounting for the presence of important morphological structures, the sutures. Sutures are articulations in which the margins of adjacent bones are united by fibrous or bony tissue in the CFS. They function to hold the bones of the skull together while allowing for mechanical stress transmission and deformation (i.e. distortion during childbirth, cyclic loading from muscle activity, forces from therapeutic mechanical devices and traumatic impacts) [10]. Sutures play different functions during the different stages of development. In early development the sutures provide high flexibility to allow for enlargement of the head around the eyes, brain and other organs. The sutures in the CSF can be divided into two groups based on their location: cranial and facial sutures. Cranial sutures undergo most of their growth during these early stages of development, whereas facial sutures are most active during adolescence. The adult CFS is viewed as a stable and static entity with sutures primarily functioning as shock absorbers to dissipate stresses transmitted through the skull[11-19].

Suture morphology changes from a simple flat joint in postnatal stages (which must stay patent to function) to a joint with differing degrees of interdigitation and interlocking projections in adulthood [20]. Such changes in suture morphology in healthy adults or in craniosynostosis patients remain unclear but are thought to be related to mechanical, genetic and hormonal factors[21, 22]. Under normal conditions, sutures in the human skeleton have been reported to be fully fused by late adulthood[20]. However, recent advances in micro-computed tomography allow for detailed investigations of the internal surfaces of the sutures and have shown that they remain partially open even beyond the seventh decade, with various degrees of connectivity across the suture gap (as presented in Chapter 3)[23].

The relationship between the morphological aspects of the sutures and the mechanical demands based on dietary habits in animals has been investigated through various studies such as herring *et al.(*1972) and Jaslow *et al*. (1989 and 1990). A study by Jaslow *et al*. (1990) using bone/suture samples from goats was the first to investigate the contribution of sutural

morphology in animals to the function of the CFS. The work by Jaslow *et al*. confirmed prior postulations put forward about the biomechanical behaviour of sutures which associated highly interdigitated sutures with mechanical advantage during mastication. However, to date there is no data to support that findings from studies on animal sutures are representative of the mechanical response of sutures in the human CFS. Differences in suture material properties and morphology between species may result in differences in mechanical response [24]. Experimental testing of CFS sutures in human bone samples is needed to determine their biomechanical behaviour and to identify species specific similarities and/or differences.

The aim of this study is to determine how the mechanical property of bending strength differs between CFS bones with and without sutures. It further investigates how bending strength is impacted by sutural interdigitation and tests the hypothesis that the bending strength of sutures is elevated with increased sutural interdigitation. Findings from this study will be compared to the results of Jaslow *et al.* to evaluate to similarities and/or differences between human and animal (goat) suture behaviour.

5.3 Materials and Methods

Six fresh frozen human cadaver heads (three males and three females, average age 76 years) were obtained through the Division of Anatomy at the University of Toronto. The study was conducted at Sunnybrook Health Sciences Center in accordance with the research board ethics guidelines. The heads were used to obtain test specimens of bone and sutures. Four sutures were studied: (1) sagittal suture, (2) coronal suture, (3) frontozygomatic suture (FZ), and (4) zygomaticotemporal suture (ZT) (Figure 5-1). The heads were dissected of all soft issue and stripped of the periosteum. A total of 20 sutures/bone samples and 9 bone only samples (adjacent to the sutures) were excised from the heads. Samples were cut to 10 mm wide by 15 to 20 mm long. Specimen thickness ranged from 2 to 8 mm. Because most of the samples were irregularly shaped, each specimen was individually trimmed using an Isomet saw (IsoMet® Low Speed Saw, Buehler Canada) to produce relatively uniform samples that resembled straight beams.

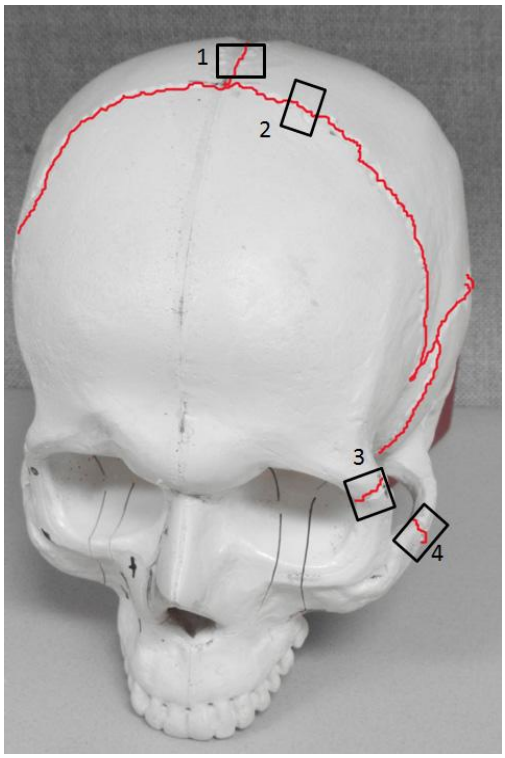

Figure 5-1: The location of the four sutures excised from the CF: (1) sagittal suture, (2) coronal suture, (3) frontozygomatic suture (FZ), and (4) zygomaticotemporal suture (ZT)

The samples were µCT scanned at an isotropic voxel size of 14µm (GE Explore Locus, General Electric Company). Two hydroxyapatite phantoms were scanned with the bone samples to quantify the bone mineral density. The µCT scans were used to obtain information about the geometry and sutural morphology of the specimens. Using tools in the imaging software AmiraDev (Amira 5.2.2, Visage Imaging, San Diego, CA) the sample width (w), mean thickness (h), and bone mineral density were measured. The degree of interdigitation (Interdigitation Index I.I.) of each suture was estimated from the µCT scans by generating 3D surfaces and tracing the path of the suture external surface and dividing that length by the straight distance between the two ends of the suture[25]. The length of the external path of the suture was measured using a custom built tool in AmiraDev (Amira 5.2.2, Visage Imaging, San Diego, CA). The length of the suture was measured as the sum of the straight distance between multiple landmarks placed over the suture line (refer to appendix E for a detailed standard operating procedure).

A custom-made three point bending fixture was used to perform the bending test. Prior to testing, the samples were thawed to room temperature. The samples were loaded as beams in three point-bending using a Bionix 858 Material Testing Systems (MTS Systems, Eden Prairie, MN). Each sample was loaded at mid-span on the external suture surface to simulate external loading on the CFS and sutures. Bending tests of the specimens were performed at a slow displacement rate of 0.8 mm/s[26] (Figure 5-2.) Each sample was loaded to fracture (indicated by force measurement of approximately zero). To standardize for size differences between the samples, the bending strength was calculated based on the elastic beam theory:

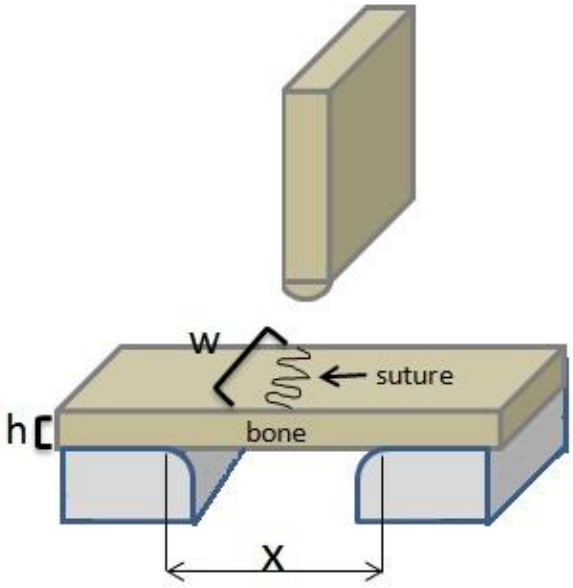

Figure 5-2: Three-point bending setup with bone sample containing suture (h is bone thickness and w is bone width). The span length (x) was 12mm. The radii of the loading nose and supports were 2mm.

$$\sigma_{max} = \frac{Mc}{I}$$

Where:

σ_{max}: Bending strength (Pa)

M=Fd : maximum bending moment (Nm)

F: peak force (N)

d: half the span length (m)

c: l/2 mean specimen thickness (m)

I= $(wh^3)/12$: second moment of area (m^4)

w: specimen width (m)

h: mean specimen thickness(m)

Linear regression analysis was used to determine if the interdigitation index predicts bending strength, controlling for density due to the different ages of the CFS samples. A Wilcoxon rank sum test was run to assess differences in bending strength between bone samples containing sutures and bone samples without sutures (Note: this nonparametric test was chosen due to the small sample sizes in the no suture bone group).

5.4 Results

Bone samples with and without sutures were loaded to failure in bending. The results are summarized in Figure 5-3 in which the bending strength is plotted against the interdigitation index. The average bending strength for bones without sutures was 243 ±63 MPa, 14% higher than bones containing sutures (average 213 ± 93 MPa). However, the Wilcoxon rank sum test result showed no statistical differences between these two groups (P=0.2). In the specimens containing sutures, regression showed bending strength increased significantly with increasing in I.I. (R=0.701, P=0.002). The highest I.I. was found in the sagittal suture samples while the lowest I.I. was found in the zygomaticotemporal suture samples. There was no relationship found between bone density alone and bending strength (P=0.321).

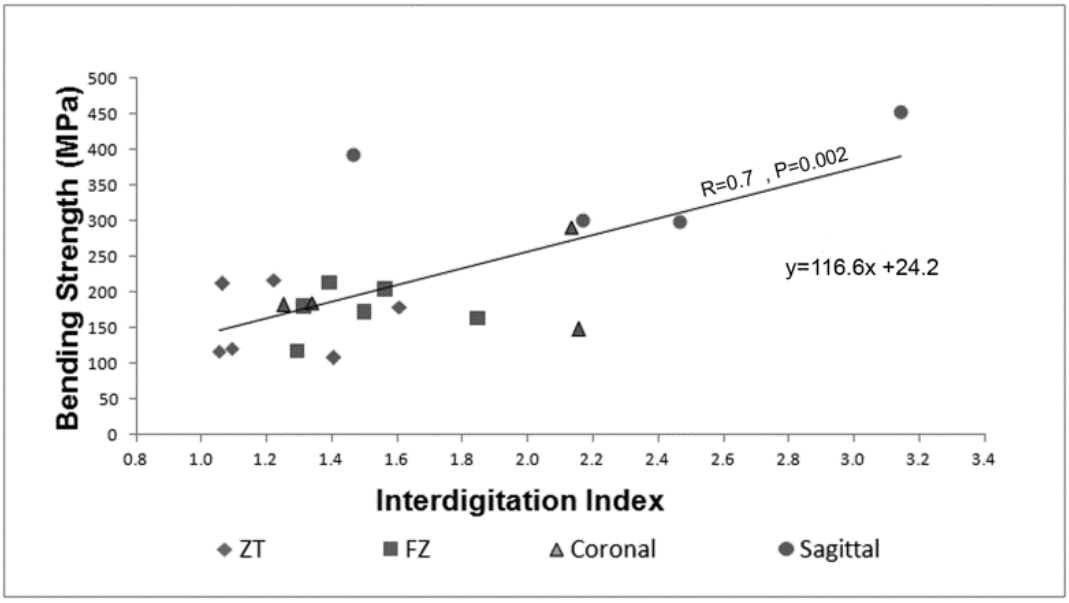

Figure 5-3: Bending strength vs. interdigitation index for bone samples containing zygomaticotemporal (ZT), frontozygomatic (FZ), coronal and sagittal sutures

5.5 Discussion

The present study tested the bending strength of CFS bones with and without sutures and analyzed the relationship between bending strength and the interdigitation of sutures. The average bending strength of bone samples without sutures was 14% higher than average strength of bone samples with suture, however this difference was not statistically significant. While a higher bending strength of bones without sutures was expected, the non-significant difference was much lower than differences previously reported in samples obtained from goats. In the study by Jaslow *et al.* the bending strength was on average approximately 40% higher in goat cranial bones without sutures (259MPa) than cranial bones with sutures [26]. Yet the most highly interdigitated sutures in this study (I.I. from 4 to 6) when loaded slowly yielded similar bending strength to the cranial bones without sutures. Previous work by Hubbard *et al*. on cranial sutures and cranial bones from human calvarium, found that cranial sutures under quasistatic loading are generally as strong in bending as cranial bones without sutures. The bending strength of bone samples without sutures are similar in the present study (243MPa) to values reported by Jaslow

et al. and cortical bone bending strength reported by other investigators (average of 256 MPa)[27, 28].

Differences in bending strength in the presence of sutures between humans and animals may be explained by variation in suture morphology. It is possible that the inner structure of human sutures, which exhibit changes in I.I. and connectivity throughout their thickness, may restrict bending motion within the collagen of the suture itself and require all bending to occur through the calcified tissue. Alternatively, the elasticity of the collagen may allow bending motion to occur until the bony edges of the suture are in contact, leading to fracture when the bony elements fail. The mechanical behaviour of sutures in the human CFS may behave differently to that of goats due to functional differences (i.e dietary habits and head butting). Further study and experimentation examining motion at the suture gap during loading and the initiation of failure is needed to better understand the behaviour of the overall bone/suture complex.

The samples failed either by separation through the suture or by fracture of the sample away from the suture site (Figure 5-4). Of the twenty suture beams samples tested, thirteen samples (7 cranial and 6 facial) failed by suture separation, indicating that the sutures were generally weaker in bending than the adjacent cranial bones. The other seven sutures (1 cranial and 6 facial) failed at the supporting column site. In three point bending test samples are expected to fail at a consistent location, yet in this study ½ of facial suture samples failed at the location of the supporting column. Upon closer investigation of the internal morphology of the samples it appeared that these samples had trabecular mesh with cortical bone shell toward the edges making them weaker than the center where they were primarily composed of dense cortical bone. This difference in internal structure between the samples may have led to the variations in fracture location. Samples breaking at the suture were found to have a higher average bending strength than samples breaking away from the suture.

Bone undergoes considerable yield and plastic deformation prior to failure, violating the basic assumption of elastic beam theory and resulting in an overestimation of bending strength. In general, although widely used, analyses of bone based on beam theory are limited in their assumption that the material properties of the bone are homogeneous and isotropic[29, 30]. The influence of such variations in material properties is generally assumed to be insignificant, but the presence of sutures in the bone samples may elevate the error attributed to this violation.

Despite these limitations, application of beam theory to bone samples has been shown to provide useful information when used as a mean to compare relative differences, as utilized in this study[29].

This study also analyzed the relationship between bending strength and the interdigitation of sutures, finding interdigitation to be positively correlated to bending strength. The findings of the highest average I.I. in the sagittal suture samples and the lowest average I.I. in the zygomaticotemporal suture samples is consistent with observations reported in Chapter 3 where more interdigitations were present in cranial sutures than facial sutures[23]. This could be related to the mechanical demand of different region of the CFS. Although the difference in the I.I. was small between the different sample groups, an increase in average bending strength was observed with sagittal suture group having the highest bending strength and the zygomaticotemporal suture group having the lowest bending strength. The significant increase in bending strength with increase in I.I. (P=0.002) is consistent with findings by Jaslow *et al.* from suture samples obtained from goats.

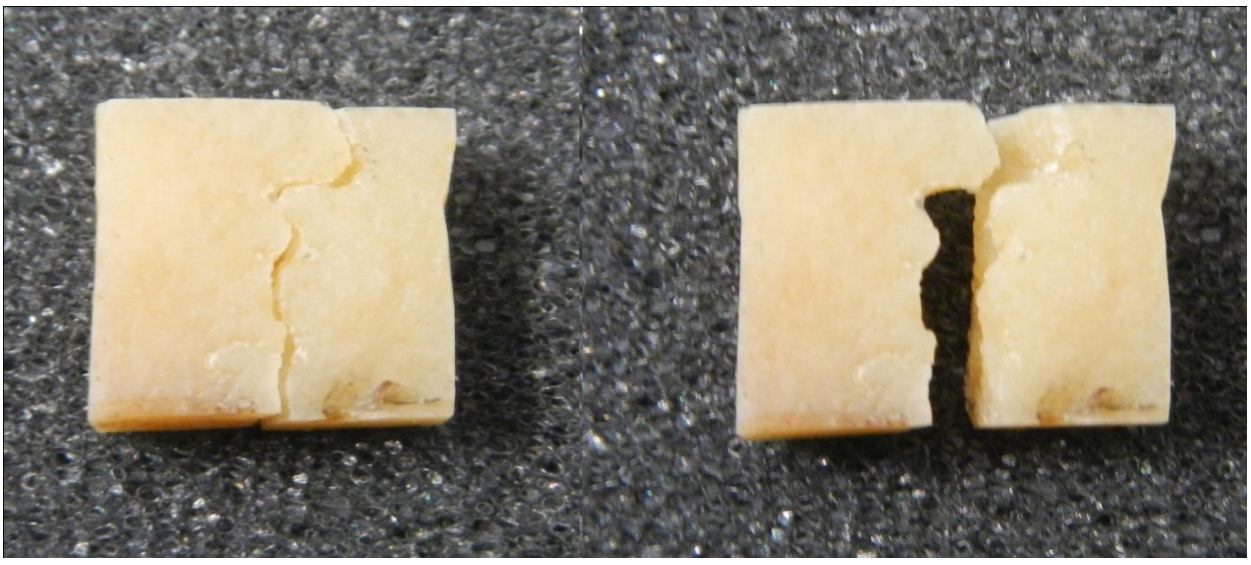

Figure 5-4: Bone containing coronal suture separated at suture site

The complexity and curvature of the CFS bones limited the ability to obtain larger test samples with longer suture segments. In particular, the degree of interdigitation of cranial sutures varies along the suture line and can differ greatly based on location (rostral or caudal). Obtaining

multiple bone segments with a wider range of sutural interdigitations was not feasible due to the higher degree of curvature in the caudal end of the cranium. This limited the suture to be excised from the rostral end of the heads. Furthermore, the irregular shape of the bone restricted our ability to use other sutures in the CFS such as the zygomaticomaxillary suture, which is located closer to areas of bite force transmission. Testing sutures positioned at different distances from areas of bite force would provide more information about the role of suture morphology in load transmission in the CFS. The number of available fresh frozen cadaver heads limited the sample size and as such the variability of the sutural interdigitations. The limited sample size also prevented the evaluation of behaviour at differing loading speeds (i.e. potential differences in mechanical behaviour resulting under faster impact loading). The interdigitating sutural interfaces are geometrically complex, and their configuration varies highly with site in a single CFS and between subjects.

Overall, this work yields important information about human CFS sutures, an important aspect in characterization of the mechanical response of the CFS due to internal and external loading. Cranial sutures have a higher I.I. and bending strength than facial sutures. The brain case and facial skeleton might be developed and evolved for different functions yielding differing morphology and mechanical response of the sutures in these sites. The bending strength of CFS sutures was positively correlated to I.I. but not to bone density alone. Sutural morphology varies considerably within human skulls and between different species. Such differences that exist in human sutures as compared to sutures from other species motivate utilizing human specific CFS models in future work.

5.6 References

1. Hardt N, Kuttenberger J, ebrary I. Craniofacial trauma. 2010:278. Available from: http://link.library.utoronto.ca/eir/EIRdetail.cfm?Resources__ID=1157113&T=F.

2. Hylander WL, Johnson KR. In vivo bone strain patterns in the zygomatic arch of macaques and the significance of these patterns for functional interpretations of craniofacial form. *Am J Phys Anthropol.* 1997;102:203-232.

3. Rudderman RH, Mullen RL. Biomechanics of the facial skeleton. *Clin Plast Surg.* 1992;19:11-29.

4. Orringer JS, Barcelona V, Buchman SR. Reasons for removal of rigid internal fixation devices in craniofacial surgery. *J Craniofac Surg.* 1998;9:40-44.

5. Nagase DY, Courtemanche DJ, Peters DA. Plate removal in traumatic facial fractures: 13-year practice review. *Ann Plast Surg.* 2005;55:608-611.

6. Kasrai L, Hearn T, Gur E, et al. A biomechanical analysis of the orbitozygomatic complex in human cadavers: Examination of load sharing and failure patterns following fixation with titanium and bioresorbable plating systems. *J Craniofac Surg.* 1999;10:237-243.

7. Herring SW, Teng S, Huang X, et al. Patterns of bone strain in the zygomatic arch. *Anat Rec.* 1996;246:446-457.

8. Oyen OJ, Tsay TP. A biomechanical analysis of craniofacial form and bite force. *Am J Orthod Dentofacial Orthop.* 1991;99:298-309.

9. Szwedowski TD, Whyne CM, Fialkov JA. Toward characterization of craniofacial biomechanics. *J Craniofac Surg.* 2010;21:202-207.

10. Mao JJ, Wang X, Kopher RA. Biomechanics of craniofacial sutures: Orthopedic implications. *Angle Orthod.* 2003;73:128-135.

11. Buckland-Wright JC. Bone structure and the patterns of force transmission in the cat skull (felis catus). *J Morphol.* 1978;155:35-61.

12. Jaslow CR. Mechanical properties of cranial sutures. *J Biomech.* 1990;23:313-321.

13. Jaslow CR, Biewener AA. Strain patterns in the horncores, cranial bones and sutures of goats (capra hircus) during impact loading. *J Zool.* 1995;235:193-210. Available from: http://dx.doi.org/10.1111/j.1469-7998.1995.tb05137.x.

14. Herring SW, Teng S. Strain in the braincase and its sutures during function. *Am J Phys Anthropol.* 2000;112:575-593.

15. Byron CD, Borke J, Yu J, et al. Effects of increased muscle mass on mouse sagittal suture morphology and mechanics. *Anat Rec A Discov Mol Cell Evol Biol.* 2004;279:676-684.

16. Rayfield EJ. Cranial mechanics and feeding in tyrannosaurus rex. *Proc Biol Sci.* 2004;271:1451-1459.

17. Pritchard JJ, SCOTT JH, GIRGIS FG. The structure and development of cranial and facial sutures. *J Anat.* 1956;90:73-86.

18. Rafferty KL, Herring SW, Marshall CD. Biomechanics of the rostrum and the role of facial sutures. *J Morphol.* 2003;257:33-44.

19. Rayfield EJ. Using finite-element analysis to investigate suture morphology: A case study using large carnivorous dinosaurs. *Anat Rec A Discov Mol Cell Evol Biol.* 2005;283:349-365.

20. Rice DP. Developmental anatomy of craniofacial sutures. *Front Oral Biol.* 2008;12:1-21.

21. Herring SW. Mechanical influences on suture development and patency. *Front Oral Biol.* 2008;12:41-56.

22. Persson M, Magnusson BC, Thilander B. Sutural closure in rabbit and man: A morphological and histochemical study. *J Anat.* 1978;125:313-321.

23. Maloul A, Fialkov J, Hojjat SP, et al. A technique for the quantification of the 3D connectivity of thin articulations in bony sutures. *J Biomech.* 2010;43:1227-1230.

24. Carmody KA, Mooney MP, Cooper GM, et al. Relationship of premaxillary bone and its sutures to deciduous dentition in nonhuman primates. *Cleft Palate Craniofac J.* 2008;45:93-100.

25. Rafferty KL, Herring SW. Craniofacial sutures: Morphology, growth, and in vivo masticatory strains. *J Morphol.* 1999;242:167-179.

26. Jaslow CR. Mechanical properties of cranial sutures. *J Biomech.* 1990;23:313-321.

27. Burstein AH, Currey JD, Frankel VH, et al. The ultimate properties of bone tissue: The effects of yielding. *J Biomech.* 1972;5:35-44.

28. Currey JD. Mechanical properties of bone tissues with greatly differing functions. *J Biomech.* 1979;12:313-319.

29. Burstein AH, Wright TM. *Fundamentals of Orthopaedic Biomechanics.* Baltimore: Williams & Wilkins, 1994.

30. Seeman E, Delmas PD. Bone quality--the material and structural basis of bone strength and fragility. *N Engl J Med.* 2006;354:2250-2261.

5.7 Appendix E

Standard operating procedure:

1. Determine the location of the sample to be excised by outlining the bone edges on the head with a pencil
2. Use a dremel to excise the samples
3. Use an Isomet saw to shape the sample to produce relatively uniform samples that resembled straight beams
4. Place each sample in a plastic bag and label it with sample name and head ID
5. Scan the samples in a µCT scanner at a 14µ resolution (GE Explore Locus, General Electric Company)
6. Make sure to place bone phantoms with each scan (Skyscan phantoms)
7. Use a three point bending fixture with span of 12mm and 2mm radii of curvature for supports and loading nose.
8. Attach the three point bending fixture to a Material Testing Station (MTS)
9. Place each sample on the supporting columns
10. Load the sample at a rate of 0.8mm/s to failure
11. Note the location of the fracture in the samples containing sutures
12. Record the peak force at failure for each sample

Data Analysis

Samples containing sutures:

1. Open each sample scan in AmiraDev software
2. Using the landmarks module measure the thinness and width of each sample
3. Measure each value three times
4. Generate an isosurface from the scan
5. Using the custom built in tool called DistSum place landmarks along the suture path on the surface
6. Make sure landmarks are places very close to each other
7. DistSum will output the length of the suture along the path
8. Use the first and last landmarks on the suture path to measure the straight distance between the suture ends

9. Calculate I.I. for each suture by dividing the suture length along the suture path by the straight distance between the suture ends
10. To calculate the bending strength use the following equation and the peak force, suture thickness, suture width and span of testing fixture

$$\sigma_{max} = \frac{Mc}{I}$$

Where:
σ_{max}: Bending strength (Pa)
M=Fd : maximum bending moment (Nm)
F: peak force (N)
d: half the span length (m)
c: l/2 mean specimen thickness (m)
I= (wh^3)/12 : second moment of area (m^4)
w: specimen width (m)
h: mean specimen thickness(m)

Samples without sutures:

1. Open each sample scan in AmiraDev software
2. Using the landmarks module measure the thinness and width of each sample
3. Measure each value three times
4. Calculate bending strength as in step 10

<u>Density Quantification:</u>

1. Open sample scan in AmiraDev software
2. Identify the two bone phantoms in the scan
3. Using the segmentation module in Amira segment the area representing each phantom
4. Using the histogram tool in Amira find the average intensity of each phantom
5. The lower intensity phantom will correspond to 0.25 mg/cm^3 bone density and the higher intensity phantom will correspond to 0.75 mg/cm^3
6. Using the intensity and density values find the linear equation for correlating intensity to density
7. Using the segmentation module in Amira segment the bone sample in each scan
8. Quantify the mean intensity for the bone
9. Using the equation in step 6 convert the intensity to bone density for each sample

CHAPTER 6
In Vitro Quantification of Strain Patterns in the Craniofacial Skeleton due to Masseter and Temporalis Activity

6.1 Abstract

Many complications in craniofacial surgery can be attributed to a lack of characterization of facial skeletal strain patterns. This study aims to delineate human midfacial strain patterns under uniform muscle loading. The left sides of 5 fresh frozen human cadaveric heads were dissected of all soft tissues except the temporalis and masseter muscles. Tensile forces were applied to the free mandibular ends of the muscles. Maxillary alveolar arches were used to restrain the skulls. Eight strain gauges were bonded to the surface of the midface to measure the strain under single muscle loading conditions (100N). Maxillary strain gauges revealed a biaxial load state for both muscles. Thin antral bone experienced high maximum principal tensile strains (Maximum of 685.5με) and high minimum principal compressive strains (Maximum of -722.44 με). Similar biaxial patterns of lower magnitude were measured on the zygoma (Maximum of 208.59 με for maximum principal strains and -78.11 με for minimum principal strains). Results, consistent for all specimens and counter to previously accepted concepts of biomechanical behaviour of the midface under masticatory muscle loading, included high strain in the thin maxillary antral wall, rotational bending through the maxilla and zygoma, and a previously under-estimated contribution of the temporalis muscle. This experimental model produced repeatable strain patterns quantifying the mechanics of the facial skeleton. These new, counter-intuitive findings underscore the need for accurate characterization of craniofacial strain patterns to address problems in current treatment methods and develop robust design criteria.

6.2 Introduction

In spite of new technologies and methods of osteosynthesis in the field of craniomaxillofacial surgery, patients continue to experience significant complications. Assumptions about craniofacial loading and strain patterns have led to hardware related complications, often resulting in the need for re-operation[1-4]. The complex skeletal anatomy and the intricate soft tissue and muscular system of the craniofacial region present significant challenges for replication and strain quantification. A functional adaptation theory has been proposed to describe the development of the craniofacial skeleton (CFS) stating that "facial bones are optimized for countering masticatory loads, i.e. that they exhibit minimum material and maximum strength for countering cyclical loading regimes"[5]. Furthermore, the standard approach in understanding craniofacial biomechanics has been based on the "buttress" anatomy and "beam" hypothesis[6-9]. This approach has been utilized to reduce the complex structure of the CFS into simpler and therefore more easily understood structures[10-12]. This has led to the development of osteosynthetic treatment regimens that are based on simplified mechanical models of craniofacial loading and strain distribution. However, the stresses and strains present in the CFS are not easily understood due to the complex bone morphology, the complexity of muscle loading and the variations in bone elastic properties. As a consequence of this lack of understanding, it has been suggested that osteosynthetic fixation techniques have been either "over" or "under-engineered" with the result of a significant rate of fixation hardware related complications the latter often leading to re-operation[1, 4].

A great volume of literature has been published on appropriate treatment for common CFS fractures. The issue of greatest attention has been the amount and location of hardware required to stabilize fractured bones against subsequent forces (primarily mastication) that may displace them. In spite of the multitude of methods of fracture stabilization studied, there is no consensus as to the optimal amount and location of fixation hardware to optimize treatment of the CFS. One of the more common reasons for re-operation is the removal of fixation devices, a consequence of over-engineering[3, 13, 14]. Designing devices and treatments for the CFS without accounting for the actual complexities of the true mechanical environment continues to result in sub-optimal treatment modalities. Characterizing the biomechanical environment of the CFS is essential for developing techniques that address its structure and function effectively.

Previous experimental work has been conducted on both cadaveric heads and primates to understand the biomechanical behaviour of healthy intact and reconstructed parts of the most complex part of the CFS, the midfacial region[5,15-28]. Earlier attempts to characterize the strain patterns produced in the midfacial region by the masseter and temporalis muscles were conducted by Endo *et al.*[11, 12]. In these studies canvas sheets were glued onto the masticatory muscular attachments to apply forces to the skull. Since then methods of force application in studies on cadaveric heads have not attempted to replicate true loading through the muscle-bone interface. Loading scenarios ranged from pulleys and rope systems to direct compressive forces applied to the zygomatic body; yet the direction and magnitude of these applied loads were unrelated to the anatomic pull of the muscles of mastication. For example, a study by Kasrai *et al.* was conducted by applying cyclic load to a contact point on the zygomatic body while another study by Alberts *et al.* was conducted by applying the force directly through the palate[29, 30]. These methods of force applications do not account for complex anatomic factors such as the hyperelastic behaviour of the muscles, which can affect strain patterns in the bone[31]. Such approaches limit studies aimed at characterizing the strain patterns of the CFS for the purpose of optimizing treatment methods and reducing patient morbidity.

More sophisticated biomechanical approaches have been used to delineate the forces and strain patterns of the CFS *in vivo*[5, 16, 17, 28]. The studies by Oyen *et al.* were conducted on monkeys to characterize strain patterns due to mastication by stimulating contractions of the jaw elevator muscles[16, 17]. Similarly *in vivo* studies by Hylander et *al.* and Ross et *al.* were conducted in macaques to measure strains in the midfacial region during mastication[5]. Although the force application in *in vivo* studies represents the most appropriate approach to measure strains in the CFS, the ethical considerations in humans and the limitations in placing multiple strain gauges on the CFS limits investigation of the strain in the full human CFS.

Computational modeling has also been utilized to quantify the biomechanical behaviour of the CFS[18, 20-26, 31-35]. The development of experimentally validated finite element (FE) models presents a robust method to generate full field information throughout the CFS under multiple loading configurations. However, due to the complexities in generating these FE models, to date these computationally intensive studies have generally been limited to single specimen specific model[31, 34, 36]. Single specimen results may not be reflective of general strain patterns due to the variety of morphologic differences between individuals. Characterizing patterns that can be

applied generally in practice and design requires consistent analysis of multiple specimens, taking into account previously unaccounted for mechanical constructs such as the muscle bone interface. The objective of the present study is to characterize and quantify the strain patterns in the midfacial region of the human CFS under muscle loading. It is hypothesized that strain patterns in the midfacial region of the CFS will yield consistent patterns despite morphologic variation.

6.3 Methods

Five fresh frozen human cadaveric heads of two males and three females (average age 86 years) were obtained through the Division of Anatomy at the University of Toronto. The study was conducted at Sunnybrook Health Sciences Center in accordance with the research board ethics guidelines. Prior to mechanical testing a CT scan was acquired for each of the 5 cadaveric heads at a voxel size of 0.488mm (Light speed VCT GE Medical Systems, GE Healthcare, Waukesha, WI). Before scanning, radiopaque fiducial markers were affixed to four positions on the CFS to provide a 3D coordinate system for subsequent data processing. The locations were the occipital region, the parietal temporal bone, the front of the maxilla directly above the incisors region and the mid-forehead.

After scanning, the left sides of the 5 cadaveric heads were dissected of all soft tissues except for the temporalis and masseter muscles. The masseter muscle was released from its insertion in the mandibular angle to allow load application. Similarly, the caudal end of the temporalis muscle was released by means of *coronoidotomy* using a surgical saw and thus keeping a small fragment of the coronoid to be used for load transmission during mechanical testing. The fascial attachments of the temporalis muscle were detached from the zygomatic arch to allow free motion of the muscle. Dehydration of the muscles during testing was minimized by regularly applying saline solution to the bodies of both muscles.

To mimic the mastication forces on the CFS, aluminum interface plates were affixed along the free end of the muscles using Ti-Cron 1/0 sutures (Syneture Inc., Covidien, Mansfield, MA). The maxillary occlusal arch was used as the restraint position for the skulls to mimic occlusion during mastication. A specially designed fixture and bone cement were used to stabilize the skull through the occlusal arch during mechanical testing (Figure 6-1). In the edentulous heads (3 specimens) four surgical screws (4.5mm diameter x 30 mm length cortex screw) were inserted

vertically into the maxillary alveolar bone, two on either side of midline for better anchorage of the cement.

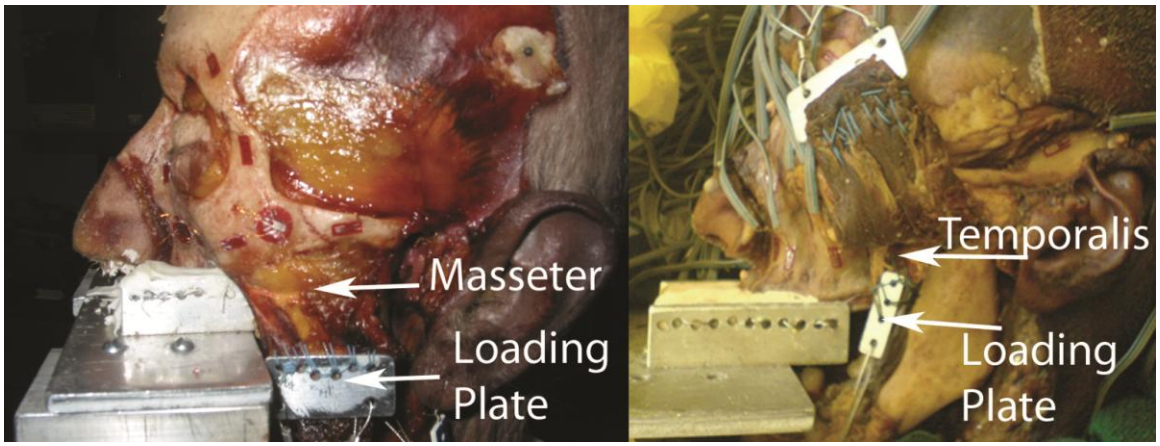

Figure 6-1: Masseter interface plate configuration (*left*) and Temporalis interface plate configuration (*right*)

Each skull was mounted on the Bionix 858 Material Testing Systems (MTS Systems, Eden Prairie, MN). A stainless steel wire was used to provide a link between the interface plates attached to the muscles and the tensile force actuator on the MTS. Strain gauges were bonded to the CFS surfaces and digitized using a microscribe (Immersion Corp., San Jose, CA) prior to testing. The fiducials were digitized to be able to determine the exact locations of the strains on 3D surfaces generated from the CT scans. A total of 6 uniaxial and 2 rosette strain gauges (FLA-3-11-3LT, Tokyo Sokki Kenkyujo Co.,Ltd., Tokyo, Japan) were bonded to the bony surface of the midfacial region of the CFS (Figure 6-2).

The location of the two rosette strain gauges (3 and 6) and four uniaxial strain gauges (1,2,7,8) were standardized using anatomical land marks such as the Nasofrontal suture (1), Naso-maxillary Suture (2), Infraorbital foramen (3), Zygomaticotemporal suture (6), frontozygomatic suture (7 and 8). The location of strain gauges 4 and 5 were not standardized and varied between specimens to obtain additional information about strain in other regions of the mid-facial area. To ensure strong bonding of the strain gauges to the bone surface the periosteum was dissected away and a dremel equipped with a polishing brush was used to ensure clean bone surfaces. The curvature and presence of multiple bony articulations dictated the regions where the strain

gauges could be mounted. Loading of the skull consisted of single muscle (masseter then temporalis) loading in tension to 100N (3 times) at a rate of 1cm/min. The 100N force application was chosen to represent bite force. This force is below the bite force reported by other studies [30, 37]. However, during mechanical testing a force higher than 100N would tear the muscle with repeated loading therefore the force had to be lowered to 100N (refer to appendix F for a detailed standard operating procedure).

Strain is a measure of the amount of deformation of a body due to applied force. It is a dimensionless unit equalling the change in object length divided by its original length. Tensile strain is measured as a positive value and compressive strain as negative value. The maximum and minimum principles strains are the largest tensile strains and the largest compressive strains, respectively. Strain was measured using a data acquisition system (DAQBOOK/2000a – signal conditioner w/ a DBK43a, IOTECH, Cleveland, Ohio). To assess the agreement between the strains measured from the five specimens an intraclass correlation coefficient test was used. Intraclass correlation coefficient is a measure of the relative similarity of quantities within sets of elements which possess common characteristics. The coefficient is used as a general descriptive statistics whose maximal value is +1 if all quantities in the group have the same value[38, 39].

6.4 Results

In this study the measured strains for all 5 specimens under masseter and temporalis loading are summarized in Table 6-1 and Table 6-2 presented visually in Figure 6-2. In all specimens the rosette strain gauge located on the maxilla revealed a biaxial load state under both temporalis and masseter loading. Under masseter loading in all five heads the thin maxillary anterior antral wall experienced high maximum principal tensile strains (average angle 33° clockwise from the facial vertical axis) ranging from 139.68 to 685.5με and high minimum principal compressive strains ranging from -172.43 to -722.44με. Similar strain patterns (average angle 16° clockwise from the facial vertical axis) were found in the same location in 4 out of 5 heads under temporalis loading with a maximum principal tensile strains ranging from 100.16 to 454.11με and minimum principal compressive strains ranging from -102.90 to -489.98με.

Table 6-1: *In vitro* strain measurements (mean and standard deviation) under a 100N tensile load applied through the masseter.

Masseter Muscle Loading (100N)					
Specimen	SP1	SP2	SP3	SP4	SP5
Gauge Number	Strain (με)	Strain (με)	Strain (με)	Strain (με)	Strain (με)
1	-8.89±1.8	----------	-43.36±3.29	-1.69±0.72	-2.96±0.58
2	46.67±1.28	17.8±3.65	31.51±2.29	-7.48±4.77	-3.9±0.22
3a*	-182.05±2.61	-722.44±28.77	-463.55±8.72	-475.92±17.96	-172.43±1.81
3b**	174.66±5.89	685.5±26.86	139.68±2.59	314.07±7.33	254.98±4.60
4	-63.68±7.13	-59.15±3.84	-248±3.29	-179.4±7.63	-47.05±0.93
5	177.38±2.18	-22.44±1.00	63.06±1.93	40.09±53.2	78.11±4.94
6a*	-66.32±3.68	-54.47±2.57	-68.16±4.33	22.64±1.93	-78.1±1.32
6b**	208.59±2.80	102.07±1.47	168.15±4.67	92.47±2.37	97.23±1.09
7	153.89±3.68	160.28±4.86	290.64±4.00	97.73±1.38	100.18±1.2
8	10.38±0.33	4.91±0.41	5.13±1.1	11.4±2.01	2.12±8.06

* Minimum Principal Strain from rosette ** Maximum Principal Strain from rosette

με: microstrain

Table 6-2: *In vitro* strain measurements (mean and standard deviation) a 100N tensile load applied through the temporalis.

Temporalis Muscle Loading (100N)					
Specimen	SP1	SP2	SP3	SP4	SP5
Gauge Number	Strain (με)	Strain (με)	Strain (με)	Strain (με)	Strain (με)
1	-6.94±1.47	----------	6.99	-2.03±0.35	5.12±0.21
2	-8.21±0.49	3.81±2.63	6.44	-6.67±1.85	-1.57±0.17
3a*	-176.72±5.76	-462.01±10.83	-489.98	-445.23±14.03	-102.90±1.71
3b**	258.94±9.27	454.11±9.22	100.16	295.03±8.15	367.86±6.99
4	-18.50±6.12	-57.64±2.48	-279.90	-139.55±3.04	-58.14±1.68
5	164.03±2.18	29.77±0.79	58.70	35.67±3.91	-65.39±1.12
6a*	-8.06±3.91	-3.22±0.86	-17.66	-2.04±2.93	-63.85±2.70
6b**	86.07±0.99	34.16±0.88	32.25	71.97±2.75	71.51±2.09
7	5.98±4.59	16.16±0.58	-37.81	-8.05±3.21	-43.37±0.90
8	-6.00±0.88	-10.75±1.10	14.61	-10.11±0.90	-7.34±1.98

* Minimum Principal Strain from rosette ** Maximum Principal Strain from rosette

με: microstrain

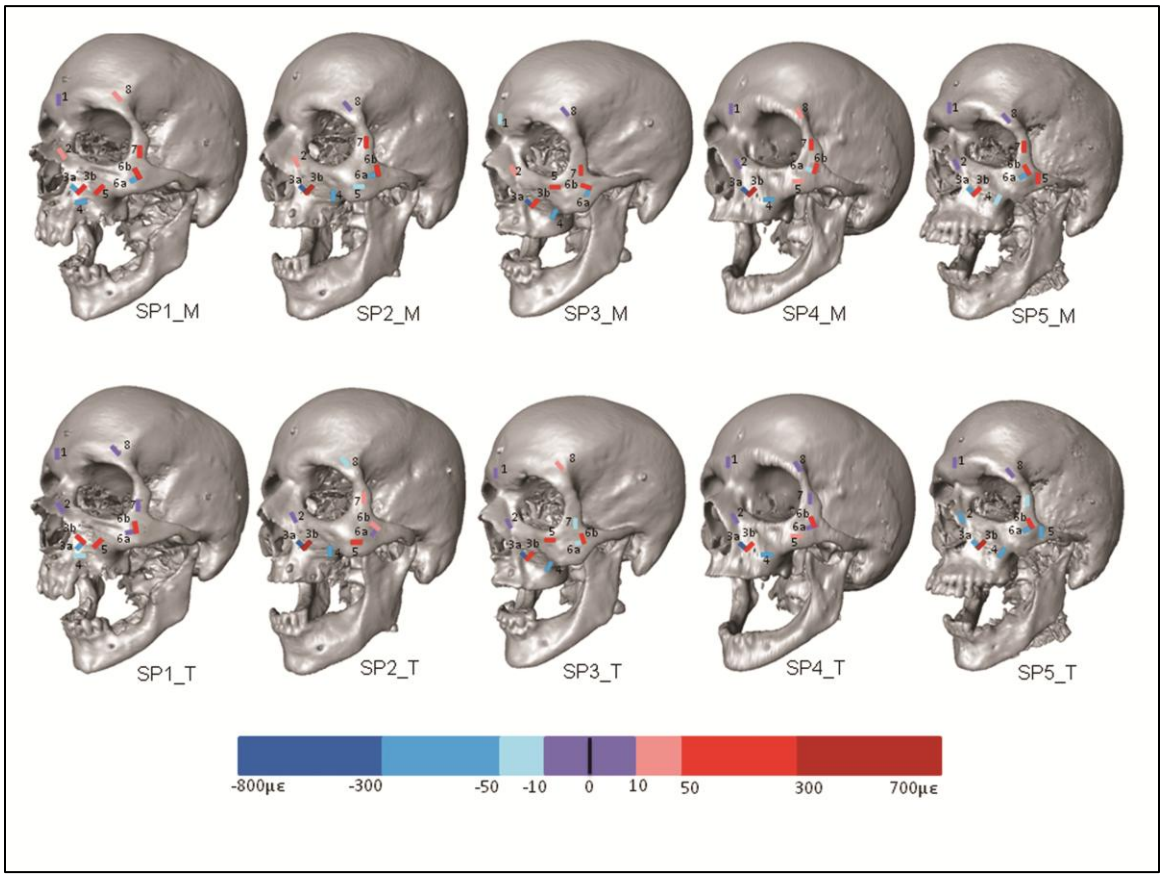

Figure 6-2: CT generated specimen specific 3D models of the five cadaveric heads with strain gauge positions and *in vitro* strain measurements. The upper row represents strains generated through Masseter muscle loading and the lower row represents strains generated through Temporalis muscle loading.

Similar biaxial strain patterns of lower magnitude were measured on the zygoma under both temporalis and masseter loading except for one specimen (SP4_M). Under masseter loading the rosette strain gauge on the zygoma revealed maximum principal tensile strains (average angle 18° counter clockwise from the face long axis) ranging from 92.47 to 208.59 με and minimum principal compressive strains ranging from -78.11 to 22.64 με. Temporalis loading revealed lower strain magnitudes with maximum principal tensile strains (average angle 12° counter clockwise from the face long axis) ranging from 32.25 to 86.07 με and minimum principal compressive strains ranging from -2.04 to -63.85με. The strain measured from SP2 at the location of gauge 1 was not used for analysis due to the detachment of the strain gauge during

the loading. Unlike other specimens SP3 was loaded only one time up to 100 N as the muscles were in bad conditions and tearing of the muscles occurred during the second loading.

Uniaxial strain gauges revealed high tensile strains on the frontal process of the zygoma during masseter loading (maximum 290.64 με). Uniaxial strain gauges also revealed that low strains were present in the supraorbital rim, nasal and frontal bones during masseter and temporalis loading. In spite of the morphological differences between the 5 heads, the overall strain patterns were similar in 4 out of the 5 heads for each of the muscle loading conditions. The statistical analysis showed that the intraclass correlation coefficient (excluding strain gauge 1 due to missing data) for the masseter and temporalis muscles loading cases were 0.73 and 0.77 (good to excellent reproducibility), respectively. However, when strains measured from gauges 4 and 5 were excluded from the statistical analysis due to large variations in the gauge locations, the intraclass correlation coefficient for the masseter and temporalis muscles loading cases improved to 0.75 and 0.81 (excellent reproducibility), respectively.

6.5 Discussion

This study successfully quantified strains generated through muscle loading in the midface region of 5 cadaveric specimens. The overall strain patterns were found to be consistent despite morphological variations between the CFSs, absence or presence of teeth and gender. The biomechanical behaviour in the midfacial region with masticatory muscle loading revealed some unexpected strain patterns. Although the highest magnitude strains were found in the maxillary buttresses, strains over the maxillary anterior antral wall were surprisingly high given the thinness of that bone. This is counter to assumptions classically made about the form-function relationship in the CFS, which would imply that little strain is experienced by thin bone structures. Furthermore, the strain directions revealed that the maxilla and zygoma undergo bending in the coronal and sagittal planes during both masseter and temporalis loading (Figure 6-3). These unexpected patterns of mechanical behaviour highlight the importance of a full and accurate characterization of the biomechanical behaviour of the CFS for the optimization of reconstructive and osteosynthetic technologies.

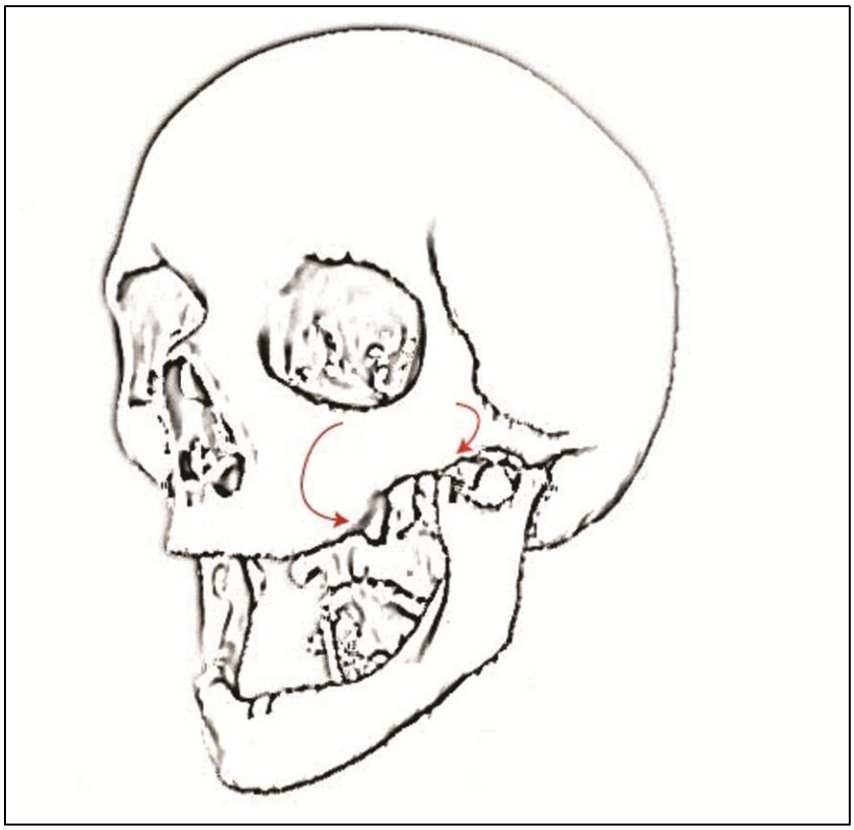

Figure 6-3: Bending direction of the zygoma (red arrows) due to muscle loading.

Several studies have identified the masseter muscle as the primarily displacing force in the CFS and a main contributor to the strains produced in the face[17, 40-42]. When loading through this muscle, high tensile strains were produced in the zygomatic complex and high compressive strains in the vertical maxillary buttress. In this study high tensile strains were predominant in the frontal process of the zygoma in all five specimens (Gauge 7). Similar findings were reported by Endo *et al.* when applying forces to canvas sheets glued onto the muscular attachment[11, 12]. These high tensile strains in the frontal process explain the deformation and stretching observed in the failure of fixation plates in this region[29]. Also, the direction of the bilateral maximum and minimum strains on the zygoma (gauges 6a & 6b) combined with the cephalo-lateral tensile maximum principal strains in the superior portion of the maxilla indicate that the zygoma is subjected to a bending moment. This bending in the midfacial region due to torsion of the zygomatic arch was also reported by Ross's *in vivo* study on macaques[28]. The similarity of this

deformation patterns to those observed by Ross's *in vivo* study support the use of this *in vitro* model to characterize the biomechanical behaviour of the human CFS. The cephalo-lateral direction of strain on the superior maxilla and the bending of the zygoma produces tensile strains in the inferior orbital rim. This strain pattern in the orbital rim could cause screw failure (pullout) which is consistent with the results reported by Kasrai *et al*. about screw failure in that region. These strain patterns due to the loading through the masseter are important in understanding hardware failure patterns reported by other investigators.

The predominant presence of the tensile strains in the zygomatic complex was also reported from *in vivo* studies of primates. The direction of these tensile strains reported in our study is consistent with *in vivo* results[16, 17, 28]. The *in vivo* studies by Oyen *et al*. on monkeys, conducted to measure strain in the frontal process by simulating the mastication muscles, revealed that the strains observed in the outer cortical surface of the zygoma are predominantly tensile. Although the strain measured in our study is generated through individual muscle loading only, it resembles strains produced by isometric forceful occlusion in primate *in vivo* studies lending validity to our model [15-17]. The *in vivo* study by Hylander *et al*. (1997) on 5 macaques to measure strains during mastication on the zygomatic arch, showed that the direction of the maximum principal strain is cephalad and anterior. This is similar to the direction of principal strain our rosette strain gauges (6a & 6b) revealed on the body of the zygoma close to the anterior region of the zygomatic arch. Based on our study and previous *in vivo* studies it appears that the cephalad tensile strains in the frontal process of the zygoma and anterior portion of the zygomatic arch are the predominant strains. Moreover, the magnitude of the strain in the supraorbital and glabellar regions is very little compared to strain levels recorded in other regions of the face. These findings emphasize earlier arguments that this region cannot be modelled as a beam [43]. According to the beam theory the strain should always be high in the midsection of the beam (i.e. glabellar region) and decrease toward the ends due to bending. However, the strains measured in the supraorbital region were not consistent for all skulls and did not follow a set pattern.

Traditionally the temporalis muscle has been considered to originate from the temporal fossa alone[44,45], but recent studies have shown that the temporalis muscle also originates from the lateral margin of the orbit, frontal process and body of the zygoma[40]. This extended area of origin can explain the strain patterns observed in the current study when loading through the temporalis muscle. When pulling the temporalis muscle down, the attachment of the temporalis

to the inner cortex of the zygoma results in loading similar to the masseter muscle. This loading resulted in similar strain patterns in both the zygoma and the maxilla as occur via loading through the masseter muscle. These findings are non-intuitive as it was believed that the temporalis muscle does not, through its origin, produce much force on the zygoma. The impact of the temporalis muscle on the strain patterns in the upper-facial region is a newly described phenomenon, indicating a potentially significant role that the temporalis muscle plays in applying forces to the upper and midfacial regions consequently producing high strains. To date, the impact of the temporalis muscle loading on the zygoma has been overlooked; the present results indicate an important role this muscle has in producing strains in both the zygoma and maxilla.

In spite of morphologic differences, the strains were found to be relatively consistent between the five CFSs (correlation coefficients of 0.75 for masseter muscle and 0.81 for temporalis muscle). This consistency bodes well for the use of generalized models in the development of new osteosynthetic technologies and reconstructive techniques rather than subject-specific models for design criteria.

That said, age and disease related morphological differences and subsequent strain and load differences will require further consideration in future model development. This study was conducted to develop a better understanding of the biomechanical behaviour of the CFS due to uniform static muscle loading. Although the aim of this study was not to replicate the concerted, complex physiology of facial and masticatory muscle loading, it aims to capture and characterize many of the previously un-described and uncharacterized aspects of the latter. In particular, the contribution of the unique mechanical and anatomic character of the masticatory muscular origins, in spite of being shown to effect strain patterns, has been largely ignored in previous models. Furthermore, boundary conditions of the occlusal arch have never before been utilized in an *in vitro* model to accurately mimic bite force loading.

Inter-specimen consistency and corroboration of our results with published *in vivo* data supports the use of this experimental model for validation of specimen specific FE models of the CFS. That the results of this study show some counterintuitive and surprising patterns of strain, consistent between specimens, underscores the importance of developing FE models. The latter will allow for the replication of more complex multi-muscle physiologic loading for full field

strain analysis and ultimately for design criteria in the development and optimization of reconstructive techniques and technologies.

6.6 References

1. Francel, T. J., Birely, B. C., Ringelman, P. R., et al. The fate of plates and screws after facial fracture reconstruction. *Plast. Reconstr. Surg.* 90, 1992: 568-573.

2. Orringer, J. S., Barcelona, V., Buchman, S. R. Reasons for removal of rigid internal fixation devices in craniofacial surgery. *J. Craniofac. Surg.* 9, 1998: 40-44.

3. Regev, E., Shiff, J. S., Kiss, A., et al. Internal fixation of mandibular angle fractures: A meta-analysis. *Plast. Reconstr. Surg.* 125, 2010: 1753-1760.

4. Jack, J. M., Stewart, D. H., Rinker, B. D., et al. Modern surgical treatment of complex facial fractures: A 6-year review. *J. Craniofac. Surg.* 16, 2005: 726-731.

5. Hylander, W. L., Johnson, K. R. In vivo bone strain patterns in the zygomatic arch of macaques and the significance of these patterns for functional interpretations of craniofacial form. *Am. J. Phys. Anthropol.* 102, 1997: 203-232.

6. Weinmann, J. P. *Bone and Bones : Fundamentals of Bone Biology*, St. Louis: C.V. Mosby, 1947.

7. Sicher, H. *Oral Anatomy*, 6th ed. Ed., Saint Louis: Mosby, 1975.

8. Nagasao, T., Nakajima, T., Kimura, A., et al. The dynamic role of buttress reconstruction after maxillectomy. *Plast. Reconstr. Surg.* 115, 2005: 1328-40; discussion 1341.

9. Rodriguez, E. D., Bluebond-Langner, R., Park, J. E., et al. Preservation of contour in periorbital and midfacial craniofacial microsurgery: Reconstruction of the soft-tissue elements and skeletal buttresses. *Plast. Reconstr. Surg.* 121, 2008: 1738-47; discussion 1748-9.

10. Rudderman, R. H., Mullen, R. L. Biomechanics of the facial skeleton. *Clin. Plast. Surg.* 19, 1992: 11-29.

11. Endo, B. Experimental studies on the mechanical significance of the form of the human facial skeleton. *J. Fac. Sci. Univ. Tokyo* 3, 1966: 1-106.

12. Endo, B. Analysis of stresses around the orbit due to masseter and temporalis muscles respectively. *J. Anthropol. Soc. Nippon* 78, 1970: 251-266.

13. Nagase, D. Y., Courtemanche, D. J., Peters, D. A. Plate removal in traumatic facial fractures: 13-year practice review. *Ann. Plast. Surg.* 55, 2005: 608-611.

14. Schortinghuis, J., Bos, R. R., Vissink, A. Complications of internal fixation of maxillofacial fractures with microplates. *J. Oral Maxillofac. Surg.* 57, 1999: 130-4; discussion 135.

15. Hylander, W. L., Picq, P. G., Johnson, K. R. Masticatory-stress hypotheses and the supraorbital region of primates. *Am. J. Phys. Anthropol.* 86, 1991: 1-36.

16. Oyen, O. J., Tsay, T. P. A biomechanical analysis of craniofacial form and bite force. *Am. J. Orthod. Dentofacial Orthop.* 99, 1991: 298-309.

17. Oyen, O. J., Melugin, M. B., Indresano, A. T. Strain gauge analysis of the frontozygomatic region of the zygomatic complex. *J. Oral Maxillofac. Surg.* 54, 1996: 1092-5; discussion 1095-6.

18. Strait, D. S., Wang, Q., Dechow, P. C., et al. Modeling elastic properties in finite-element analysis: How much precision is needed to produce an accurate model? *Anat. Rec. A. Discov. Mol. Cell. Evol. Biol.* 283, 2005: 275-287.

19. Vinyard, C. J., Ravosa, M. J., Wall, C. E., et al. *Primate Craniofacial Function and Biology*, New York ; London: Springer, 2008. Pp. 496.

20. Strait, D. S., Weber, G. W., Neubauer, S., et al. The feeding biomechanics and dietary ecology of australopithecus africanus. *Proc. Natl. Acad. Sci. U. S. A.* 106, 2009: 2124-2129.

21. Wang, Q., Smith, A. L., Strait, D. S., et al. The global impact of sutures assessed in a finite element model of a macaque cranium. *Anat. Rec. (Hoboken)* 293, 2010: 1477-1491.

22. Wang, Q., Wright, B. W., Smith, A., et al. Mechanical impact of incisor loading on the primate midfacial skeleton and its relevance to human evolution. *Anat. Rec. (Hoboken)* 293, 2010: 607-617.

23. Chalk, J., Richmond, B. G., Ross, C. F., et al. A finite element analysis of masticatory stress hypotheses. *Am. J. Phys. Anthropol.* 145, 2011: 1-10.

24. Ross, C. F., Hylander, W. L. In vivo and in vitro bone strain in the owl monkey circumorbital region and the function of the postorbital septum. *Am. J. Phys. Anthropol.* 101, 1996: 183-215.

25. Ross, C. F. In vivo function of the craniofacial haft: The interorbital "pillar". *Am. J. Phys. Anthropol.* 116, 2001: 108-139.

26. Ross, C. F., Metzger, K. A. Bone strain gradients and optimization in vertebrate skulls. *Ann. Anat.* 186, 2004: 387-396.

27. Ross, C. F., Patel, B. A., Slice, D. E., et al. Modeling masticatory muscle force in finite element analysis: Sensitivity analysis using principal coordinates analysis. *Anat. Rec. A. Discov. Mol. Cell. Evol. Biol.* 283, 2005: 288-299.

28. Ross, C. F., Berthaume, M. A., Dechow, P. C., et al. In vivo bone strain and finite-element modeling of the craniofacial haft in catarrhine primates. *J. Anat.* 218, 2011: 112-141.

29. Kasrai, L., Hearn, T., Gur, E., et al. A biomechanical analysis of the orbitozygomatic complex in human cadavers: Examination of load sharing and failure patterns following fixation with titanium and bioresorbable plating systems. *J. Craniofac. Surg.* 10, 1999: 237-243.

30. Alberts, L. R., Phillips, K. O., Tu, H. K., et al. A biologic model for assessment of osseous strain patterns and plating systems in the human maxilla. *J. Oral Maxillofac. Surg.* 61, 2003: 79-88.

31. Szwedowski, T. D., Whyne, C. M., Fialkov, J. A. Toward characterization of craniofacial biomechanics. *J. Craniofac. Surg.* 21, 2010: 202-207.

32. Ravosa, M. J., Johnson, K. R., Hylander, W. L. Strain in the galago facial skull. *J. Morphol.* 245, 2000: 51-66.

33. Curtis, N. Craniofacial biomechanics: An overview of recent multibody modelling studies. *J. Anat.* 218, 2011: 16-25.

34. Szwedowski, T. D., Fialkov, F., Whyne, C. Sensitivity analysis of a validated subject-specific finite element model of the human craniofacial skeleton . *Proceedings of the Institution of Mechanical Engineers. Part H, Journal of engineering in medicine* 224, 2010: 1-10.

35. Strait, D. S., Wang, Q., Dechow, P. C., et al. Modeling elastic properties in finite-element analysis: How much precision is needed to produce an accurate model? *Anat. Rec. A. Discov. Mol. Cell. Evol. Biol.* 283, 2005: 275-287.

36. Provatidis, C., Georgiopoulos, B., Kotinas, A., et al. In vitro validated finite element method model for a human skull and related craniofacial effects during rapid maxillary expansion. *Proc. Inst. Mech. Eng. H.* 220, 2006: 897-907.

37. Raadsheer, M. C., van Eijden, T. M., van Ginkel, F. C., et al. Contribution of jaw muscle size and craniofacial morphology to human bite force magnitude. *J. Dent. Res.* 78, 1999: 31-42.

38. Haggard, E. A. *Intraclass Correlation and the Analysis of Variance. with an Appendix by Hari C. Gupta*, New York: Dryden Press, 1958.

39. Johnson, N. L., Kotz, S., Read, C. B. *Encyclopedia of Statistical Sciences*, New York: Wiley, 1982; 1988.

40. Barry, C. P., Ryan, W. J., Stassen, L. F. Anatomical study of factors contributing to zygomatic complex fracture instability in human cadavers. *Plast. Reconstr. Surg.* 119, 2007: 637-40; discussion 641.

41. Deveci, M., Eski, M., Gurses, S., et al. Biomechanical analysis of the rigid fixation of zygoma fractures: An experimental study. *J. Craniofac. Surg.* 15, 2004: 595-602.

42. Karlan, M. S., Cassisi, N. J. Fractures of the zygoma. A geometric, biomechanical, and surgical analysis. *Arch. Otolaryngol.* 105, 1979: 320-327.

43. Picq, P. G., Hylander, W. L. Endo's stress analysis of the primate skull and the functional significance of the supraorbital region. *Am. J. Phys. Anthropol.* 79, 1989: 393-398.

44. Agur, A. M. R., Lee, M. J., Grant, J. C. B. *Grant's Atlas of Anatomy*, 9th Ed., Baltimore: Williams & Wilkins, 1991.

45. Moore, K. L., Dalley, A. F. *Clinically Oriented Anatomy*, 4th Ed., Philadelphia: Lippincott Williams & Wilkins, 1999.

6.7 Appendix F

Standard operating procedure:

Specimen Preparation

1. Place the fresh frozen heads in the fridge 24 hours prior to testing
2. Make an incision to the left side of the head extending from the frontal bone, around the temporalis to the ear, then down towards the base of the neck
3. Release the left masseter muscle from the insertion into the angle of the mandible using a surgical elevator
4. Raise the master muscle to expose the temporalis insertion into the coronoid
5. Fracture the base of the coronoid using a surgical chisel
6. Make sure to preserve the insertion of the temporalis into the remaining coronoid fragment for load transmission during mechanical testing
7. Remove the remaining soft tissues in order to expose the surface of the bones
8. Make sure the periosteum is dissected away from the left maxilla, nasal bones, orbit and zygoma
9. Before scanning place radio-opaque fiducial markers on the bone surface in order to provide a 3D coordinate system for subsequent data processing
10. Place the fiducials at the following locations: at the root of the zygomatic arch in the temporal bone and, the front of the maxilla directly above the incisors and at the bridge of the nose just under the orbit
11. Remove any mercury fillings in the teeth
12. Mercury fillings can be removed using a standard Dremel tool with a countersunk engraving bit
13. Scan the cadaver heads using a clinical CT scanner (Light speed VCT GE Medical Systems, GE Healthcare)

Loading

1. Attach aluminum interface plates to the dissected masseter and temporalis muscles using Ti-Cron 1-4 metric sutures (Syneture Inc., Covidien)
2. Make sure the sutures threaded well through the body of the muscles
3. Place a steel wire between the teeth force

4. Place the teeth inside a specially designed fixture to mimic bite conditions
5. Pour polymethylmethacrylate (bone cement) into the fixture to fully immerse the teeth and the steel wire
6. Wait for the bone cement to cure and become rigid
7. Place the head on a Mechanical Testing Station (MTS Bionix)
8. Make sure the head is elevated above the base to provide space for force redirections pulleys
9. Connect a stainless steel 500 lb test wire to provide a link between the interface plates of the masseter and temporalis and the tensile force actuator on the MTS
10. Place a pulley under the head on the MTS to be used to redirect the force from the hydraulic actuator in the approximate native direction of the masseter or temporalis muscles
11. Bound the strain gauges to bone surface using the M-Bond 200 Adhesive Kit
12. Using a Microscribe 3DX digitize the location of the strain gauges and fiducials fixed to the head
13. Connect the strain gauges to a data acquisition system DAQBOOK
14. Apply a 100N force to masseter muscle and measure the strain
15. Repeat step 14 two more times
16. Apply 100N force to the temporalis muscle
17. Repeat step 16 two more times
18. The strain magnitude experienced by each strain gauge during loading will be recorded in a file and saved on the laptop connected to the data acquisition system DAQBOOK
19. Open the clinical CT scan of each head in AmiraDev software
20. Identify the location of the fiducials on the bone surface. Fiducials appear as bright circles in the scan
21. Generate an Isopsurface for each head
22. Using the data obtained in step 12 and the location of the fiducials in the scan determine the location of each strain gauge
23. Use the 3D head surface and strain data to visualize the strains measured using the strain gauges

CHAPTER 7
General Discussion

7.1 Summary

The five studies presented in this thesis provide new insight into the biomechanical behaviour of thin bone structures in the CFS. Each study examined different *morphological and geometrical* aspects of thin bony structures and their impact on the local biomechanical behaviour through image processing techniques, mechanical testing and FE analysis. Characterizing the local mechanical behaviour of thin bone structures is important for understanding the global impact of loading on strain patterns in the CFS. The findings of these studies can also be applied to other regions of thin bone structures in the human skeleton to better understand their biomechanical behaviour.

The biomechanical behaviour of the CFS can be studied through *in vivo*, *in vitro* and computational experimentation. *In vivo* studies can provide the most accurate representation of complex material properties, geometry and physiological loading conditions. However, conducting *in vivo* studies on the human CFS is limited by ethical considerations. Animal *in vivo* experiments can provide material, geometry and physiologic loading information, however, differences in the morphology between animals and humans limit the transferability of findings from such studies to humans. Moreover, ethical considerations limit the researchers' ability to conduct comprehensive *in vivo* studies on animals. Many of the limitations (i.e. restricted access to bone surfaces) associated with *in vivo* studies can be resolved using an *in vitro* approach. *In vitro* experiments on cadaver CFS facilitates access to sites difficult to reach and allows evaluation of the role of human morphology on biomechanical behaviour. However, *in vitro* experiments must accept changes in tissue elastic properties tissues postmortem, the use of non-physiological loading forces, and the inability to represent complex loading from various muscles. Computational modeling using the FE method can mitigate some of these issues by implementing complex representations of material properties, geometry and loading based on 3D imaging. However, validation of FE models is essential and is often accomplished through direct comparisons to *in vitro* testing data. *In vitro* validation of FE models provides an assessment of

how accurately geometry and material properties have been modeled under conditions in which loads and constraints can be tightly controlled. Once a model is validated under simplified loading, its biomechanical behaviour can be evaluated under more complex physiologic loading conditions.

The accuracy of FE models of thin bone structures is highly dependent on both geometry and material property assignment [1-3]. Recent advances in imaging technology have made it possible to capture and digitally reconstruct skeletal geometry at the micro-level and beyond, thereby facilitating the generation of detailed FEM of bony structures [4-9]. However, the relatively large voxel size in clinical images limits the ability to capture accurate information about geometry and material properties of thin bone regions and complex articulations (i.e. sutures) which are important components of CFS models.

The inaccurate measurement of cortical bone thickness from clinical CT scans due to image degradation limits the ability to use such measurements to generate accurate FE models. This limitation can be encountered when using CT images at various locations in the human skeleton. Similar to the CFS, the pelvis and scapula are composed of a mixture of thin bone regions as cortical shell only, thicker cortex, and areas of cortical shell surrounding a trabecular mesh. Validated models of the CFS and pelvis by Szwedowski *el al.* and Anderson *et al.* have reported high sensitivities to changes in cortical thickness in their FE models [1, 3]. In both studies slight deviations in cortical thickness resulted in significant changes to strain distributions. Szwedowski *el al.* found that modeling cortical bone thickness based on clinical CT data measurements provided the best correlation to experimental in vitro data (r=0.73). However, areas of thin bone (i.e. sinus wall) exhibited the highest deviations from the experimentally measured strain values (46% less strain in the FE models). Similarly, image degradation has a negative impact on scan intensity, which commonly used to define bone material properties (i.e. *Young's modulus*)[10]. High FE model sensitivity was also found based on bone material property assignment. Qualitative examination of the clinical CT scans used by Szwedowski *el al.* revealed blurring along the boundaries of thin bone regions which results in overestimation of cortical bone thickness during CT image segmentation. These findings motivate the initial research questions addressed in this thesis: Are cortical bone thickness and material properties obtained from clinical CT images of the CFS accurate enough to produce robust FE models? .

The first study confirmed previously reported clinical CT based overestimation of cortical bone width measurements and accompanying underestimation of intensity values [11-13]. It further demonstrated that image voxel size has a large effect on FE modeled biomechanical behaviour, with large voxel size resulting in greatly reduced maximum principal strains. As such, this study confirmed that relatively large voxel sizes used in clinical CT images is a significant problem for generating accurate FE models of the CFS and limits successful experimental validation of such models. The importance of these findings is not limited to FE models of the CFS but applies to all structures in the human skeleton where thin cortical bone is present. Furthermore, accurate cortical bone thickness measurements are important for evaluating skeletal integrity with respect to the impact of new and existing therapies targeted to bone and the suitability of thin bone structures for hardware insertion[14, 15].

Confirming the significant impact of image degradation on cortical bone thickness measurement, material properties and ultimately strain magnitude has motivated development of an automated method to correct thin bone geometry and X-Ray intensity information from clinical CT images (beyond the scope of this thesis). Analysis of the CFS in its physiologic environment requires full skull model generation, limiting the CT resolution that can be utilized, due to the size of the resultant data sets. The resolution of clinical CT images are further limited due to radiation dose. As such, it is important to develop such algorithms to improve the robustness of clinical data sets through the digital reduction of image blurring. If image post-procession can be shown to yield accurate geometry and material properties for thin cortical bone structures in the CFS from clinical CT images, this may have a large impact towards improving the accuracy of CFS FE models.

The overarching goal of the second, third and fourth studies was to characterize the local biomechanical behaviour of suture/bone structures in the CFS. There have been numerous *in vivo* and *in vitro* strain gauge studies which have attempted to characterize the strain across CFS sutures [16-21, 21-25], These studies have identified important mechanical features of patent sutures and have suggested that the CFS with unfused sutures does not behave mechanically as rigid body (i.e. in young children). Although it is clear that sutures in the CFS influence the strain flow, their impact on adult CFS biomechanics and their biomechanical properties remain poorly

defined. Two main issues have limited the current state of knowledge of CFS sutures. The first is the lack of complete understanding of the localized biomechanical behaviour of sutures, which is essential to characterize the global impact of sutures on the CFS. The second is the extent of which the information about suture biomechanics derived from animals is representative of the biomechanics of human CFS sutures, knowing that species-specific bone cell dynamics may produce different patterns of suture and bone biomechanics [26].

The suture studies presented in this thesis aimed at addressing these two issues through combination of FE analysis, imaging techniques and mechanical testing. To date, there has been a disconnect between studies conducted to examine the overall impact of sutures on the CFS and studies investigating the local biomechanical behaviour [25, 27-31]. Suture biomechanics can be impacted by many factors such as loading type, morphology, and bone and suture material properties. The lack of knowledge about the impact of these factors has limited researchers from accounting for these factors in global CFS models. Yet, full CFS FE models developed without accounting for suture morphology may lead to biased results. A clear understanding of the morphology and localized behaviour of the sutures, as presented in chapter 4, is an important step in determining their impact on the global behaviour of the CFS.

Prior to the publication of the study presented in chapter 3, little information was available about the internal 3D morphology of human cranial and facial sutures. Suture morphology was primarily defined based on surface interdigitations or 2D histologic sections [32-34]. Advances in μCT imaging allowed for internal visualization of the suture morphology but no information was available about the degree of connectivity across the bony interdigitations. The work in this thesis introduced a new parameter with which to quantify suture morphology: suture connectivity. Suture connectivity, defined as the degree of bony bridging between the adjacent surfaces of the suture gap, allows for both quantification and 3D visualization of connectivity across the suture gap and a better understanding of suture development. Applications for this skeletal connectivity measurement technique extend beyond adult CFS suture morphology. For example, this technique could be applied to study morphological changes in children with craniosynostosis to develop a better understanding of fusion in the internal surface of the suture or extended to quantify connectivity through healing fractures.

Previously developed FE models of the CFS have been limited by not accounting for the presence of sutures [1, 3]. The present work has clearly demonstrated that sutures in the adult CFS are not fully fused and may play a complex role in strain transmission. Incorrect assumptions of fusion may lead to biased interpretations of strain gage results on a global scale and lead to misrepresentation and interpretation of CFS FE model results. Better understanding of the local biomechanical behaviour of sutures and sutural patency may help refine FE models and increase the ability of such models to represent the complex thin bone anatomy, load transmission and fracture patterns seen in the CFS.

In chapter 4 the local biomechanical behaviour of sutures was evaluated computationally considering differing loading directions (parallel, perpendicular and pressure), suture morphology (connectivity and interdigitations) and material properties (isotropic and orthotropic). The use of FE models allowed quantification of the individual and combined impact of these parameters. Prior FE work modeling suture behaviour has investigated only parallel loading scenarios [28-31]. Yet, sutures in the CFS can experience complex loading due to muscle, mastication and impact forces. As such, it is important to understand the impact of multiple loading directions when characterizing the biomechanical behaviour of sutures/bone complexes. Connectivity across the suture has also been neglected in previous computational models. Using the data obtained from Chapter 3 an average connectivity was assigned to sutures in the FE models with varying interdigitation indexes. This allowed for evaluation of the combined impact of interdigitation and connectivity on suture mechanical behaviour. This study also was the first to integrate information about fiber orientation obtained from histological sections of human sutures into a FE suture model.

The influence of sutures on strain patterns holds important implications for the attempts to investigate strain distributions throughout the CFS using FE models. Chapters 2 to 4 analyzed the impact of multiple factors on local suture mechanics, allowing the identification of factors which may be critical in developing accurate FE models. Though the general strain flow and strain gradients may not necessarily change based on the presence of sutures in full CFS FE models, strain patterns will likely be altered locally at areas close to the sutures. This has been demonstrated in previous studies on the Macaque skull, which have shown that the presence or absence of patent sutures has only a subtle effect on strain patterns over the whole skull, but

leads to some sizeable shifts in localized areas (such as the posterior zygomatic arch and anterior midface) [27, 35, 36]. Furthermore, the same studies have shown that even though sutures had a minimum impact on the strain patterns, they resulted in much larger changes in the full CFS strain energy. These animal studies along with the results presented in this thesis highlight the need to include sutures in full CFS models. Yet the precise method with which to incorporate sutures in full CFS FE models is yet to be solved and represents an important technical question. Whether sutures should be modeled using their complex interdigitating morphology with connectivity, or as simplified structures depends on the scale of the research question and the biomechanical parameters to be evaluated.

The final study presented in Chapter 6 focused on experimental testing of the full CFS. This work measured local strain magnitudes and directions at multiple regions in the CFS under simplified muscle loading. In this study, strain gauges placed over the maxillary sinus wall (thin cortical bone alone) demonstrated the presence of high strains in thin bone regions in the midfacial area, similar to strains found in the zygomatic buttress (thick cortical shell over trabecular mesh). Regions of thin cortical bone such as the maxillary sinus wall were previously believed to play a minimum role in load bearing the CFS [37, 38]. This finding emphasize the importance of accurately modeling the geometry and material properties of thin cortical bone regions as they play a critical role in load bearing in the CFS. Furthermore, the types (compression and tensile) and orientation of strains in the midfacial region confirm the complex loading experienced by bones of the CFS, even due to simplified muscle forces. This further highlights the importance of characterizing the varying biomechanical behaviour of the craniofacial sutures under different loading scenarios.

Overall, the findings from the five studies presented in this thesis have added to scientific knowledge of the CFS with respect to it complex morphology, limitations of current clinical imaging and biomechanical behaviour of thin bone structures and their articulations. While the focus of this thesis was in characterizing thin bony structures in the CFS, application of the developed methodologies and results can be extended to other regions of the skeletal system.

7.2 Limitations

The current work has provided new insights into the morphology and mechanics of thin bone structures that can aid in characterizing the biomechanical behaviour of the CFS. While the strengths of this work have added to the field of bone biomechanics, several limitations exist in the research methods employed for the presented studies. Specific limitations of each study have been discussed in their individual chapters, but there are some overall limitations that are common between the studies. The limited access to fresh frozen human heads did not allow for the analysis of large numbers of samples; this restricted the ability of this work, in some instances, to yield comprehensive conclusions or demonstrate statistically significant results. Furthermore the age of the human tissue analysed in this thesis (range 65-101 years) represents only the later stages of adult life. Extending these analyses to CFS tissue from children and younger adults would yield additional insights into the biomechanical behaviour of thin bone structures and their articulations throughout the maturation process. Since the sutures in the CFS undergo major changes in their morphology over the human life span to meet varying mechanical demands, studying samples from different age groups is essential for full characterization of the biomechanical behaviour of the sutures in the adult CFS. Obtaining cadaveric tissue remains a challenge in biomedical research, which emphasizes the need to develop alternative approaches, such as CT image based patient specific computational modeling, to study CFS behaviour.

In Chapter 2, images were generated by downsampling high resolution μCT scans of bone samples to represent clinical CT imges. The downsampled images generated from high resolution μCT scans, however, have less noise than is present in images acquired using clinical CT at a similar voxel size and, as such, do not fully represent an equivalent image quality. The presence of increased noise in clinical CT images represents a worst case scenario of image quality degradation due to increased noise, not present in our simulated low resolution images. The negative impact of blurring seen in the simulated images would be further magnified by the presence of noise in clinical images, increasing the potential impact of our findings.

The developed technique for quantifying suture connectivity required manual user interventions to improve the segmentation in the suture region. The imaging software AmiraDev (Amir 5.2.2, Visage Imaging, San Diego, CA) was used to conduct the semi-automated segmentation of the

suture gap and bony bridging. However, the ability to fully automate the segmentation was limited due to the morphological complexity of the sutures. The manual segmentation interventions were time consuming to ensure accurate definition of suture and bone boundaries in each slice in the μCT stack. Due to the segmentation intensive nature of the technique, the relationship between connectivity and bending strength of the 20 additional sutures studied in Chapter 5 was not included. The semi-automated technique presented demonstrated the feasibility of image based 3D connectivity quantifications in sutures. Future work developing a fully automated segmentation method is required to allow wider application of this technique to mulitple sutures with various morphological complexities. As the CFS contains 17 sutures with varying amounts of interdigitation and connectivity [39], an automated segmentation method could be used to examine differences between these sutures. Quantifying suture morphology at different developmental stages may further be used to better understand internal morphological changes to suture and CFS growth.

Idealized FE models of CFS sutures were used to quantify the impact of morphological features, loading direction and material property assignments on mechanical behaviour. An additional specimen specific FE suture model was shown to follow similar trends in terms of strain energy and von Mises stress to the idealized model. Additional specimen specific models would be needed to confirm the ability of idealized data sets to represent the complexity of human sutures and to determine whether these idealized models are also able to accurately represent additional biomechanical outcome parameters (i.e. bending strength). Experimental measurement of biomechanical outcome parameters (i.e. strain) through methods such as μ-image registration would also be required to ultimately validate the specimen specific FE models.

Although the loading applied through the mastication muscles used in Chapter 6 is more relevant to CFS physiology than loading methods employed by other investigators (pulleys, rope systems and direct compressive forces applied to the bone)[40-42], it does not represent the multi-muscle physiological loading that is present *in vivo* in the CFS. In this study, the loading was applied through the two major mastication muscles (masseter and temporalis) to establish a basic understanding of CFS biomechanical behaviour. These two muscles are responsible for generating the highest loads experienced by the CFS and are easy to access in comparison to other smaller muscles. However, other muscles such as the pterygoid and digastrics provide transverse stabilization during crunching and grinding motions and will ultimately be important

for developing a comprehensive understanding of CFS biomechanical behaviour. Biting forces reported by other investigators were higher than the loading forces applied in this study [43, 44]. The ability to apply higher forces was limited by the poor conditions of the muscles in the cadaver specimens used, which resulted in tearing under higher applied loads. The lower force application may have resulted in a change to the overall strain patterns, with a non-uniform reduction in strain in some regions in the CFS that may be critical for load transmission. FE models of the CFS experimentally validated under simplified loading conditions, may be used to simulate multi-muscle forces at varying load levels to represent the complexity of CFS biomechanical behaviour.

7.3 Significance and Future Directions

In spite of the development of new technologies for application in the field of craniomaxillofacial surgery, clinicians continue to experience shortcomings and failures in these technologies, and revision operations for problematic facial hardware and reconstructive techniques continue to occur. The intricate bony anatomy of the CFS creates a complex structure with biomechanical behaviour that is challenging to understand. Characterizing the biomechanical behaviour of thin bone structures in the CFS represents an essential first step toward understanding the environment in which existing and new technologies are expected to perform.

Through this work we have expanded our understanding of important morphologic and material aspects of the biomechanical behaviour of thin bone structure in the CFS. This has been done through combining image analyses, computational modelling and mechanical testing. These methods allowed for defining the critical role of morphology and structure in shaping the biomechanical behaviour of the CFS. The semi-automated technique for quantifying 3D connectivity of sutures introduced a new a morphological parameter that can be used to better evaluate fusion in healthy and diseased sutures. Similarly, this study has identified multiple factors (i.e. connectivity, interdigitation) critical for determining the response of sutures to loading. The information presented in this thesis is a platform to guide future studies that aim to characterize the biomechanical environment in which future devices and techniques for CFS repair and reconstruction will perform.

The studies presented in this thesis provide important information about thin bone structures, which can be utilized in future characterization of the global biomechanical behaviour of the CFS. One of the motivations for this PhD project was the limitations faced by Szwedowski *et al.* in the development and validation of FE models of the full CFS[1, 45]. Quantifying the limitations of clinical CT data in representing the morphology and material properties of thin bone structures in Chapter 2 due to blurring, has led to development of an algorithm that can derive accurate local measures of cortical bone thickness and material properties from CT data through post scan image processing. Future work is needed to extend this algorithm to allow the processing of large data sets, i.e. clinical CT scans of the CFS, to reduce image blurring prior to segmentation for specimen specific FE model development. This technique will be critical in capturing the accurate geometry and material properties of very thin bone regions in the CFS (such as the maxillary sinus wall) and in accurately measuring cortical shell thickness (alone and adjacent to trabecular bone).

Biomechanical characterization of the suture/bone complex demonstrated the importance of loading direction on behaviour, which suggests that different loading scenarios might have different functional effects on CFS sutures. As such, future work should evaluate the response of the bone/suture complex to multifaceted loading corresponding to physiological conditions and the implications of this with respect to anatomic location and normal and pathologic suture morphology. Furthermore, the impact of different material properties assignment on the biomechanical behaviour should be investigated. Various material properties can be assigned to FE models based on the information reported from multiple studies[46-48]. These investigations should employ a combination of methods including FE modeling, multimodal image analysis and experimental mechanical testing to develop a comprehensive understanding of suture biomechanics.

Investigating the variations in suture morphology in the CFS is important to understand their role in the load transmission. The data presented in this thesis showed that suture morphology is not limited to the number of interdigitations but includes varying degrees of fusion between the adjacent bone surfaces. Future work may focus on investigating the internal 3D morphology of cranial and facial sutures during development. This can aid in understanding the relationship between suture loading, morphology and fusion in healthy and diseased states. Earlier attempts to understand the impact of mechanical stimuli on suture fusion have used an interdigitation

index as one measure of morphological changes[24, 49-52]. Incorporating the degree of connectivity across sutures may lead to a more physiologically relevant evaluation of the impact of mechanical stimuli on failure and fusion.

Although the suture studies presented in this thesis provided important information about the morphology and local biomechanical behaviour of sutures, this work did not address the methodological issue related to suture inclusion in full CFS FE models. With high levels of behaviour inter and intra specimen morphological variations in CFS sutures, further study is needed to optimize appropriate modeling approaches. Future investigations should aim at determining the sensitivity of morphologic factors with respect to different mechanical outcomes (i.e. strain, strain energy, *etc*.). This can be achieved by implementing a design of experiments approach combined with µCT based FE models containing various morphologies to identify how changes in morphology and their interactions (i.e. with load and material property assignments) may impact biomechanical behaviour.

Developing FE models of the human CFS can aid in understanding the distribution of loads throughout the bones of the CFS due to physiological loading. The distribution of load and resultant strain patterns are important because they form the basis upon which design criteria for new technologies and methodologies will be developed. The mechanical testing data collected for the study in this thesis can be used for validation of FE models of multiple specimens. Future direction should focus on developing multiple patient specific FE models from clinical CT scans. The FE models should be developed from scans that are processed with the correction algorithm to decrease blurring. The models should also account for suture presence and their varying morphology. In particular, future work should evaluate if models developed with sutures and based on accurate geometry and material properties will yield better correlation to mechanical testing results in comparison to the work of Szwedowski *et al*. and others[1, 45, 53, 54].

The development of multiple subject-specific CFS models validated against *in vitro* mechanical testing is not fully sufficient for understanding *in vivo* biomechanical behaviour. However, the validated FE models can be used to model *in vivo* complex physiological loading scenarios. By loading the FE models through multiple mastication muscles a more comprehensive understanding of the biomechanical behaviour of the CFS can be developed. Information obtained from *in vivo* bite force measurements and the relative recruitment levels of various

mastication muscles can be used to apply physiologic loading to a validated FE model [43, 44, 55]. The strain patterns generated through complex loading should be compared to the strain patterns generated through single muscle loading to evaluate how the strain patterns change under multi-muscle complex loading. Applying physiological loading to validated FE models of human CFS will provide information about stresses and strains that would provide clinically relevant and transferable information. The techniques and knowledge developed in this thesis can also be applied to help the wider scientific community to understand the biomechanical behaviour of thin bone structures and articulations in other parts of the human skeleton. Multi-specimen validated FE models can be used to study any skeletal anatomy or pathology, including the treatment of congenital deformities and traumatic injuries (fractures).

Successful experimental validation of the FE models can provide fundamental new insights into the local and global mechanics of the CFS, and provide a foundation to assess existing and new techniques and devices for treatment, ultimately aiding their translation to clinical practice. The characterization of the mechanical behaviour of the CFS using FE models validated through *in vitro* mechanical testing can provide an understanding of the impact of muscles on load distribution and strain patterns. It will also provide an insight to the global role the morphology plays in determining these load distributions. The validated FE models will be used to analyze more complex loading patterns that occur *in vivo* but are difficult to represent experimentally. They will be used to describe the behaviour and stability of the CFS under simple and complex loading scenarios. These FE models will provide the basis for future studies to understand the effect of changes in morphology due to diseases or injuries on strain patterns potentially using morphing techniques. Such knowledge will aid in the development of robust design criteria for new technologies. The results of these studies will provide a platform for the development of future devices and techniques for CFS repair and reconstruction. Future opportunities for analysis with such validated models are wide in considering reconstruction and replacement of bony defects, and fractures resulting from trauma, birth defects, infections and ablation of neoplasia. Ultimately, improved devices for fixation and reconstruction of the CFS will reduce the need for revision surgery due to failure or relapse along with associated costs and morbidity.

7.4 References

1. Szwedowski TD, Fialkov F, & Whyne C. Sensitivity analysis of a validated subject-specific finite element model of the human craniofacial skeleton. *Proc Inst Mech Eng [H]*. 2010.

2. Szabo BA, Babuška I. Introduction to finite element analysis. 2011:364. Available from: http://myaccess.library.utoronto.ca/login?url=http://onlinelibrary.wiley.com/book/10.1002/9781119993834.

3. Anderson AE, Peters CL, Tuttle BD, et al. Subject-specific finite element model of the pelvis: Development, validation and sensitivity studies. *J Biomech Eng.* 2005;127:364-373.

4. Dumont ER, Piccirillo J, Grosse IR. Finite-element analysis of biting behavior and bone stress in the facial skeletons of bats. *Anat Rec A Discov Mol Cell Evol Biol.* 2005;283:319-330.

5. Rayfield EJ. Using finite-element analysis to investigate suture morphology: A case study using large carnivorous dinosaurs. *Anat Rec A Discov Mol Cell Evol Biol.* 2005;283:349-365.

6. Rayfield EJ. Cranial mechanics and feeding in tyrannosaurus rex. *Proc Biol Sci.* 2004;271:1451-1459.

7. Rayfield EJ, Norman DB, Horner CC, et al. Cranial design and function in a large theropod dinosaur. *Nature.* 2001;409:1033-1037.

8. Curtis N, Kupczik K, O'higgins P, et al. Predicting skull loading: Applying multibody dynamics analysis to a macaque skull. *Anat Rec (Hoboken).* 2008;291:491-501.

9. Moazen M, Curtis N, O'Higgins P, et al. Assessment of the role of sutures in a lizard skull: A computer modelling study. *Proc Biol Sci.* 2009;276:39-46.

10. Zannoni C, Mantovani R, Viceconti M. Material properties assignment to finite element models of bone structures: A new method. *Med Eng Phys.* 1998;20:735-740.

11. Hangartner TN. Thresholding technique for accurate analysis of density and geometry in QCT, pQCT and microCT images. *J Musculoskelet Neuronal Interact.* 2007;7:9-16.

12. Hangartner TN, Gilsanz V. Evaluation of cortical bone by computed tomography. *J Bone Miner Res.* 1996;11:1518-1525.

13. Silva MJ, Wang C, Keaveny TM, et al. Direct and computed tomography thickness measurements of the human, lumbar vertebral shell and endplate. *Bone.* 1994;15:409-414.

14. van Londen GJ, Perera S, Vujevich KT, et al. Effect of risedronate on hip structural geometry: A 1-year, double-blind trial in chemotherapy-induced postmenopausal women. *Bone.* 2008;43:274-278.

15. Motoyoshi M. Clinical indices for orthodontic mini-implants. *J Oral Sci.* 2011;53:407-412.

16. Behrents RG, Carlson DS, Abdelnour T. In vivo analysis of bone strain about the sagittal suture in macaca mulatta during masticatory movements. *J Dent Res.* 1978;57:904-908.

17. Smith KK, Hylander WL. Strain gauge measurement of mesokinetic movement in the lizard varanus exanthematicus. *J Exp Biol.* 1985;114:53-70.

18. Herring SW, Mucci RJ. In vivo strain in cranial sutures: The zygomatic arch. *J Morphol.* 1991;207:225-239.

19. Rafferty KL, Herring SW. Craniofacial sutures: Morphology, growth, and in vivo masticatory strains. *J Morphol.* 1999;242:167-179.

20. Herring SW, Teng S. Strain in the braincase and its sutures during function. *Am J Phys Anthropol.* 2000;112:575-593.

21. Rafferty KL, Herring SW, Marshall CD. Biomechanics of the rostrum and the role of facial sutures. *J Morphol.* 2003;257:33-44.

22. Sun Z, Lee E, Herring SW. Cranial sutures and bones: Growth and fusion in relation to masticatory strain. *Anat Rec A Discov Mol Cell Evol Biol.* 2004;276:150-161.

23. Lieberman DE, Krovitz GE, Yates FW, et al. Effects of food processing on masticatory strain and craniofacial growth in a retrognathic face. *J Hum Evol.* 2004;46:655-677.

24. Shibazaki R, Dechow PC, Maki K, et al. Biomechanical strain and morphologic changes with age in rat calvarial bone and sutures. *Plast Reconstr Surg.* 2007;119:2167-78; 2179-81.

25. Wang Q, Dechow P, Wright B, et al. Surface strain on bone and sutures in a monkey facial skeleton: An in vitro approach and its relevance to finite element analysis. In: Vinyard CJ, Ravosa MJ, Wall CE, ebrary I, eds. *Primate Craniofacial Function and Biology.* New York ; London: Springer, 2008:149-71.

26. Carmody KA, Mooney MP, Cooper GM, et al. Relationship of premaxillary bone and its sutures to deciduous dentition in nonhuman primates. *Cleft Palate Craniofac J.* 2008;45:93-100.

27. Wang Q, Smith AL, Strait DS, et al. The global impact of sutures assessed in a finite element model of a macaque cranium. *Anat Rec (Hoboken).* 2010;293:1477-1491.

28. Borke J, Zhang G, Yu J, et al. Mechanical environment and suture complexity. *Journal of Dental Research.* 2003;82:A1505.

29. Yu J, Borke J, Zhang G. Brief synopsis of cranial sutures: Optimization by adaptation *Seminars in Pediatric Neurology.* 2004;11:249.

30. Zhang G, Borke J, Yu J. Mechanical environment and cranial suture wavy pattern. *Georgia Life Sciences Summit,Atlanta.* 2002.

31. Jasinoski SC, Reddy BD, Louw KK, et al. Mechanics of cranial sutures using the finite element method. *J Biomech.* 2010;43:3104-3111.

32. Furuya Y, Edwards MS, Alpers CE, et al. Computerized tomography of cranial sutures. part 1: Comparison of suture anatomy in children and adults. *J Neurosurg.* 1984;61:53-58.

33. Persson M, Magnusson BC, Thilander B. Sutural closure in rabbit and man: A morphological and histochemical study. *J Anat.* 1978;125:313-321.

34. Persson M. The role of sutures in normal and abnormal craniofacial growth. *Acta Odontol Scand.* 1995;53:152-161.

35. Fitton L, Kupezik K, Milne N, et al. The role of sutures in modulating strain distribution within the skull of macaca fascicularis. *American Journal Of Physical Anthropology.* 2008;138:128.

36. Milne N, Fitton L, O'Higgins P, et al. The role of the zygomaticomaxillary suture in modulating strain distribution within the skull of macaca fascicularis. *Journal of Comparative Human Biology.* 2009;60:239.

37. Hardt N, Kuttenberger J, ebrary I. Craniofacial trauma. 2010:278. Available from: http://link.library.utoronto.ca/eir/EIRdetail.cfm?Resources__ID=1157113&T=F.

38. Rudderman RH, Mullen RL. Biomechanics of the facial skeleton. *Clin Plast Surg.* 1992;19:11-29.

39. Potter SOL. *A Compend of Human Anatomy: Including the Anatomy of the Viscera.* 5th ed. Philadelphia: P. Blakiston, Son & Co., 1892.

40. Kasrai L, Hearn T, Gur E, et al. A biomechanical analysis of the orbitozygomatic complex in human cadavers: Examination of load sharing and failure patterns following fixation with titanium and bioresorbable plating systems. *J Craniofac Surg.* 1999;10:237-243.

41. Alberts LR, Phillips KO, Tu HK, et al. A biologic model for assessment of osseous strain patterns and plating systems in the human maxilla. *J Oral Maxillofac Surg.* 2003;61:79-88.

42. Endo B. Distribution of stress and strain produced in the human facial skeleton by the masticatory force *J Anthrop Soc Nippon.* 1965;73:123-136.

43. Ross CF, Dharia R, Herring SW, et al. Modulation of mandibular loading and bite force in mammals during mastication. *J Exp Biol.* 2007;210:1046-1063.

44. Peck CC, Hannam AG. Human jaw and muscle modelling. *Arch Oral Biol.* 2007;52:300-304.

45. Szwedowski TD, Whyne CM, Fialkov JA. Toward characterization of craniofacial biomechanics. *J Craniofac Surg.* 2010;21:202-207.

46. Margulies SS, Thibault KL. Infant skull and suture properties: Measurements and implications for mechanisms of pediatric brain injury. *J Biomech Eng.* 2000;122:364-371.

47. Radhakrishnan P, Mao JJ. Nanomechanical properties of facial sutures and sutural mineralization front. *J Dent Res.* 2004;83:470-475.

48. Coats B, Margulies SS. Material properties of human infant skull and suture at high rates. *J Neurotrauma.* 2006;23:1222-1232.

49. Anderson PJ, Netherway DJ, David DJ, et al. Scanning electron microscope and micro-CT evaluation of cranial sutures in health and disease. *J Craniofac Surg.* 2006;17:909-919.

50. Byron CD, Borke J, Yu J, et al. Effects of increased muscle mass on mouse sagittal suture morphology and mechanics. *Anat Rec A Discov Mol Cell Evol Biol.* 2004;279:676-684.

51. Jafari A, Shetty KS, Kumar M. Study of stress distribution and displacement of various craniofacial structures following application of transverse orthopedic forces--a three-dimensional FEM study. *Angle Orthod.* 2003;73:12-20.

52. Michael Andrew Miroue. The human facial sutures: A morphological and histological study of age changes from 20 to 95 years. 1975.

53. Wang Q, Wright BW, Smith A, et al. Mechanical impact of incisor loading on the primate midfacial skeleton and its relevance to human evolution. *Anat Rec (Hoboken).* 2010;293:607-617.

54. Chalk J, Richmond BG, Ross CF, et al. A finite element analysis of masticatory stress hypotheses. *Am J Phys Anthropol.* 2011;145:1-10.

55. Raadsheer MC, van Eijden TM, van Ginkel FC, et al. Contribution of jaw muscle size and craniofacial morphology to human bite force magnitude. *J Dent Res.* 1999;78:31-42.